Eur. Phys. J. C (2015) 75:231
DOI 10.1140/epjc/s10052-015-3436-3

THE EUROPEAN PHYSICAL JOURNAL C

Regular Article - Experimental Physics

Determination of spin and parity of the Higgs boson in the $WW^* \to e\nu\mu\nu$ decay channel with the ATLAS detector

ATLAS Collaboration[⋆]

CERN, 1211 Geneva 23, Switzerland

Received: 13 March 2015 / Accepted: 1 May 2015 / Published online: 27 May 2015

Abstract Studies of the spin and parity quantum numbers of the Higgs boson in the $WW^* \to e\nu\mu\nu$ final state are presented, based on proton–proton collision data collected by the ATLAS detector at the Large Hadron Collider, corresponding to an integrated luminosity of 20.3 fb^{-1} at a centre-of-mass energy of $\sqrt{s} = 8$ TeV. The Standard Model spin-parity $J^{CP} = 0^{++}$ hypothesis is compared with alternative hypotheses for both spin and CP. The case where the observed resonance is a mixture of the Standard-Model-like Higgs boson and CP-even ($J^{CP} = 0^{++}$) or CP-odd ($J^{CP} = 0^{+-}$) Higgs boson in scenarios beyond the Standard Model is also studied. The data are found to be consistent with the Standard Model prediction and limits are placed on alternative spin and CP hypotheses, including CP mixing in different scenarios.

1 Introduction

This paper presents studies of the spin and parity quantum numbers of the newly discovered Higgs particle [1,2] in the $WW^* \to e\nu\mu\nu$ final state, where only final states with opposite-charge, different-flavour leptons (e, μ) are considered. Determining the spin of the newly discovered resonance and its properties under charge-parity (CP) conjugation is of primary importance to firmly establish its nature, and in particular whether it is the Standard Model (SM) Higgs boson or not. Compared to the previous ATLAS publication [3], this paper contains significant updates and improvements: the SM Higgs-boson hypothesis is compared with improved spin-2 scenarios. The case where the observed resonance[1] has $J^P = 1^+$ or 1^- is not studied in this paper as it is already excluded by previous publications both by the ATLAS [3] and CMS collaborations [4].

To simulate the alternative Higgs-boson hypotheses, the MadGraph5_aMC@NLO [5] generator is adopted. It includes terms of higher order (α_S^3) in the Lagrangian, in contrast to the JHU [6,7] event generator used in the previous publication [3]. In the context of this study, the 1-jet final state, which is more sensitive to contributions from the higher-order terms, is analysed, in addition to the 0-jet final state.

Furthermore, the parity of the Higgs resonance is studied by testing the compatibility of the data with a beyond-the-Standard-Model (BSM) CP-even or CP-odd Higgs boson [8]. Finally, the case where the observed resonance is a mixed CP-state, namely a mixture of a SM Higgs boson and a BSM CP-even or CP-odd Higgs boson, is investigated.

This study follows the recently published $H \to WW^*$ analysis [9] in the 0- and 1-jet channels with one major difference: the spin and parity analysis uses multivariate techniques to disentangle the various signal hypotheses and the backgrounds from each other, namely Boosted Decision Trees (BDT) [10]. The reconstruction and identification of physics objects in the event, the simulation and normalisation of backgrounds, and the main systematic uncertainties are the same as described in Ref. [9]. This paper focuses in detail on the aspects of the spin and parity analysis that differ from that publication.

The outline of this paper is as follows: Sect. 2 describes the theoretical framework for the spin and parity analysis, Sect. 3 discusses the ATLAS detector, the data and Monte Carlo simulation samples used. The event selection and the background estimates are described in Sects. 4 and 5, respectively. The BDT analysis is presented in Sect. 6, followed by a description of the statistical tools used and of the various uncertainties in Sects. 7 and 8, respectively. Finally, the results are presented in Sect. 9.

2 Theoretical framework for the spin and parity analyses

In this section, the theoretical framework for the study of the spin and parity of the newly discovered resonance is discussed. The effective field theory (EFT) approach is adopted

[1] In the following the abbreviated notation J^P is used instead of J^{CP}.

⋆ e-mail: atlas.publications@cern.ch

in this paper, within the Higgs characterisation model [8] implemented in the MadGraph5_aMC@NLO [5] generator. Different hypotheses for the Higgs-boson spin and parity are studied. Three main categories can be distinguished: the hypothesis that the observed resonance is a spin-2 resonance, a pure CP-even or CP-odd BSM Higgs boson, or a mixture of an SM Higgs and CP-even or CP-odd BSM Higgs bosons. The latter case would imply CP violation in the Higgs sector. In all cases, only the Higgs boson with a mass of 125 GeV is considered. In case of CP mixing, the Higgs boson would be a mass eigenstate, but not a CP eigenstate.

The approach used by this model relies on an EFT, which by definition is only valid up to a certain energy scale Λ. This Higgs characterisation model considers that the resonance structure recently observed corresponds to one new boson with $J^P = 0^{\pm}$, $1^{\pm}$ or 2^+ and with mass of 125 GeV, assuming that any other BSM particle exists at an energy scale larger than Λ. The EFT approach has the advantage of being easily and systematically improvable by adding higher-dimensional operators in the Lagrangian, which effectively corresponds to adding higher-order corrections, following the same approach as that used in perturbation theory. The Λ cutoff scale is set to 1 TeV in this paper, to account for the experimental results from the LHC and previous collider experiments that show no evidence of new physics at lower energy scales. More details can be found in Ref. [8]. In the EFT approach adopted, the Higgs-boson couplings to particles other than W bosons are ignored as they would impact the signal yield with no effects on the $H \rightarrow WW^*$ decay kinematics, which is not studied in this analysis.

This section is organised as follows. Higgs-like resonances in the framework of the Higgs characterisation model are introduced in Sects. 2.1.1 and 2.2.1, for spin-2 and spin-0 particles, respectively. The specific benchmark models under study are described in Sects. 2.1.2 and 2.2.2.

2.1 Spin-2 theoretical model and benchmarks

2.1.1 Spin-2 theoretical model

Given the large number of possible spin-2 benchmark models, a specific one is chosen, corresponding to a graviton-inspired tensor with minimal couplings to the SM particles [11]. In the spin-2 boson rest frame, its polarisation states projected onto the parton collision axis can take only the values of ± 2 for the gluon fusion (ggF) process and ± 1 for the $q\bar{q}$ production process. For the spin-2 model studied in this analysis, only these two production mechanisms are considered. The Lagrangian $\mathcal{L}_2^p$ for a spin-2 minimal coupling model is defined as:

$$\mathcal{L}_2^p = \sum_{p=V,f} -\frac{1}{\Lambda}\kappa_p T_{\mu\nu}^p X_2^{\mu\nu}, \quad (1)$$

where $T_{\mu\nu}^p$ is the energy-momentum tensor, $X_2^{\mu\nu}$ is the spin-2 particle field and V and f denote vector bosons (Z, W, γ and gluons) and fermions (leptons and quarks), respectively. The κ_p are the couplings of the Higgs-like resonance to particles, e.g. κ_q and κ_g label the couplings to quarks and gluons, respectively.

With respect to the previous publication [3], the spin-2 analysis presented in this paper uses the MadGraph5_aMC@NLO [5] generator, which includes higher-order tree-level QCD calculations. As discussed in the following, these calculations have an important impact on the Higgs-boson transverse momentum $p_{\mathrm{T}}^{\mathrm{H}}$ distribution, compared to the studies already performed using a Monte Carlo (MC) generator at leading order [6,7]. In fact, when κ_q is not equal to κ_g (non-universal couplings), due to order-α_{S}^3 terms, a tail in the $p_{\mathrm{T}}^{\mathrm{H}}$ spectrum appears.

For leading-order (LO) effects, the $q\bar{q}$ and ggF production processes are completely independent, but the beyond-LO processes contain diagrams with extra partons that give rise to a term proportional to $(\kappa_q - \kappa_g)^2$, which grows with the centre-of-mass energy squared of the hard process (s) as $s^3/(m^4\Lambda^2)$ (where m is the mass of the spin-2 particle), and leads to a large tail at high values of $p_{\mathrm{T}}^{\mathrm{H}}$. The distributions of some spin-sensitive observables are affected by this tail. For a more detailed discussion, see Ref. [8]. This feature appears in final states with at least one jet, which indeed signals the presence of effects beyond leading order. Therefore, the 1-jet category is analysed in addition to the 0-jet category in this paper, in order to increase the sensitivity for these production modes. Figure 1 shows the $p_{\mathrm{T}}^{\mathrm{H}}$ distribution for the 0- and 1-jet final states at generator level after basic selection requirements (the minimum p_{T} required for the jets used for this study is 25 GeV). Three different signal hypotheses are shown: one corresponding to universal couplings, $\kappa_g = \kappa_q$, and two examples of non-universal couplings. The tail at high values of $p_{\mathrm{T}}^{\mathrm{H}}$ is clearly visible in the 1-jet category for the cases of non-universal couplings.

This $p_{\mathrm{T}}^{\mathrm{H}}$ tail would lead to unitarity violation if there were no cutoff scale for the validity of the theory. By definition, in the context of the EFT approach, at a certain scale Λ, new physics should appear and correct the unitarity-violating behaviour, even below the scale Λ. There is a model-dependent theoretical uncertainty on the p_{T} scale at which the EFT would be corrected by new physics: this uncertainty dictates the need to study benchmarks that use different $p_{\mathrm{T}}^{\mathrm{H}}$ cutoffs, as discussed in the following subsection.

2.1.2 Choice of spin-2 benchmarks

Within the spin-2 model described in the previous section, a few benchmarks, corresponding to a range of possible sce-

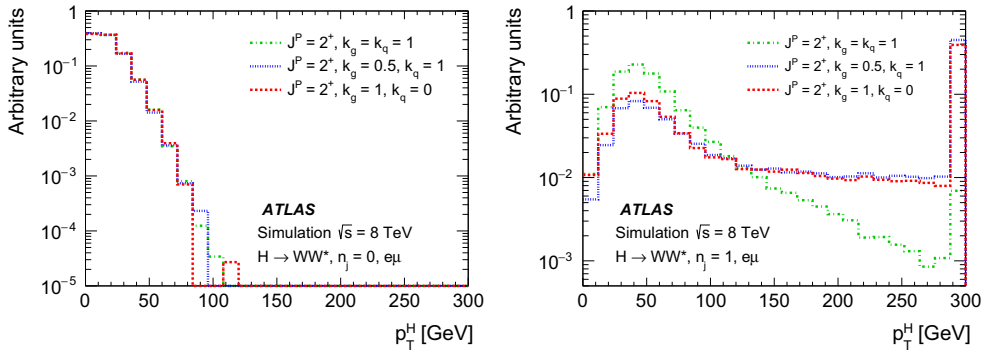

Fig. 1 The distribution of the transverse momentum of the Higgs boson, $p_{\mathrm{T}}^{\mathrm{H}}$, at the Monte Carlo event-generator level for 0-jet (*left*) and 1-jet (*right*) final states. Three spin-2 signal hypotheses are shown: $\kappa_g = \kappa_q = 1$, $\kappa_g = 0.5$, $\kappa_q = 1$ and $\kappa_g = 1$, $\kappa_q = 0$. The *last bin* in each plot includes the overflow

narios, are studied in this paper. In order to make sensible predictions for the spin-sensitive observables in the case of non-universal couplings, a cutoff on the Higgs-boson transverse momentum is introduced at a scale where the EFT is assumed to still be valid: this is chosen to be one-third of the scale Λ, corresponding to $p_{\mathrm{T}} < 300$GeV. On the other hand, the lowest possible value up to which the EFT is valid by construction is the mass of the resonance itself; therefore it is important to study the effect of a threshold on $p_{\mathrm{T}}^{\mathrm{H}}$ at 125 GeV.

Five different hypotheses are tested against the data:

- universal couplings: $\kappa_g = \kappa_q$;
- $\kappa_g = 1$ and $\kappa_q = 0$, with two $p_{\mathrm{T}}^{\mathrm{H}}$ cutoffs at 125 and 300 GeV;
- $\kappa_g = 0.5$ and $\kappa_q = 1$, with two $p_{\mathrm{T}}^{\mathrm{H}}$ cutoffs at 125 and 300 GeV.

The case $\kappa_g = 0$ and $\kappa_q = 1$ is not considered here, because it leads to a $p_{\mathrm{T}}^{\mathrm{H}}$ distribution which disagrees with the data, as shown in the $H \to \gamma\gamma$ and $H \to ZZ$ differential cross-section measurements [12,13].

2.2 Spin-0 and CP-mixing theoretical models and benchmarks

2.2.1 Spin-0 and CP-mixing theoretical models

In the case where the spin of the Higgs-like resonance is zero, there are several BSM scenarios that predict the parity of the Higgs particle to be either even or odd [14]. Another interesting possibility is that the Higgs-like resonance is not a CP eigenstate, but a mixture of CP-even and CP-odd states. This would imply CP violation in the Higgs sector, which is possible in the context of the Minimal Supersymmetric Standard Model [15] or of two Higgs-doublet models [16]. This CP violation might be large enough to explain the prevalence of matter over antimatter in the universe.

In the adopted EFT description, the scalar boson has the same properties as the SM Higgs boson, and its interactions with the SM particles are described by the appropriate operators. The BSM effects are expressed in terms of interactions with SM particles via higher-dimensional operators.

The effective Lagrangian $\mathcal{L}_0^W$ adopted for this study, in order to describe the interactions of W bosons with scalar and pseudoscalar states, is expressed as:

$$\begin{aligned}\mathcal{L}_0^W = \Big\{ & c_\alpha \kappa_{\mathrm{SM}} [g_{\mathrm{HWW}}\, W_\mu^+ W^{-\mu}] \\ & - \frac{1}{2}\frac{1}{\Lambda}[c_\alpha \kappa_{\mathrm{HWW}}\, W_{\mu\nu}^+ W^{-\mu\nu} + s_\alpha \kappa_{\mathrm{AWW}}\, W_{\mu\nu}^+ \widetilde{W}^{-\mu\nu}] \\ & - \frac{1}{\Lambda} c_\alpha [(\kappa_{\mathrm{H}\partial\mathrm{W}}\, W_\nu^+ \partial_\mu W^{-\mu\nu} + h.c.)] \Big\} X_0, \end{aligned} \tag{2}$$

where $W_{\mu\nu} = \partial_\mu W_\nu^\pm - \partial_\nu W_\mu^\pm$, $\widetilde{W}_{\mu\nu} = 1/2 \cdot \epsilon_{\mu\nu\rho\sigma} W^{\rho\sigma}$ and $\epsilon_{\mu\nu\rho\sigma}$ is the Levi-Civita tensor, while X_0 represents the spin-0 Higgs-boson field [8]. In the SM, the coupling of the Higgs boson to the W bosons is given by g_{HWW}, while the angle α describes the mixing between CP-even and CP-odd states. The notation $c_\alpha \equiv \cos\alpha$, $s_\alpha \equiv \sin\alpha$ is used in the Lagrangian. The dimensionless coupling parameters κ_i are real and describe CP violation in the most general way. The parameter κ_{SM} describes the deviations of the Higgs-boson coupling to the vector boson W from those predicted by the SM, while κ_{AWW} and κ_{HWW} are the BSM CP-odd and CP-even coupling parameters, respectively.[2] The mixing between the CP-even SM Higgs boson and the CP-even BSM Higgs boson can be achieved by changing the relative strength of the couplings κ_{SM} and κ_{HWW}. The $\cos\alpha$ term multiplies both the SM and BSM CP-even terms in the Lagrangian and therefore its

[2] The Lagrangian terms associated to the higher-dimensional operators are called in this paper *BSM CP-even* and *BSM CP-odd Higgs bosons*.

value does not change the relative importance of those contributions. This is different from the mixing of CP-even and CP-odd states, as a $\sin\alpha$ term multiplies the CP-odd state in the Lagrangian. The last term of the Lagrangian is due to derivative operators which are relevant in the case one of the two vector bosons is off-shell.

The higher-dimensional operator terms in the Lagrangian are the terms that contain κ_{AWW} and κ_{HWW} and are suppressed by a factor $1/\Lambda$. The SM Higgs boson is described by the first term of the Lagrangian, corresponding to the following choice of parameters: $\kappa_{\mathrm{SM}} = 1$, $\kappa_{\mathrm{AWW}} = \kappa_{\mathrm{HWW}} = 0$ and $|c_\alpha| = 1$. The derivative operator (the $\kappa_{\mathrm{H}\partial\mathrm{W}}$ term) described in the Lagrangian of Eq. (2) would modify the results below the sensitivity achievable with the available data statistics. In fact, the effects on the kinematic distributions introduced by the derivative operator in the same range of variation of κ_{HWW} are at most 10–20 % of the ones produced by κ_{HWW} itself. Since the present analysis is barely sensitive to κ_{HWW}, the even smaller $\kappa_{\mathrm{H}\partial\mathrm{W}}$ variations are not studied further, and the corresponding term in the Lagrangian is neglected.

2.2.2 Choice of CP benchmarks

The following approach to study different CP hypotheses under the assumption of a spin-0 hypothesis is taken in this paper. First of all, in the fixed-hypothesis scenario, the cases where the observed resonance is a pure BSM CP-even or CP-odd Higgs boson are considered. In addition, the mixing between the CP-even SM and BSM CP-odd or CP-even Higgs bosons is studied. In the CP-odd case, the mixing depends on the value of κ_{AWW} and on the mixing angle α. As can be deduced from Eq. (2), varying α or κ_{AWW} has an equivalent effect on the kinematic variable distributions; therefore in this paper only the α parameter is varied while κ_{AWW} is kept constant. The scan range of α covers the entire range from $-\pi/2$ to $\pi/2$ as the final state kinematic distributions differ for positive and negative values of α. On the other hand, the mixing between the CP-even SM and CP-even BSM Higgs bosons depends exclusively on the value of κ_{HWW} and not on the value of α.

To summarise, four hypotheses are tested against the data in this paper (for the cutoff value $\Lambda = 1$ TeV):

- Compare the SM Higgs-boson case with the pure BSM CP-even case, defined as $\kappa_{\mathrm{SM}} = 0$, $\kappa_{\mathrm{AWW}} = 0$, $\kappa_{\mathrm{HWW}} = 1$, $c_\alpha = 1$.
- Compare the SM Higgs-boson case with the BSM CP-odd case, defined as $\kappa_{\mathrm{SM}} = 0$, $\kappa_{\mathrm{AWW}} = 1$, $\kappa_{\mathrm{HWW}} = 0$, $c_\alpha = 0$.
- Scan over $\tan\alpha$: under the assumption of a mixing between a CP-even SM Higgs boson and a CP-odd BSM Higgs boson. The mixing parameter is defined as $(\tilde{\kappa}_{\mathrm{AWW}}/\kappa_{\mathrm{SM}})\cdot\tan\alpha$, where $\tilde{\kappa}_{\mathrm{AWW}} = (1/4)\cdot(v/\Lambda)\cdot\kappa_{\mathrm{AWW}}$, v is the vacuum expectation value and $\tan\alpha$ is the only variable term (corresponding to variations of c_α between -1 and 1). The other parameters are set as follows: $\kappa_{\mathrm{SM}} = 1$, $\kappa_{\mathrm{AWW}} = 1$, $\kappa_{\mathrm{HWW}} = 0$.
- Scan over κ_{HWW}: under the assumption of a mixing between a CP-even SM Higgs boson and a CP-even BSM Higgs boson. The mixing parameter is defined as $\tilde{\kappa}_{\mathrm{HWW}}/\kappa_{\mathrm{SM}}$, where $\tilde{\kappa}_{\mathrm{HWW}} = (1/4)\cdot(v/\Lambda)\cdot\kappa_{\mathrm{HWW}}$ and the only variable term is κ_{HWW} (corresponding to variations of $\tilde{\kappa}_{\mathrm{HWW}}/\kappa_{\mathrm{SM}}$ between -2.5 and 2.5). For larger values of this ratio, the kinematic distributions of the final-state particles asymptotically tend to the ones obtained in presence of a pure CP-even BSM Higgs boson. The latter is used as the last point of the scan. The other parameters are set as follows: $\kappa_{\mathrm{SM}} = 1$, $\kappa_{\mathrm{AWW}} = 0$, $c_\alpha = 1$.

In the case of CP-mixing, only one MC sample is generated (see Sect. 3), and all other samples are obtained from it by reweighting the events on the basis of the matrix element amplitudes derived from Eq. (2). The precision of this procedure is verified to be better than the percent level. The mixing parameters used to produce this sample are chosen such that the kinematic phase space for all CP-mixing scenarios considered here was fully populated, and the values of the parameters are: $\kappa_{\mathrm{SM}} = 1$, $\kappa_{\mathrm{AWW}} = 2$, $\kappa_{\mathrm{HWW}} = 2$, $c_\alpha = 0.3$.

In addition, it is interesting to study the case where the SM, the BSM CP-even and the CP-odd Higgs bosons all mix. Unfortunately, in the $H \to WW^*$ channel, the present data sample size limits the possibility to constrain such a scenario, which would imply a simultaneous scan of two parameters $\tan\alpha$ and κ_{HWW}. In particular this is due to the lack of sensitivity in the κ_{HWW} scan, consequently, as already stated, both the two and the three parameter scans, including in addition the derivative operators, are not pursued further. These studies are envisaged for the future.

3 ATLAS detector, data and MC simulation samples

This section describes the ATLAS detector, along with the data and MC simulation samples used for this analysis.

3.1 The ATLAS detector

The ATLAS detector [17] is a multipurpose particle detector with approximately forward-backward symmetric cylindrical geometry and a near 4π coverage in solid angle.[3]

[3] The experiment uses a right-handed coordinate system with the origin at the nominal pp interaction point at the centre of the detector. The positive x-axis is defined by the direction from the origin to the centre of the LHC ring, the positive y-axis points upwards, and the z-axis

The inner tracking detector (ID) consists of a silicon-pixel detector, which is closest to the interaction point, a silicon-strip detector surrounding the pixel detector, both covering up to $|\eta| = 2.5$, and an outer transition–radiation straw-tube tracker (TRT) covering $|\eta| < 2$. The ID is surrounded by a thin superconducting solenoid providing a 2 T axial magnetic field.

A highly segmented lead/liquid-argon (LAr) sampling electromagnetic calorimeter measures the energy and the position of electromagnetic showers over $|\eta| < 3.2$. The LAr calorimeter includes a presampler (for $|\eta| < 1.8$) and three sampling layers, longitudinal in shower depth, up to $|\eta| < 2.5$. LAr sampling calorimeters are also used to measure hadronic showers in the end-cap ($1.5 < |\eta| < 3.2$) and both the electromagnetic and hadronic showers in the forward ($3.1 < |\eta| < 4.9$) regions, while an iron/scintillator tile sampling calorimeter measures hadronic showers in the central region ($|\eta| < 1.7$).

The muon spectrometer (MS) surrounds the calorimeters and is designed to detect muons in the pseudorapidity range $|\eta| < 2.7$. The MS consists of one barrel ($|\eta| < 1.05$) and two end-cap regions. A system of three large superconducting air-core toroid magnets provides a magnetic field with a bending integral of about 2.5 T·m (6 T·m) in the barrel (end-cap) region. Monitored drift-tube chambers in both the barrel and end-cap regions and cathode strip chambers covering $2.0 < |\eta| < 2.7$ are used as precision measurement chambers, whereas resistive plate chambers in the barrel and thin gap chambers in the end-caps are used as trigger chambers, covering up to $|\eta| = 2.4$.

A three-level trigger system selects events to be recorded for offline analysis. The first-level trigger is hardware-based, while the higher-level triggers are software-based.

3.2 Data and Monte Carlo simulation samples

The data and MC simulation samples used in this analysis are a subset of those used in Ref. [9] with the exception of the specific spin/CP signal samples produced for this paper.

The data were recorded by the ATLAS detector during the 2012 LHC run with proton–proton collisions at a centre-of-mass energy of 8 TeV, and correspond to an integrated luminosity of 20.3 fb^{-1}. This analysis uses events selected by triggers that required either a single high-p_{T} lepton or two leptons. Data quality requirements are applied to reject events recorded when the relevant detector components were not operating correctly.

Dedicated MC samples are generated to evaluate all but the W+jets and multi-jet backgrounds, which are estimated using data as discussed in Sect. 5. Most samples use the POWHEG [18] generator, which includes corrections at next-to-leading order (NLO) in α_{S} for the processes of interest. In cases where higher parton multiplicities are important, ALPGEN [19] or SHERPA [20] provide merged calculations at tree level for up to five additional partons. In a few cases, only leading-order generators (such as ACERMC [21] or GG2VV [22]) are available. Table 1 shows the event generator and production cross-section times branching fraction used for each of the signal and background processes considered in this analysis.

The matrix-element-level Monte Carlo calculations are matched to a model of the parton shower, underlying event and hadronisation, using either PYTHIA6 [23], PYTHIA8 [24], HERWIG [25] (with the underlying event modelled by JIMMY [26]), or SHERPA. Input parton distribution functions (PDFs) are taken from CT10 [27] for the POWHEG and SHERPA samples and CTEQ6L1 [28] for the ALPGEN + HERWIG and ACERMC samples. The Drell–Yan (DY) sample (Z/γ^*+jets) is reweighted to the MRST PDF set [29].

The effects of the underlying event and of additional minimum-bias interactions occurring in the same or neighbouring bunch crossings, referred to as pile-up in the following, are modelled with PYTHIA8, and the ATLAS detector response is simulated [30] using either GEANT4 [31] or GEANT4 combined with a parametrised GEANT4-based calorimeter simulation [32].

For the signal, the ggF production mode for the $H \to WW^*$ signal is modelled with POWHEG + PYTHIA8 [33,34] at $m_{\mathrm{H}} = 125$GeV for the SM Higgs-boson signal in the spin-2 analysis, whereas MADGRAPH5_AMC@NLO [5] is used for the CP analysis. The $H + 0, 1, 2$ partons samples are generated with LO accuracy, and subsequently showered with PYTHIA6. For the BSM signal, the MADGRAPH5_aMC@NLO generator is used in all cases. For the CP analysis, all samples (SM and BSM) are obtained by using the matrix-element reweighting method applied to a CP-mixed sample, as mentioned in Sect. 2.2.1, to provide a description of different CP-mixing configurations. The PDF set used is CTEQ6L1. To improve the modelling of the SM Higgs-boson p_{T}, a reweighting scheme is applied that reproduces the prediction of the next-to-next-to-leading-order (NNLO) and next-to-next-to-leading-logarithms (NNLL) dynamic-scale calculation given by the HRES2.1 program [35,36]. The BSM spin-0 Higgs-boson p_{T} is reweighted to the same distribution.

Cross-sections are calculated for the dominant diboson and top-quark processes as follows: the inclusive WW cross-section is calculated to NLO with MCFM [37]; non-

Footnote 3 continued
is along the beam direction. Cylindrical coordinates (r, ϕ) are used in the plane transverse to the beam, with ϕ the azimuthal angle around the beam axis. Transverse components of vectors are indicated by the subscript T. The pseudorapidity is defined in terms of the polar angle θ as $\eta = -\ln\tan(\theta/2)$. The angular distance between two objects is defined as $\Delta R = \sqrt{(\Delta\eta)^2 + (\Delta\phi)^2}$.

Table 1 Monte Carlo samples used to model the signal and background processes. The corresponding cross-sections times branching fractions, $\sigma \cdot \mathcal{B}$, are quoted at $\sqrt{s} = 8$TeV. The branching fractions include the decays $t \to Wb$, $W \to \ell\nu$, and $Z \to \ell\ell$ (except for the process $ZZ \to \ell\ell\,\nu\nu$). Here ℓ refers to e, μ, or τ. The neutral current $Z/\gamma^* \to \ell\ell$ process is denoted Z or γ^*, depending on the mass of the produced lepton pair. The parameters κ_g, κ_q are defined in Sect. 2.1.1, while $\kappa_{\rm SM}$, $\kappa_{\rm HWW}$, $\kappa_{\rm AWW}$, c_α are defined in Sect. 2.2.1

Process	MC generator	Filter	$\sigma \cdot \mathcal{B}$(pb)
Signal samples used in $J^P = 2^+$ analysis			
SM $H \to WW^*$	POWHEG + PYTHIA8		0.435
$\kappa_g = \kappa_q$	MADGRAPH5_aMC@NLO + PYTHIA6		–
$\kappa_g = 1, \kappa_q = 0$	MADGRAPH5_aMC@NLO + PYTHIA6		–
$\kappa_g = 0.5, \kappa_q = 1$	MADGRAPH5_aMC@NLO + PYTHIA6		–
Signal samples used in CP-mixing analysis			
$c_\alpha = 0.3, \kappa_{\rm SM} = 1$	MADGRAPH5_aMC@NLO + PYTHIA6		–
$\kappa_{\rm HWW} = 2, \kappa_{\rm AWW} = 2$			
Background samples			
WW			
$q\bar{q} \to WW$ and $qg \to WW$	POWHEG + PYTHIA6		5.68
$gg \to WW$	GG2VV + HERWIG		0.196
Top quarks			
$t\bar{t}$	POWHEG + PYTHIA6		26.6
Wt	POWHEG + PYTHIA6		2.35
$tq\bar{b}$	ACERMC + PYTHIA6		28.4
$t\bar{b}$	POWHEG + PYTHIA6		1.82
Other dibosons (VV)			
$W\gamma$	ALPGEN + HERWIG	$p_{\rm T}^{\gamma} > 8$ GeV	369
$W\gamma^*$	SHERPA	$m_{\ell\ell} \leq 7$ GeV	12.2
WZ	POWHEG + PYTHIA8	$m_{\ell\ell} > 7$ GeV	12.7
$Z\gamma$	SHERPA	$p_{\rm T}^{\gamma} > 8$ GeV	163
$Z\gamma^*$	SHERPA	min. $m_{\ell\ell} \leq 4$ GeV	7.31
ZZ	POWHEG + PYTHIA8	$m_{\ell\ell} > 4$ GeV	0.733
$ZZ \to \ell\ell\,\nu\nu$	POWHEG + PYTHIA8	$m_{\ell\ell} > 4$ GeV	0.504
Drell –Yan			
Z/γ^*	ALPGEN + HERWIG	$m_{\ell\ell} > 10$ GeV	16500

resonant gluon fusion is calculated and modelled to LO in $\alpha_{\rm S}$ with GG2VV, including both WW and ZZ production and their interference; $t\bar{t}$ production is normalised to the calculation at NNLO in $\alpha_{\rm S}$, with resummation of higher-order terms to NNLL accuracy, evaluated with TOP++2.0 [38]; single-top-quark processes are normalised to NNLL, following the calculations from Refs. [39,40] and [41] for the s-channel, t-channel, and Wt processes, respectively.

The WW background and the dominant backgrounds involving top-quark production ($t\bar{t}$ and Wt) are modelled using the POWHEG + PYTHIA6 event generator [42–45]. For WW, WZ, and ZZ production via non-resonant vector boson scattering, the SHERPA generator provides the LO cross-section and is used for event modelling. The negligible vector-boson-scattering (VBS) ZZ process is not shown in Table 1 but is included in the background modelling for completeness. The process $W\gamma^*$ is defined as associated $W+Z/\gamma^*$ production, containing an opposite-charge same-flavour lepton pair with invariant mass $m_{\ell\ell}$ less than 7 GeV. This process is modelled using SHERPA with up to one additional parton. The range $m_{\ell\ell} > 7$ GeV is simulated with POWHEG + PYTHIA8 and normalised to the POWHEG cross-section. The use of SHERPA for $W\gamma^*$ is due to the inability of POWHEG + PYTHIA8 to model invariant masses down to the production threshold. The SHERPA sample requires two leptons with $p_{\rm T} > 5$ GeV and $|\eta| < 3$. The jet multiplicity is corrected using a SHERPA sample generated with $0.5 < m_{\ell\ell} < 7$ GeV and up to two additional partons, while the total cross-section is corrected using the ratio of the MCFM NLO to SHERPA LO calculations in the same restricted mass range. A similar procedure is used to model $Z\gamma^*$, defined as Z/γ^* pair production with one same-flavour opposite-charge lepton pair having $m_{\ell\ell} \leq 4$ GeV and the other having $m_{\ell\ell} > 4$ GeV.

The $W\gamma$ and DY processes are modelled using ALPGEN + HERWIG with merged tree-level calculations of up to five jets. The merged samples are normalised to the NLO calculation of MCFM (for $W\gamma$) or the NNLO calculation of DYNNLO [46] (for DY). The $W\gamma$ sample is generated with the requirements $p_{\mathrm{T}}^{\gamma} > 8\,\mathrm{GeV}$ and $\Delta R(\gamma, \ell) > 0.25$.

A SHERPA sample is used to accurately model the $Z(\rightarrow \ell\ell)\gamma$ background. The photon is required to have $p_{\mathrm{T}}^{\gamma} > 8\,\mathrm{GeV}$ and $\Delta R(\gamma, \ell) > 0.1$; the lepton pair must satisfy $m_{\ell\ell} > 10\,\mathrm{GeV}$. The cross-section is normalised to NLO using MCFM. Events are removed from the ALPGEN + HERWIG DY samples if they overlap with the kinematics defining the SHERPA $Z(\rightarrow \ell\ell)\gamma$ sample.

4 Event selection

The object reconstruction in terms of leptons, jets, and missing transverse momentum, as well as the lepton identification and isolation criteria, which were optimised to minimise the impact of the background from misidentified isolated prompt leptons, are the same as described in detail in Ref. [9]: these aspects are therefore not discussed in this paper. The selection criteria and the analysis methodology used for the spin/CP studies described here are different however, since they are motivated not only by the need to distinguish the background processes from the Higgs-boson signal, but also by the requirement to optimise the separation power between different signal hypotheses. Thus, several selection requirements used in Ref. [9] are loosened or removed in the selection described below.

This section is organised in four parts. First, the event preselection is described, followed by the discussion of the spin- and parity-sensitive variables. These variables motivate the choice of topological selection requirements in the 0-jet and 1-jet categories described in the last two sections. All selection criteria are summarised in Table 2 and the corresponding expected and observed event yields are presented in Table 3.

4.1 Event preselection

The $WW \rightarrow e\nu\mu\nu$ final state chosen for this analysis consists of $e\mu$ pairs, namely pairs of opposite-charge, different-flavour, identified and isolated prompt leptons. This choice is based on the expected better sensitivity of this channel compared to the same-flavour channel, which involves a large potential background from $Z/\gamma^{*} \rightarrow ee/\mu\mu$ processes. The preselection requirements are designed to reduce substantially the dominant background processes to the Higgs-boson signal (see Sect. 5) and can be summarised briefly as follows:

- The leading lepton is required to have $p_{\mathrm{T}} > 22$ GeV to match the trigger requirements.
- The subleading lepton is required to have $p_{\mathrm{T}} > 15$ GeV.
- The mass of the lepton pair is required to be above 10 GeV.
- The missing transverse momentum in the event is required to be $p_{\mathrm{T}}^{\mathrm{miss}} > 20$ GeV.
- The event must contain at most one jet with $p_{\mathrm{T}} > 25\,\mathrm{GeV}$ and $|\eta| < 4.5$. The jet p_{T} is required to be higher than 30 GeV in the forward region, $2.4 < |\eta| < 4.5$, to minimise the impact of pile-up.

Table 2 List of selection requirements in the signal region adopted for both the spin and CP analyses. The $p_{\mathrm{T}}^{\mathrm{H}}$ selection requirement (*) is applied to all samples when testing the spin-2 benchmarks with non-universal couplings

Variable	Requirements
Preselection	
N_{leptons}	Exactly 2 with $p_{\mathrm{T}} > 10$GeV, $e\mu$, opposite sign
$p_{\mathrm{T}}^{\ell_1}$	>22 GeV
$p_{\mathrm{T}}^{\ell_2}$	>15 GeV
$m_{\ell\ell}$	>10 GeV
$p_{\mathrm{T}}^{\mathrm{miss}}$	>20 GeV
0-jet selection	
$p_{\mathrm{T}}^{\ell\ell}$	>20 GeV
$m_{\ell\ell}$	<80 GeV
$\Delta\phi_{\ell\ell}$	<2.8
$p_{\mathrm{T}}^{\mathrm{H}}$	<125 or 300 GeV (*)
1-jet selection	
b-veto	No b-jets with $p_{\mathrm{T}} > 20$ GeV
$m_{\tau\tau}$	$< m_Z - 25$ GeV
m_{T}^{ℓ}	>50 GeV
$m_{\ell\ell}$	<80 GeV
$\Delta\phi_{\ell\ell}$	<2.8
m_{T}	<150 GeV
$p_{\mathrm{T}}^{\mathrm{H}}$	<125 or 300 GeV(*)

This analysis considers only $e\mu$ pairs in the 0-jet and 1-jet categories for the reasons explained in Sect. 1. Each category is analysed independently since they display rather different background compositions and signal-to-background ratios.

4.2 Spin- and CP-sensitive variables

The shapes of spin- and CP-sensitive variable distributions are discussed in this section for the preselected events.

Figures 2 and 3 show the variables used to discriminate different spin-2 signal hypotheses from the SM Higgs-boson hypothesis for the 0-jet and the 1-jet category, respectively. For both the 0-jet and the 1-jet categories, the most sensitive variables are $p_{\mathrm{T}}^{\ell\ell}$ (transverse momentum of the

Table 3 Expected event yields in the signal regions (SR) for the 0- and 1-jet categories (labelled as 0j and 1j, respectively). For the dominant backgrounds, the expected yields are normalised using the control regions defined in Sect. 5. The expected contributions from various processes are listed, namely the ggF SM Higgs-boson production (N_{ggF}), and the background contribution from WW (N_{WW}), top quark (top-quark pairs $N_{t\bar{t}}$, and single-top quark N_t), Drell–Yan Z/γ^* to $\tau\tau$ ($N_{\mathrm{DY},\tau\tau}$), misidentified leptons ($N_{W+\mathrm{jets}}$), $WZ/ZZ/W\gamma$ (N_{VV}) and Drell–Yan Z/γ^* to $ee/\mu\mu$ ($N_{\mathrm{DY,SF}}$). The total sum of the backgrounds (N_{bkg}) is also shown together with the data. Applying the $p_{\mathrm{T}}^{\mathrm{H}}$ requirement in the 0-jet category does not change substantially the event yields, while it has an effect in the 1-jet category, as expected. The errors on the ratios of the data over total background, N_{bkg}, only take into account the statistical uncertainties on the observed and expected yields

	N_{ggF}	N_{WW}	$N_{t\bar{t}}$	N_t	$N_{\mathrm{DY},\tau\tau}$	$N_{W+\mathrm{jets}}$	N_{VV}	$N_{\mathrm{DY,SF}}$	N_{bkg}	Data	Data/N_{bkg}
0j SR	218	2796	235	135	515	366	311	32	4390	4730	1.08 ± 0.02
1j SR	77	555	267	103	228	123	131	5.8	1413	1569	1.11 ± 0.03
1j SR: $p_{\mathrm{T}}^{\mathrm{H}} < 300$ GeV	77	553	267	103	228	123	131	5.8	1411	1567	1.11 ± 0.03
1j SR: $p_{\mathrm{T}}^{\mathrm{H}} < 125$ GeV	76	530	259	101	224	121	128	5.8	1367	1511	1.11 ± 0.03

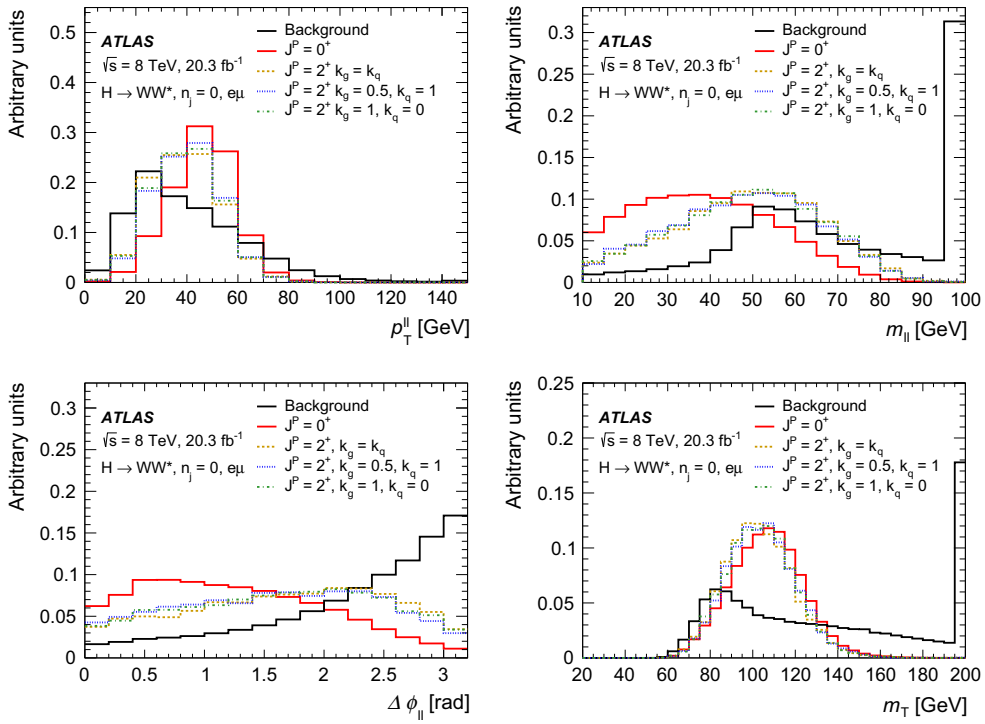

Fig. 2 Expected normalised Higgs-boson distributions of the transverse momentum of the dilepton system $p_{\mathrm{T}}^{\ell\ell}$, the dilepton mass $m_{\ell\ell}$, the azimuthal angular difference between the leptons $\Delta\phi_{\ell\ell}$ and and the transverse mass m_{T} for the $e\mu$+0-jet category. The distributions are shown for the SM signal hypothesis (*solid red line*) and for three spin-2 hypotheses, namely $J^P = 2^+$, $\kappa_g = 0.5$, $\kappa_q = 1$ (*dashed yellow line*), $J^P = 2^+$, $\kappa_g = 1$, $\kappa_q = 0$ (*blue dashed line*) and $J^P = 2^+$, $\kappa_g = \kappa_q$ (*green dashed line*). The expected shapes for the sum of all backgrounds, including the data-derived W+jets background, is also shown (*solid black line*). The *last bin* in each plot includes the overflow

dilepton system), $m_{\ell\ell}$, $\Delta\phi_{\ell\ell}$ (ϕ angle between the two leptons) and m_{T} (transverse mass of the dilepton and missing momentum system). These variables are the same as those used for the spin-2 analysis in the previous publication [3].

Similarly, Figs. 4 and 5 show the the variables that best discriminate between an SM Higgs boson and a BSM CP-even or CP-odd signal, respectively. The BSM CP-even variables are the same as those used in the spin-2 analysis, apart from the $p_{\mathrm{T}}^{\mathrm{miss}}$ variable which is substituted for m_{T}. The variables for the CP-odd analysis are $m_{\ell\ell}$, $E_{\ell\ell\nu\nu}$, Δp_{T}, $\Delta\phi_{\ell\ell}$, where $E_{\ell\ell\nu\nu} = p_{\mathrm{T}}^{\ell_1} - 0.5p_{\mathrm{T}}^{\ell_2} + 0.5p_{\mathrm{T}}^{\mathrm{miss}}$, $p_{\mathrm{T}}^{\ell_1}$ and $p_{\mathrm{T}}^{\ell_2}$ are respectively the transverse momenta of the leading and subleading leptons, and Δp_{T} is the absolute value of their difference.

The CP-mixing analysis studies both the positive and negative values of the mixing parameter, as explained in Sect. 2.2.2. In the BSM CP-even benchmark scan, for negative values of the mixing parameter, interference between the SM and BSM CP-even Higgs-boson couplings causes a cancellation that drastically changes the shape of the

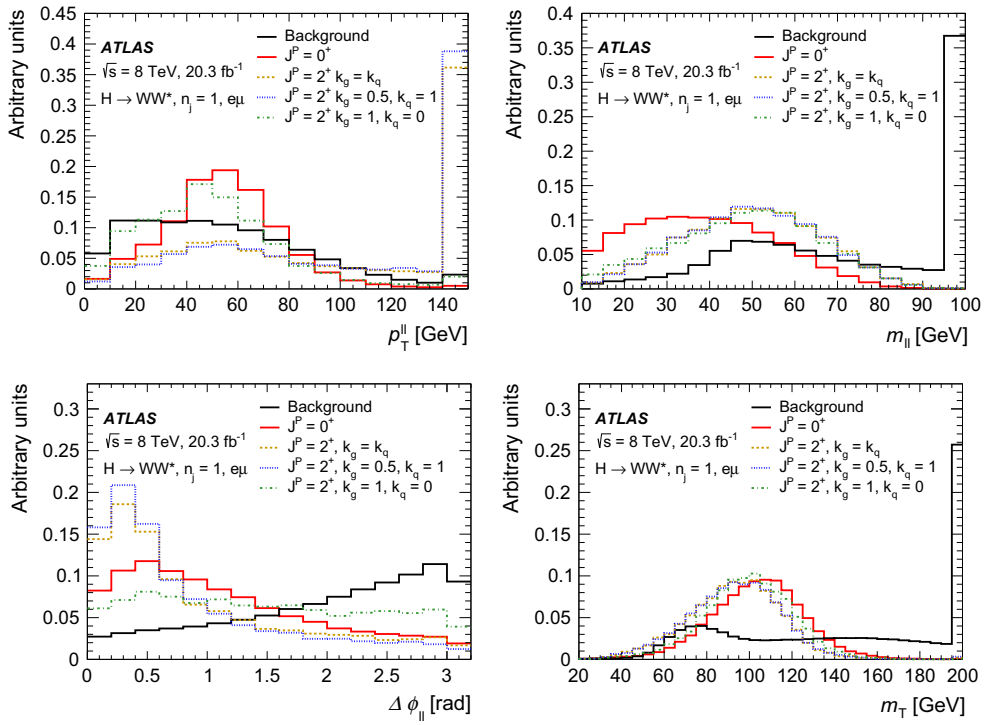

Fig. 3 Expected normalised Higgs-boson distributions of $p_{\mathrm{T}}^{\ell\ell}$, $m_{\ell\ell}$, $\Delta\phi_{\ell\ell}$ and m_{T} for the $e\mu$+1-jet category. The distributions are shown for the SM signal hypothesis (*solid red line*) and for three spin-2 hypotheses, namely $J^P = 2^+, \kappa_g = 0.5, \kappa_q = 1$ (*dashed yellow line*), $J^P = 2^+$, $\kappa_g = 1, \kappa_q = 0$ (*blue dashed line*) and $J^P = 2^+, \kappa_g = \kappa_q$ (*green dashed line*). The expected shapes for the sum of all backgrounds, including the data-derived W+jets background, is also shown (*solid black line*). The *last bin* in each plot includes the overflow

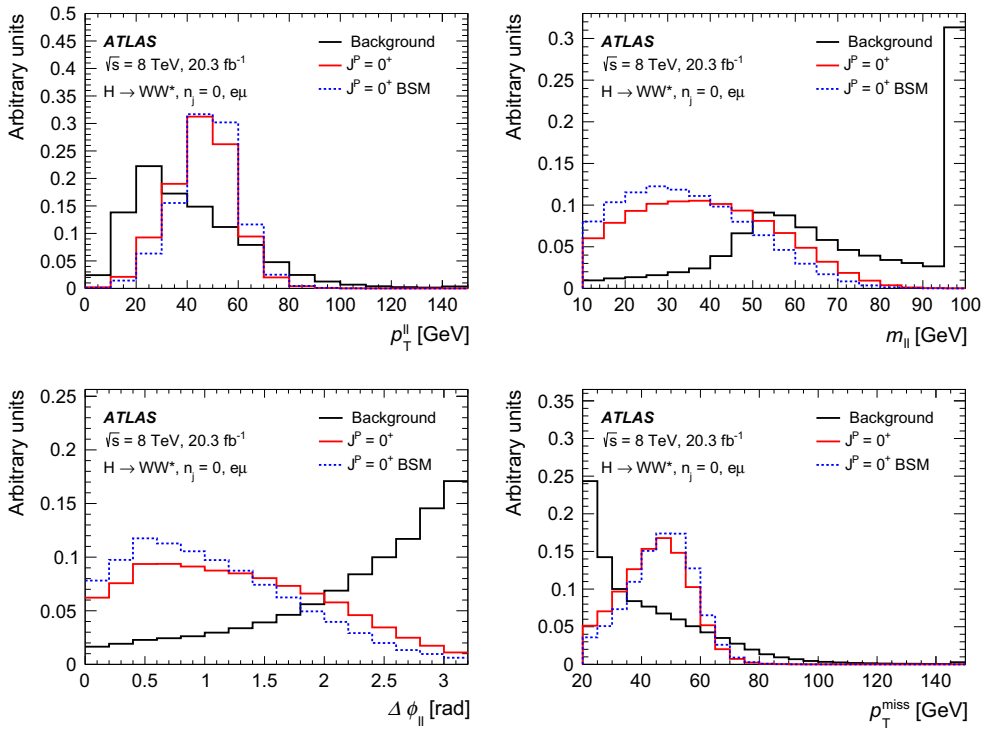

Fig. 4 Expected normalised Higgs-boson distributions of $p_{\mathrm{T}}^{\ell\ell}$, $m_{\ell\ell}$, $\Delta\phi_{\ell\ell}$ and the missing transverse momentum $p_{\mathrm{T}}^{\mathrm{miss}}$ for the $e\mu$+0-jet category. The distributions are shown for the SM signal hypothesis (*solid red line*) and for the BSM CP-even signal (*dashed line*). The expected shapes for the sum of all backgrounds, including the data-derived W+jets background, is also shown (*solid black line*). The *last bin* in each plot includes the overflow

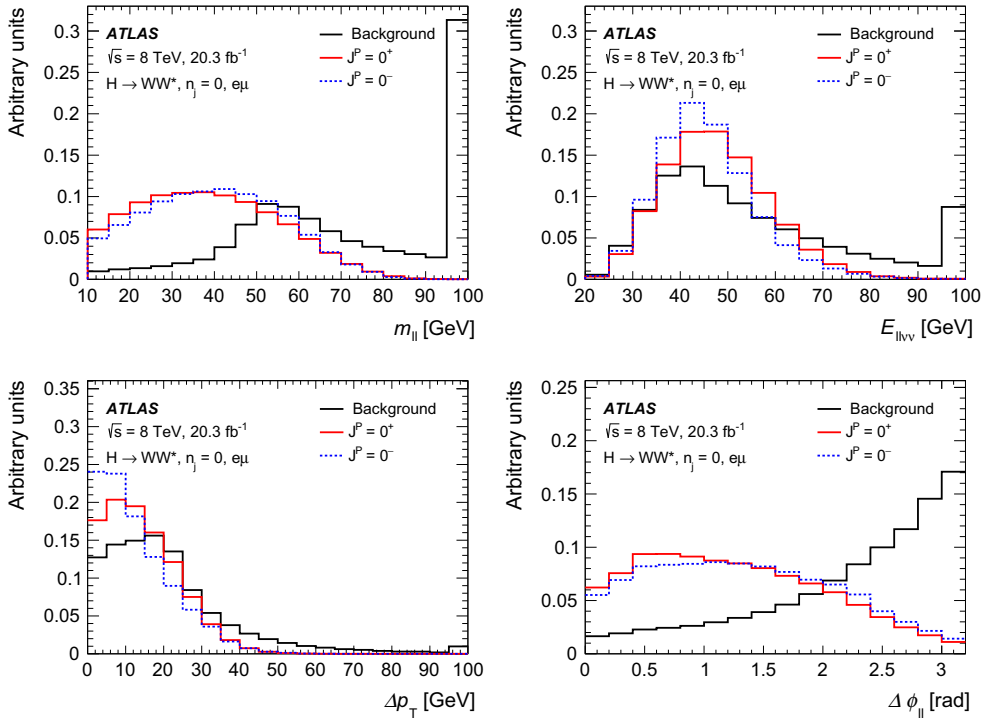

Fig. 5 Expected normalised Higgs-boson distributions of $m_{\ell\ell}$, the $E_{\ell\ell\nu\nu}$ variable defined in Sect. 4.2, the difference between the transverse momenta of the leading and subleading leptons Δp_{T} and $\Delta\phi_{\ell\ell}$ for the $e\mu$+0-jet category. The distributions are shown for the SM signal hypothesis (*solid red line*) and for the BSM CP-odd signal (*dashed line*). The expected shapes for the sum of all backgrounds, including the data-derived W+jets background, is also shown (*solid black line*). The *last bin* in each plot includes the overflow

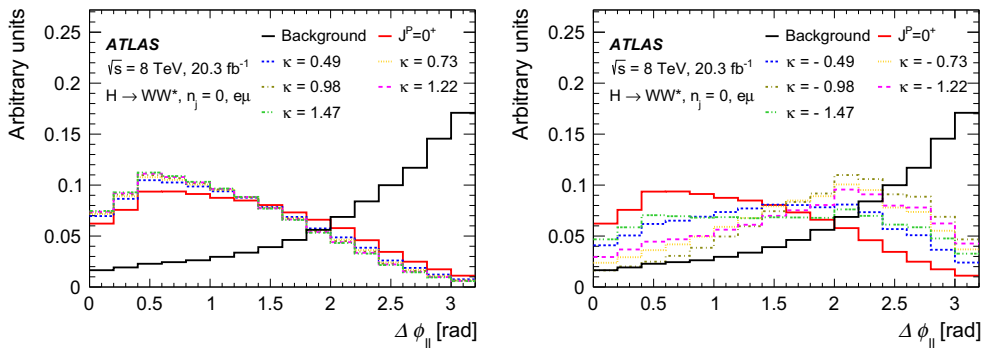

Fig. 6 Expected normalised Higgs-boson distributions of $\Delta\phi_{\ell\ell}$ for the $e\mu$+0-jet category. The distributions are shown for the SM signal hypothesis (*solid red line*) and for different mixing hypotheses of the SM Higgs and CP-even BSM Higgs bosons, corresponding to positive (*left*) and negative (*right*) values of the mixing parameter $\tilde{\kappa}_{HWW}/\kappa_{\mathrm{SM}}$ (abbreviated to κ in the legend). The expected shapes for the sum of all backgrounds, including the data-derived W+jets background, is also shown (*solid black line*). The *last bin* in each plot includes the overflow

discriminating variable distributions. As an example, Fig. 6 shows the distribution of $\Delta\phi_{\ell\ell}$ for the SM Higgs boson together with the distributions for several different values of the CP-mixing parameter.

While for positive values of $\tilde{\kappa}_{\mathrm{HWW}}/\kappa_{\mathrm{SM}}$ (Fig. 6, left) and for the SM Higgs-boson hypothesis, the $\Delta\phi_{\ell\ell}$ distribution peaks towards low values, when reaching the maximum of the interference (at about $\tilde{\kappa}_{\mathrm{HWW}}/\kappa_{\mathrm{SM}} \sim -1$), the mean of the $\Delta\phi_{\ell\ell}$ distribution slowly moves towards higher values. This significantly improves the separation power between the SM and the BSM CP-even Higgs-boson hypotheses (Fig. 6, right). For values of $\tilde{\kappa}_{\mathrm{HWW}}/\kappa_{\mathrm{SM}} < -1$, the peak of distribution gradually moves back to low values of $\Delta\phi_{\ell\ell}$, as in the case of the SM Higgs-boson hypothesis. The sum of the backgrounds is also shown on the same figure. The other CP-sensitive variables exhibit a similar behaviour in this specific region of parameter space. The impact of this feature on the results is discussed in Sect. 9.3.

4.3 Event selection in the 0-jet and 1-jet categories

Table 2 summarises the preselection requirements discussed in Sect. 4.1, together with the selections applied specifically to the 0-jet and 1-jet categories. These selection requirements are optimised in terms of sensitivity for the different spin and CP hypotheses studied while maintaining the required rejection against the dominant backgrounds. In general, they are looser than those described in Ref. [9], which were optimised for the SM Higgs boson.

Some of these looser selection requirements are applied to both the 0-jet and 1-jet categories:

- The mass of the lepton pair, $m_{\ell\ell}$, must satisfy $m_{\ell\ell} < 80$ GeV, a selection which strongly reduces the dominant WW continuum background.
- The azimuthal angle, $\Delta\phi_{\ell\ell}$, between the two leptons, must satisfy $\Delta\phi_{\ell\ell} < 2.8$.

Events in the 0-jet category are required to also satisfy $p_{\mathrm{T}}^{\ell\ell} > 20$ GeV, while events in the 1-jet category, which suffer potentially from a much larger background from top-quark production, must also satisfy the following requirements:

- No b-tagged jet [47] $p_{\mathrm{T}} > 20$ GeV is present in the event.
- Using the direction of the missing transverse momentum a τ-lepton pair can be reconstructed with a mass $m_{\tau\tau}$ by applying the collinear approximation [48]; $m_{\tau\tau}$ is required to pass the $m_{\tau\tau} < m_Z - 25$ GeV requirement to reject $Z/\gamma^* \to \tau\tau$ events.
- The transverse mass, m_{T}^{ℓ}, chosen to be the largest transverse mass of single leptons defined as $m_{\mathrm{T}}^{\ell_{\mathrm{i}}} = \sqrt{2 p_{\mathrm{T}}^{\ell_{\mathrm{i}}} p_{\mathrm{T}}^{\mathrm{miss}} (1 - \cos\Delta\phi)}$, where $\Delta\phi$ is the angle between the lepton transverse momentum and $p_{\mathrm{T}}^{\mathrm{miss}}$, is required to satisfy $m_{\mathrm{T}}^{\ell} > 50$ GeV to reject the W+jets background.
- The total transverse mass of the dilepton and missing transverse momentum system, m_{T}, is required to satisfy $m_{\mathrm{T}} < 150$ GeV.

For alternative spin-2 benchmarks with non-universal couplings, as listed in Sect. 2.1.2, an additional requirement on the reconstructed Higgs-boson transverse momentum $p_{\mathrm{T}}^{\mathrm{H}}$ is applied in the signal and control regions for all MC samples and data. The $p_{\mathrm{T}}^{\mathrm{H}}$ variable is reconstructed as the transverse component of the vector sum of the four-momenta of both leptons and the missing transverse energy.

Table 3 shows the number of events for data, expected SM signal and the various background components after event selection. The background estimation methods are described in detail in Sect. 5. Good agreement is seen between the observed numbers of events in each of the two categories and the sum of the total background and the expected signal from an SM Higgs boson. The 0-jet category is the most sensitive one with almost three times larger yields than the 1-jet category. As expected, however, the requirements on $p_{\mathrm{T}}^{\mathrm{H}}$ affect mostly the 1-jet category, which is sensitive to possible tails at high values of $p_{\mathrm{T}}^{\mathrm{H}}$, as explained in Sect. 2.1.2. Figures 7 and 8 show the distributions of discriminating variables used in the analysis after the full selection for the 0-jet and 1-jet categories, respectively. These figures show reasonable agreement between the data and the sum of all expected contributions, including that from the SM Higgs boson.

5 Backgrounds

The background contamination in the signal region (SR) is briefly discussed in the previous section. This section is dedicated to a more detailed description of backgrounds and their determination. The following physics processes relevant for this analysis are discussed:

- WW: non-resonant W-boson pair production;
- top quarks (labelled as Top): top-quark pair production ($t\bar{t}$) and single-top-quark production (t);
- misidentified leptons (labelled as W+jets): W-boson production, in association with a jet that is misidentified as a lepton, and dijet or multi-jet production with two misidentifications;
- Z/γ^* decay to $\tau\tau$ final states.

Other smaller backgrounds, such as non-WW dibosons ($W\gamma$, $W\gamma^*$, WZ and ZZ) labelled as VV in the following, as well as the very small $Z/\gamma^* \to ee$ or $\mu\mu$ contribution, are estimated directly from simulation with the appropriate theoretical input as discussed in Sect. 3.

The dominant background sources are normalised either using only data, as in the case of the W+jets background, or using data yields in an appropriate control region (CR) to normalise the MC predictions, as for WW, $Z/\gamma^* \to \tau\tau$ and top-quark backgrounds. The event selection in control regions is orthogonal to the signal region selection but as close as possible to reduce the extrapolation uncertainties from the CRs to the SR. The requirements that define these regions are listed in Table 4.

The control regions, for example the WW CR, are used to determine a normalisation factor, β, defined by the ratio of the observed to expected yields of WW candidates in the CR, where the observed yield is obtained by subtracting the non-WW contributions from the data. The estimate $B_{\mathrm{SR}}^{\mathrm{est}}$ for the background under consideration, in the SR, can be written as:

$$B_{\mathrm{SR}}^{\mathrm{est}} = B_{\mathrm{SR}} \cdot \underbrace{N_{\mathrm{CR}}/B_{\mathrm{CR}}}_{\text{Normalisation } \beta} = N_{\mathrm{CR}} \cdot \underbrace{B_{\mathrm{SR}}/B_{\mathrm{CR}}}_{\text{Extrapolation } \alpha}, \quad (3)$$

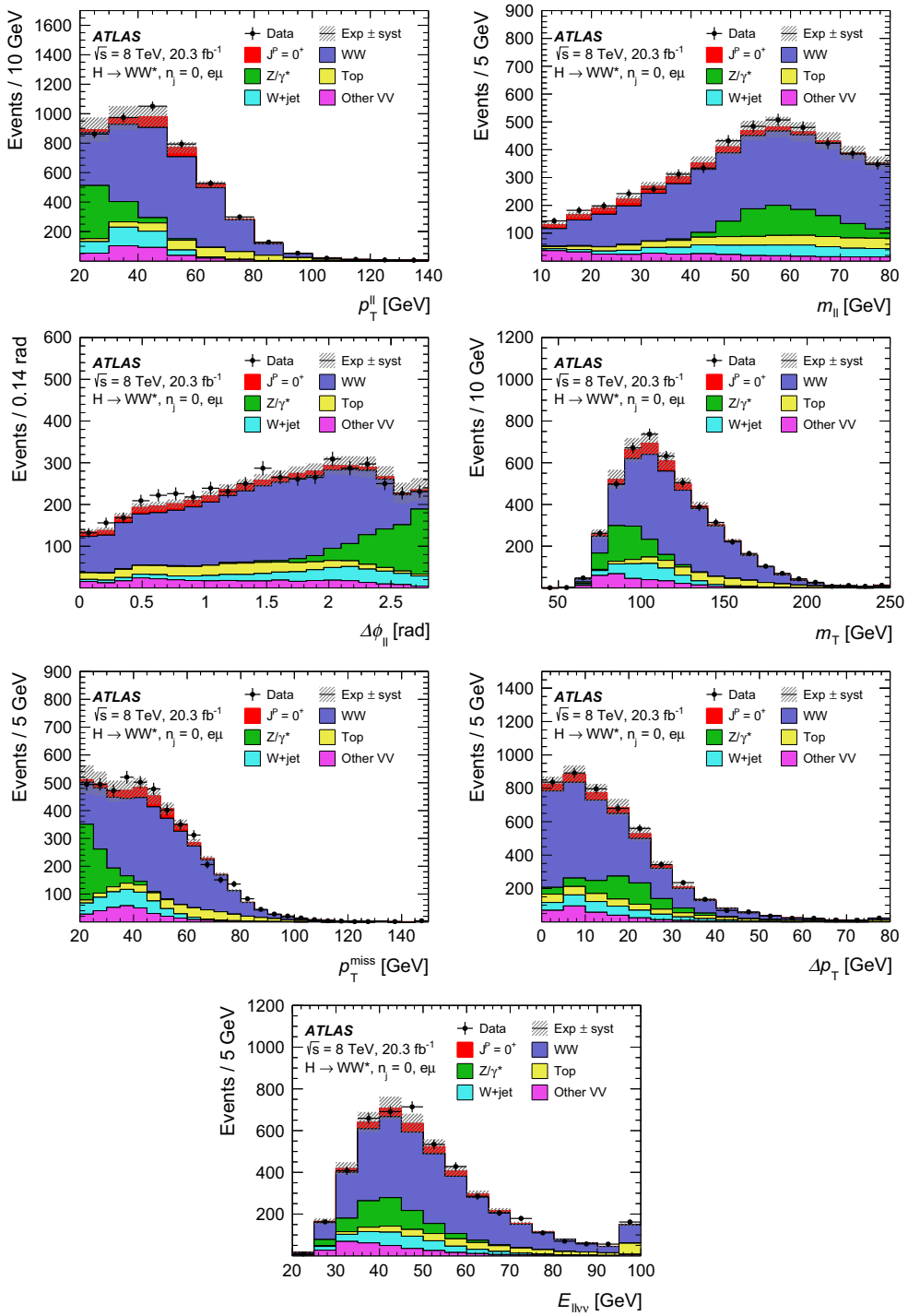

Fig. 7 Expected and observed distributions of $p_{\mathrm{T}}^{\ell\ell}$, $m_{\ell\ell}$, $\Delta\phi_{\ell\ell}$, m_{T}, $p_{\mathrm{T}}^{\mathrm{miss}}$, Δp_{T} and $E_{\ell\ell\nu\nu}$ for the 0-jet category. The *shaded band* represents the systematic uncertainties described in Sects. 5 and 8. The signal is shown assuming an SM Higgs boson with mass $m_H = 125$ GeV. The backgrounds are normalised using control regions defined in Sect. 5. The *last bin* in each plot includes the overflow

where N_{CR} and B_{CR} are the observed yield and the MC estimate in the CR, respectively, and B_{SR} is the MC estimate in the signal region. The parameter β defines the data-to-MC normalisation factor in the CR, while the parameter α defines the extrapolation factor from the CR to the SR predicted by the MC simulation. With enough events in the CR, the large theoretical uncertainties associated with estimating the background only from simulation are replaced by the

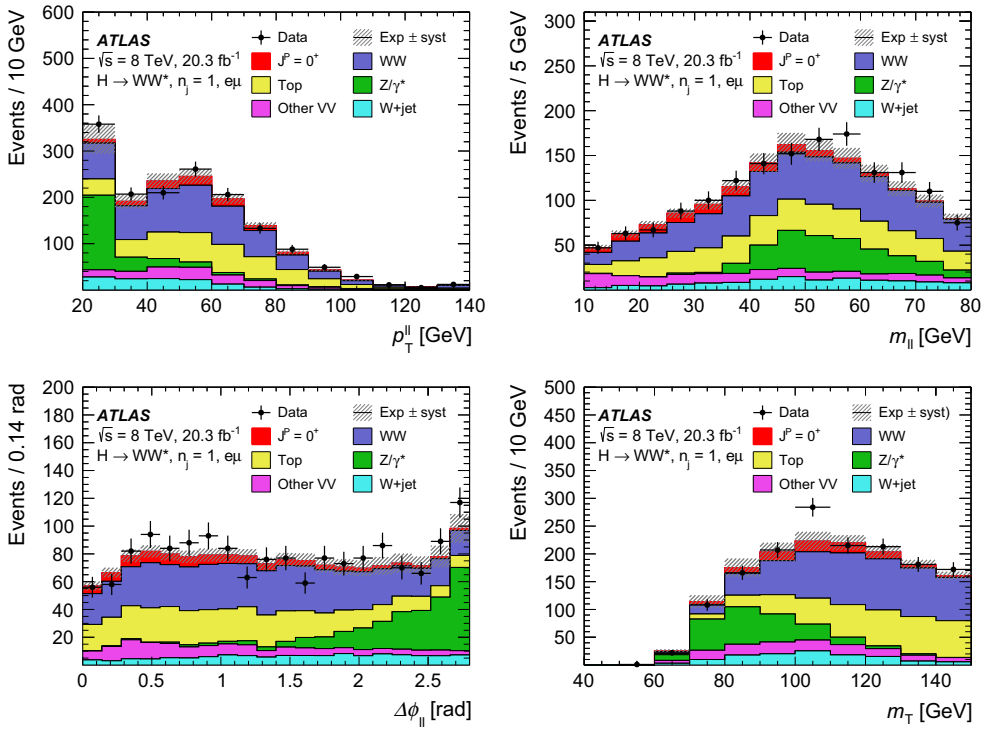

Fig. 8 Expected and observed distributions of $p_{\mathrm{T}}^{\ell\ell}$, $m_{\ell\ell}$, $\Delta\phi_{\ell\ell}$ and m_{T} for the 1-jet category. The *shaded band* represents the systematic uncertainties described in Sects. 5 and 8. The signal is shown assuming an SM Higgs boson with mass $m_H = 125$ GeV. The backgrounds are normalised using control regions defined in Sect. 5. The *last bin* in each plot includes the overflow

Table 4 List of selection criteria used to define the orthogonal control regions for WW, top-quark and $Z/\gamma^* \to \tau\tau$ backgrounds

Control region	Selection
WW CR 0-jet	Preselection, $p_{\mathrm{T}}^{\ell\ell} > 20$ GeV, $80 < m_{\ell\ell} < 150$ GeV
WW CR-1 jet	Preselection, b-veto, $m_{\tau\tau} < m_Z - 25$ GeV
	$m_{\mathrm{T}}^{\ell} > 50$ GeV, $m_{\ell\ell} > 80$ GeV
Top CR 0-jet	Preselection, $\Delta\phi_{\ell\ell} < 2.8$, all jets inclusive
Top CR 1-jet	At least one b-jet, $m_{\tau\tau} < m_Z - 25$ GeV
$Z/\gamma^* \to \tau\tau$ CR 0-jet	Preselection, $m_{\ell\ell} < 80$ GeV, $\Delta\phi_{\ell\ell} > 2.8$
$Z/\gamma^* \to \tau\tau$ CR 1-jet	Preselection, b-veto, $m_{\mathrm{T}}^{\ell} > 50$ GeV, $m_{\ell\ell} < 80$ GeV, $\lvert m_{\tau\tau} - m_Z \rvert < 25$ GeV

combination of two significantly smaller uncertainties: the statistical uncertainty on N_{CR} and the systematic uncertainty on α.

The extrapolation factor α has uncertainties which are common to all MC-simulation derived backgrounds:

- uncertainty due to higher perturbative orders in QCD not included in the MC simulation, evaluated by varying the renormalisation and factorisation scales by factors one-half and two;
- uncertainty due to the PDF choice, estimated by taking the largest difference between the nominal PDF set (e.g. CT10) and two alternative PDF sets (e.g. MSTW2008 [49] and NNPDF2.3 [50]), with the uncertainty determined from the error eigenvectors of the nominal PDF set added in quadrature;
- uncertainty due to modelling of the underlying event, hadronisation and parton shower (UE/PS), evaluated by comparing the predictions from the nominal and alternative parton shower models, e.g. PYTHIA and HERWIG.

The section is organised as follows. Section 5.1 describes the WW background – the dominant background in both the 0- and 1-jet categories. Section 5.2 describes the background from the top-quark production, the second largest background in the 1-jet category. The $Z/\gamma^* \to \tau^+\tau^-$ background

Table 5 Theoretical uncertainties (in %) on the extrapolation factor α for WW, top-quark and $Z/\gamma^* \to \tau\tau$ backgrounds. "Total" refers to the sum in quadrature of all uncertainties. The negative sign indicates anti-correlation with respect to the unsigned uncertainties for categories in the same column. The uncertainties on the top-quark background extrapolation factor in the 0-jet category are discussed in Sect. 5.2

Category	Scale	PDF	Gen	EW	UE/PS	p_{T}^{Z}	Total
WW background							
SR 0-jet	0.9	3.8	6.9	−0.8	−4.1	–	8.2
SR 1-jet	1.2	1.9	3.3	−2.1	−3.2	–	5.3
Top-quark background							
SR 1-jet	−0.8	−1.4	1.9	–	2.4	–	3.5
WW CR 1-jet	0.6	0.3	−2.4	–	2.0	–	3.2
$Z/\gamma^* \to \tau\tau$ background							
SR 0-jet	−7.1	1.3	–	–	−6.5	19	21.3
SR 1-jet	6.6	0.66	–	–	−4.2	–	7.9
WW CR 0-jet	−11.4	1.7	–	–	−8.3	16	21.4
WW CR 1-jet	−5.6	2.2	–	–	−4.8	–	7.7

is described in Sect. 5.3, while the data-derived estimate of the W+jets background is briefly described in Sect. 5.4. The extrapolation factor uncertainties are summarised in Table 5. More details can be found in Ref. [9].

5.1 Non-resonant W-boson pairs

Non-resonant W-boson pair production is the dominant (irreducible) background in this analysis. Only some of the kinematic properties allow resonant and non-resonant production to be distinguished. The WW background is normalised using a control region which differs from the signal region in having a different range of dilepton invariant mass, $m_{\ell\ell}$. The leptons from non-resonant WW production tend to have a larger opening angle than the resonant WW production. Furthermore, the Higgs-boson mass is lower than the mass of the system formed by the two W bosons. Thus, the non-resonant WW background is dominant at high $m_{\ell\ell}$ values.

The 0-jet WW control region is defined after applying the $p_{\mathrm{T}}^{\ell\ell}$ criterion by changing the $m_{\ell\ell}$ requirement to $80 < m_{\ell\ell} < 150$ GeV. The 1-jet WW control region is defined after the m_{T}^{ℓ} criterion by requiring $m_{\ell\ell} > 80$ GeV. The purity of the WW control region is expected to be 69 % in the 0-jet category and 43 % in the 1-jet category. Thus, the data-derived normalisation of the main non-WW backgrounds, the top-quark and Drell–Yan backgrounds, is applied in the WW CR as described in the following two subsections. Other small backgrounds are normalised using MC simulation. The CR normalisation is applied to the combined WW estimate independently of the production (qq, qg or gg) process. The $\Delta\phi_{\ell\ell}$ and $m_{\ell\ell}$ distributions in the WW control region are shown in Fig. 9 for the 0-jet and 1-jet final states.

Apart from the sources discussed in the previous section, the extrapolation factor α has uncertainties due to the generator choice, estimated by comparing the POWHEG + HERWIG and aMC@NLO + HERWIG generators, and due to higher-order electroweak corrections determined by reweighting the MC simulation to the NLO electroweak calculation. All uncertainties are summarised in Table 5.

5.2 Top quarks

The top-quark background is one of the largest backgrounds in this analysis. Top quarks can be produced in pairs ($t\bar{t}$) or individually in single-top processes in association with a W boson (Wt) or lighter quark(s) (single-t). The top-quark background normalisation from data is derived independently of the production process.

For the 0-jet category, the control region is defined by applying the preselection cuts including the missing transverse momentum threshold, with an additional requirement of $\Delta\phi_{\ell\ell} < 2.8$ to reduce the $Z/\gamma^* \to \tau\tau$ background. The top-quark background 0-jet CR is inclusive in the number of jets and has a purity of 74 %. The extrapolation parameter α is determined as described in Eq. (3). The value of α is corrected using data in a sample containing at least one b-tagged jet [9].

The resulting normalisation factor is 1.08 ± 0.02 (stat.). The total uncertainty on the normalisation factor is 8.1 %. The total uncertainty includes variations of the renormalisation and factorisation scales, PDF choice and parton shower model. Also the uncertainty on the $t\bar{t}$ and Wt production cross-sections and on the interference of these processes is included. An additional theoretical uncertainty is evaluated on the efficiency of the additional selection after the jet-veto requirement. Experimental uncertainties on the simulation-derived components are evaluated as well.

In the 1-jet category, the top-quark background is the second leading background, not only in the signal region

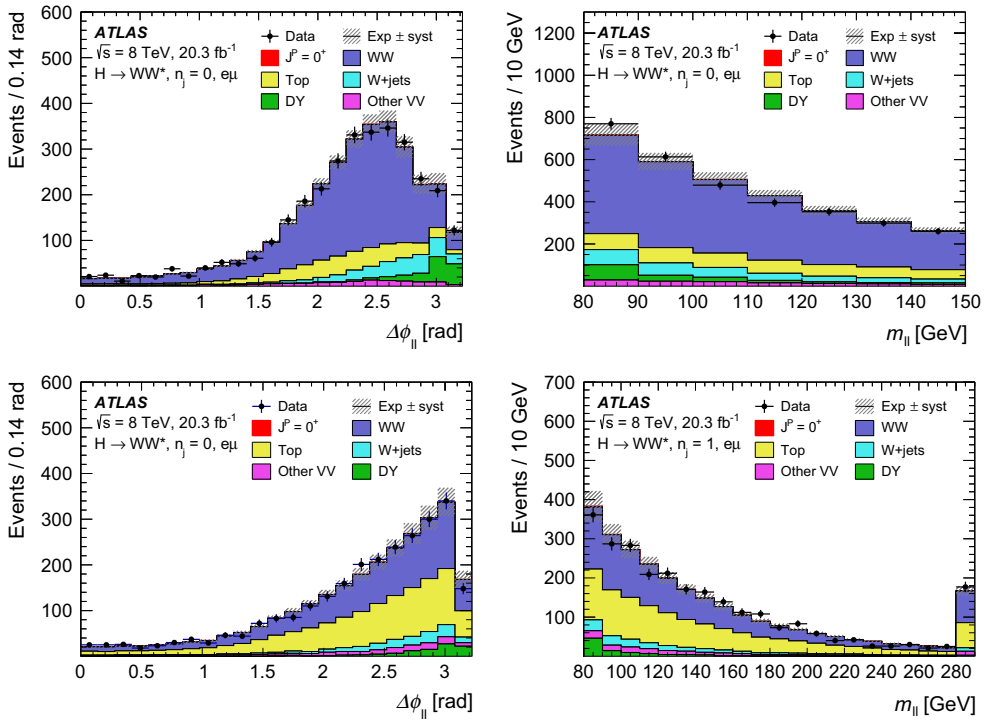

Fig. 9 The $\Delta\phi_{\ell\ell}$ and $m_{\ell\ell}$ distributions in the WW control region, for the 0-jet (*top*) and 1-jet (*bottom*) categories. The signal is shown assuming an SM Higgs boson with mass $m_H = 125$ GeV. The signal contamination is negligible for the SM as well as for the alternative hypotheses. The normalisation factors from the control regions described in Sect. 5 are applied. The *last bin* in each plot includes the overflow

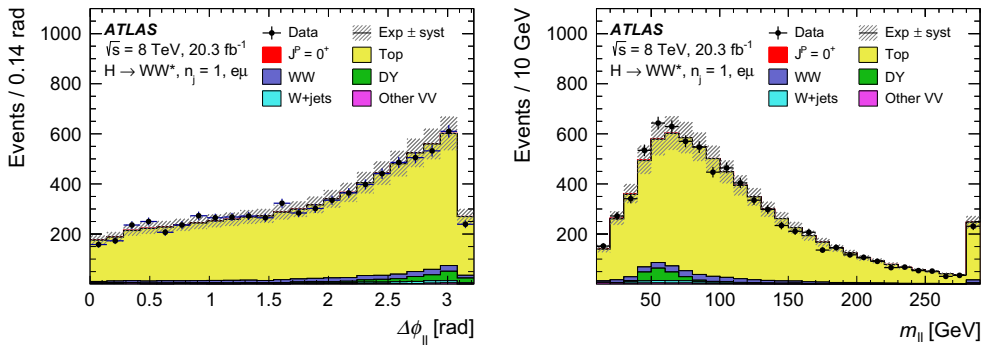

Fig. 10 The $\Delta\phi_{\ell\ell}$ and $m_{\ell\ell}$ distributions in the top-quark background control region for the 1-jet category. The signal is shown assuming an SM Higgs boson with mass $m_H = 125$ GeV. The signal contamination is negligible for the SM as well as for the alternative hypotheses. The normalisation factors from the control regions described in Sect. 5 are applied. The *last bin* in each plot includes the overflow

but also in the WW control region, where the contamination by this background is about 40 %. Thus two extrapolation parameters are defined: α_{SR} for the extrapolation to the signal region and α_{WW} for the extrapolation to the WW control region. The 1-jet top-quark background control region is defined after the preselection and requires the presence of exactly one jet, which must be b-tagged. Events with additional b-tagged jets with $20 < p_{\mathrm{T}} < 25$ GeV are vetoed, following the SR requirement. Selection criteria on m_{T}^{ℓ} and $m_{\tau\tau}$ veto are applied as well. The $\Delta\phi_{\ell\ell}$ and $m_{\ell\ell}$ distributions in the 1-jet CR are shown in Fig. 10.

The extrapolation uncertainty is estimated using the above mentioned sources of theoretical uncertainties and the additional uncertainties specific to the top-quark background: $t\bar{t}$ and single-top cross-sections and the interference between single and pair production of top quarks. A summary of the uncertainties is given in Table 5.

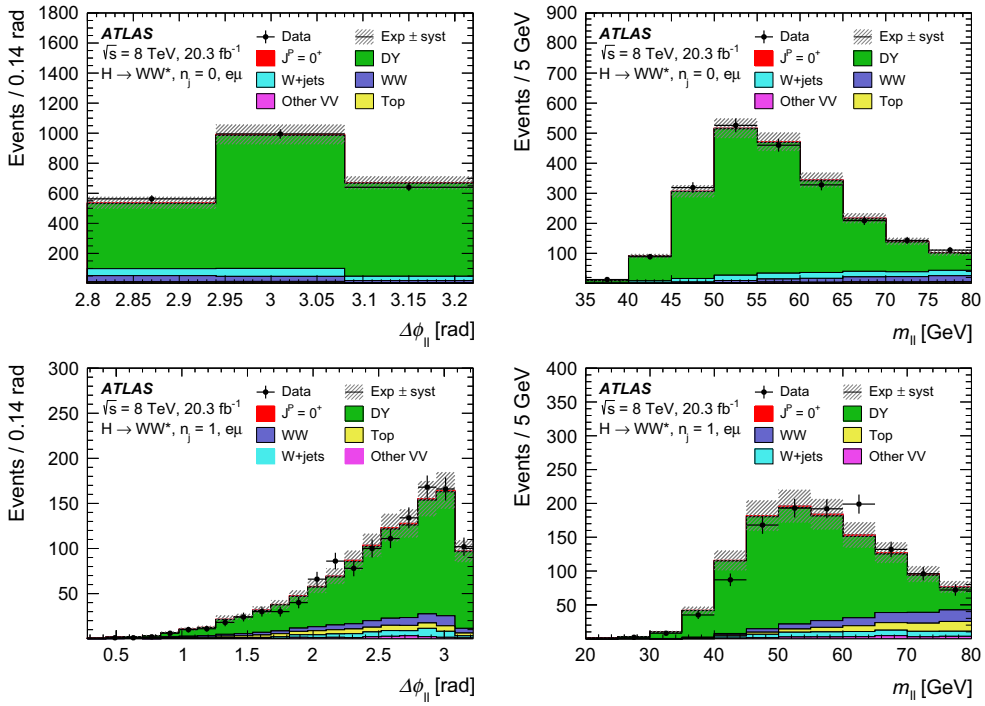

Fig. 11 The $\Delta\phi_{\ell\ell}$ and $m_{\ell\ell}$ distributions in the $Z/\gamma^* \to \tau\tau$ control region, for the 0-jet (*top*) and 1-jet (*bottom*) categories. The signal is shown assuming an SM Higgs boson with mass $m_H = 125$ GeV. The signal contamination is negligible for the SM as well as for the alternative hypotheses. The normalisation factors from the control regions described in Sect. 5 are applied

5.3 Drell–Yan

The Drell–Yan background is dominated by $Z/\gamma^* \to \tau\tau$ events with τ-leptons decaying leptonically. The $Z/\gamma^* \to \tau\tau$ 0-jet control region is defined by applying the preselection requirements, adding $m_{\ell\ell} < 80$ GeV and reversing the $\Delta\phi_{\ell\ell}$ criterion, $\Delta\phi_{\ell\ell} > 2.8$. The purity of this control region is expected to be 90 %. The $Z/\gamma^* \to \tau\tau$ 1-jet control region is defined by applying the preselection requirements, b-veto, $m_{\mathrm{T}}^{\ell} > 50$ GeV as in the signal region but requiring $|m_{\tau\tau} - m_Z| < 25$ GeV. The purity of the 1-jet control region is about 80 %.

The $Z/\gamma^* \to \tau\tau$ predictions in the 0- and 1-jet categories are estimated using the extrapolation from the control region to the signal region and to the WW control region, as there is a 4–5 % contamination of $Z/\gamma^* \to \tau\tau$ events in the WW control region. The $\Delta\phi_{\ell\ell}$ and $m_{\ell\ell}$ distributions in the $Z/\gamma^* \to \tau\tau$ control region are shown in Fig. 11 for the 0-jet and 1-jet final states.

A mismodelling of the transverse momentum of the Z boson p_{T}^{Z}, reconstructed as $p_{\mathrm{T}}^{\ell\ell}$, is observed in the DY-enriched region. The mismodelling is more pronounced in the 0-jet category. The ALPGEN + HERWIG MC generator does not adequately model the parton shower of the soft jets which balance $p_{\mathrm{T}}^{\ell\ell}$ in events with no selected jets. A correction, based on weights derived from a data-to-MC comparison in the Z mass peak, is therefore applied to MC events in bins of $p_{\mathrm{T}}^{\ell\ell}$ in the 0-jet category. The weights are applied to p_{T}^{Z} at generator-level for all lepton flavour decays.

Apart from the above mentioned sources of theoretical uncertainties, one additional uncertainty on the p_{T}^{Z}-reweighting in the 0-jet category is estimated by comparing the difference between the nominal (derived in the Z mass peak) and the alternative (derived in the Z mass peak but after the $p_{\mathrm{T}}^{\mathrm{miss}} > 20$ GeV criterion) set of weights. All uncertainties are summarised in Table 5.

5.4 Misidentified leptons

The W+jets background is estimated in the same way as in Ref. [9], where a detailed description of the method can be found. The W+jets control sample contains events where one of the two lepton candidates satisfies the identification and isolation criteria for the signal sample, and the other lepton fails to meet these criteria but satisfies less restrictive criteria (these lepton candidates are called "anti-identified"). Events in this sample are otherwise required to satisfy all of the signal selection requirements. The dominant component of this sample (85–90 %) is due to W+jets events in which a jet produces an object reconstructed as a lepton. This object may be either a non-prompt lepton from the decay of a hadron containing a heavy quark, or a particle (or particles) originating from a jet and reconstructed as a lepton candidate.

The W+jets contamination in the signal region is obtained by scaling the number of events in the data control sample by an extrapolation factor. This extrapolation factor is measured in a data sample of jets produced in association with Z bosons reconstructed in either the ee or $\mu\mu$ final state (referred to as the Z+jets control sample below). The factor is the ratio of the number of identified lepton candidates satisfying all lepton selection criteria to the number of anti-identified leptons measured in bins of anti-identified lepton p_{T} and η. Each number is corrected for the presence of processes other than Z+jets.

The composition of the associated jets – namely the fractions of jets due to the production of heavy-flavour quarks, light-flavour quarks and gluons – in the Z+jets sample and the W+jets sample are different. Monte Carlo simulation is used to correct the extrapolation factors and to determine the associated uncertainty. Other important uncertainties on the Z+jets extrapolation factor are due to the limited number of jets that meet the lepton selection criteria in the Z+jets control sample and the uncertainties on the contributions from other physics processes.

The total systematic uncertainty on the corrected extrapolation factors varies as a function of the p_{T} of the anti-identified lepton; this variation is from 29 to 61 % for anti-identified electrons and from 25 to 46 % for anti-identified muons. The systematic uncertainty on the corrected extrapolation factor dominates the systematic uncertainty on the W+jets background.

6 BDT analysis

Both the spin and the CP analysis employ a BDT algorithm[4] to distinguish between different signal hypotheses. In all cases, two discriminants are trained to separate the signals from each other, or from the various background components, using the discriminating variables described in Sect. 4.2. The resulting two-dimensional BDT output is then used to construct a binned likelihood, which is fitted to the data to test its compatibility with the SM or BSM Higgs hypotheses, using the fit procedure presented in Sect. 7.

Before the training, the same preselection and some of the selection cuts listed in Table 2 are applied to data and on all MC predictions for background and signal. The additional selection requirements adopted for both the 0- and 1-jet categories are $m_{\ell\ell} < 100$ GeV and on $p_{\mathrm{T}}^{\mathrm{H}}$ for the spin-2 non-universal coupling models. The loosening of the $m_{\ell\ell}$ requirement with respect to the one applied in the full event selection is meant to increase the number of MC events for training. In the 0-jet category a requirement $p_{\mathrm{T}}^{\ell\ell} > 20$ GeV is applied while the $\Delta\phi_{\ell\ell}$ cut is omitted, whereas the latter is needed in the 1-jet category due to the large DY background. All background samples are used in the training and each one is weighted by the corresponding production cross-section.

6.1 Spin analysis

The spin analysis presented here follows closely the strategy of Ref. [3] for the 0-jet category, while the 1-jet category has been added and is treated likewise. For each category, one BDT discriminant (called BDT_0 in the following) is trained to discriminate between the SM hypothesis and the background, and a second one (BDT_2) to discriminate between the alternative spin-2 hypotheses and the background. This results in five BDT_2 trainings for the alternative spin-2 models defined in Sect. 2.1.2 and one BDT_0 training for the SM Higgs boson.

The distributions of the input variables used for BDT_0 and BDT_2 in the 0-jet and 1-jet categories, respectively, are shown in Figs. 2 and 3 (see Sect. 4.2).

The BDT discriminant distributions (also referred to as BDT output distributions) for the 0-jet and 1-jet signal region are shown in Figs. 12 and 13 for the case of universal couplings and of non-universal ones with $p_{\mathrm{T}}^{\mathrm{H}} < 125$ GeV, respectively. The plots for non-universal couplings and $p_{\mathrm{T}}^{\mathrm{H}} < 300$ GeV are very similar to the ones obtained using the requirement $p_{\mathrm{T}}^{\mathrm{H}} < 125$ GeV except for the BSM signal distribution. The SM Higgs signal is normalised using the SM Higgs-boson production cross-section. Good agreement between data and MC simulation is observed in those distributions once the SM signal is included.

6.2 CP analysis

The CP analysis – which includes both the fixed-hypothesis test and the CP-mixing scan – uses only the 0-jet category. In this case as well, two BDT discriminants are trained: the first, BDT_0, is identical to the one described above for the spin analysis (SM Higgs-boson signal versus background, using $m_{\ell\ell}$, $p_{\mathrm{T}}^{\ell\ell}$, $\Delta\phi_{\ell\ell}$ and m_{T} as input variables, as shown in Fig. 2). The second BDT, however, called $\mathrm{BDT}_{\mathrm{CP}}$ in the following, is trained to discriminate between the SM signal and signal for the alternative hypothesis without any background component. The training obtained using the two pure CP-even or CP-odd hypotheses is then applied to all the CP-mixing scenarios. As described in Sect. 4.2, the $\mathrm{BDT}_{\mathrm{CP}}$ training uses different input variables: $m_{\ell\ell}$, $\Delta\phi_{\ell\ell}$, $p_{\mathrm{T}}^{\ell\ell}$ and $p_{\mathrm{T}}^{\mathrm{miss}}$ for the

[4] A decision tree is a collection of cuts used to classify events as signal or background. The classification is based on a set of discriminating variables (BDT input variables) on which the algorithm is trained. The input events are repeatedly split using this information. At each split, the algorithm finds the variable and the optimal selection cut on this variable, that give the best separation between signal and background. Finally, an overall output weight (BDT output) is assigned to each event: the larger the weight, the more signal-like the event is classified to be. More details can be found in Ref. [10].

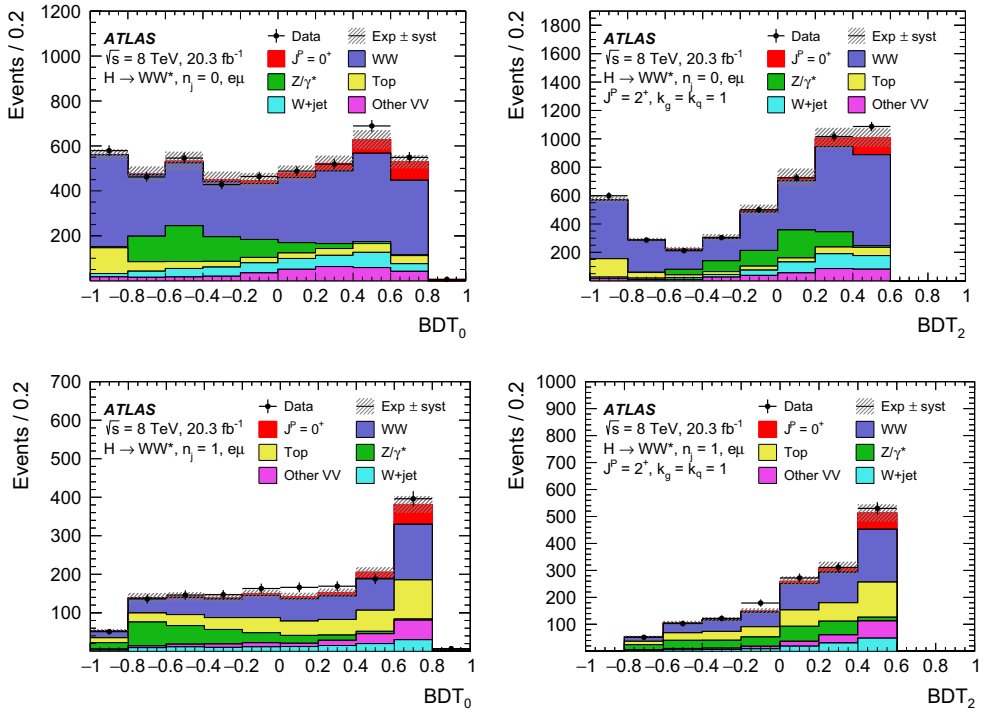

Fig. 12 The distributions of the output of BDT_0, discriminating between the SM hypothesis and the background, and BDT_2, discriminating between the alternative spin-2 hypothesis and the background, in the signal region for the spin-2 model with universal couplings. The signal is shown for the SM Higgs-boson hypothesis with $m_H = 125$ GeV. The background yields are corrected with the normalisation factors determined in the control regions

CP-even scenario, as shown in Fig. 4, and $m_{\ell\ell}$, $\Delta\phi_{\ell\ell}$, $E_{\ell\ell\nu\nu}$ and Δp_{T} for the CP-odd scenario, as shown in Fig. 5.

The different training strategy adopted for $\mathrm{BDT}_{\mathrm{CP}}$ and BDT_2 is motivated by the intrinsic difference between the spin and CP analyses: while, in the former case, the spin-2 signal is more background-like (its shape is similar to that of the dominant WW background), in the latter case, the different signal hypotheses result in shapes of the input variable distributions which are quite similar to each other, while they remain different from the background shape. Therefore, for the CP analysis, the best separation power is obtained by training $\mathrm{BDT}_{\mathrm{CP}}$ to discriminate between the SM and BSM hypotheses.

The $\mathrm{BDT}_{\mathrm{CP}}$ output distributions for the SM versus BSM CP-odd and CP-even hypotheses are shown in Fig. 14. Good agreement between data and MC simulation is also found in this case, once the SM Higgs-boson signal is included.

7 Fit procedure

This section discusses the statistical approach adopted in this paper. First, the rebinning of the two-dimensional BDT output distribution is discussed. The rebinning is applied for both analyses: the fixed-hypothesis tests and the CP-mixing analysis. Afterwards the statistical procedure for the individual analyses is presented.

The two-dimensional $\mathrm{BDT}_0 \times \mathrm{BDT}_2$ output (or $\mathrm{BDT}_0 \times \mathrm{BDT}_{\mathrm{CP}}$ for the CP analysis) distribution is unrolled row by row to a one-dimensional distribution. After the unrolling, bins with less than one background event are merged. The latter threshold is applied to the sum of weighted background events, i.e. after the normalisation to the corresponding cross-section and luminosity and the application of the post-fit scale factors to the background processes. This is done independently in the 0-jet and 1-jet categories and for all benchmarks and scans where a retraining of the BDT has occurred. Such a procedure is not intended to improve the expected sensitivity per se, rather to stabilise the fit in the presence of a large number of free parameters.

7.1 Procedure for the fixed-hypothesis test

The statistical analysis of the data employs a binned likelihood $\mathcal{L}(\varepsilon, \mu, \boldsymbol{\theta})$ constructed with one parameter of interest, ε, which represents the fraction of SM Higgs-boson events with respect to the expected signal yields, and can assume only discrete values $\varepsilon = 0$ (for the alternative ALT hypothesis) and $\varepsilon = 1$ (for the SM hypothesis).

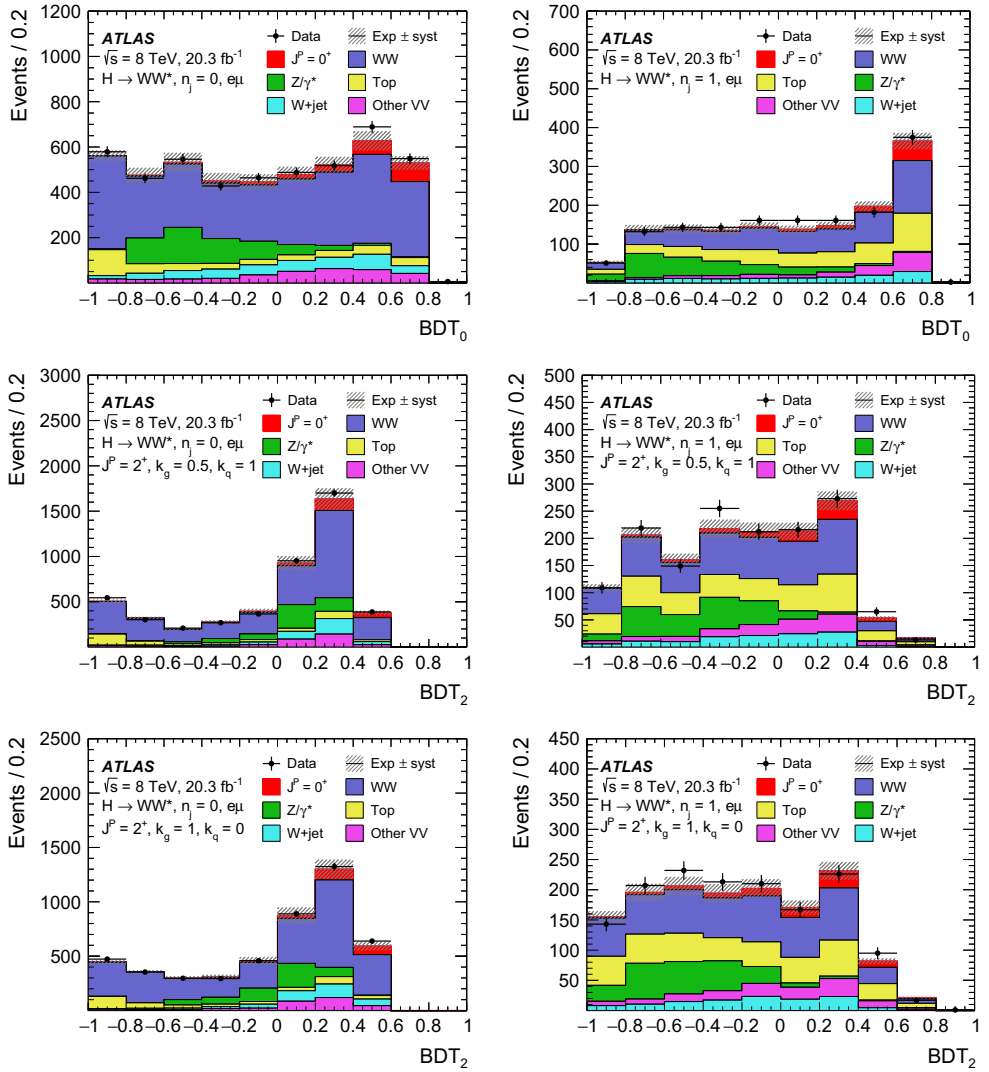

Fig. 13 BDT_0 and BDT_2 output distributions in the signal region for spin-2 models with non-universal couplings. The signal is shown for the SM Higgs-boson hypothesis with $m_H = 125$ GeV. The $p_T^H < 125$ GeV selection requirement is applied to all signal and background processes, corrected with the normalisation factors determined in the control regions

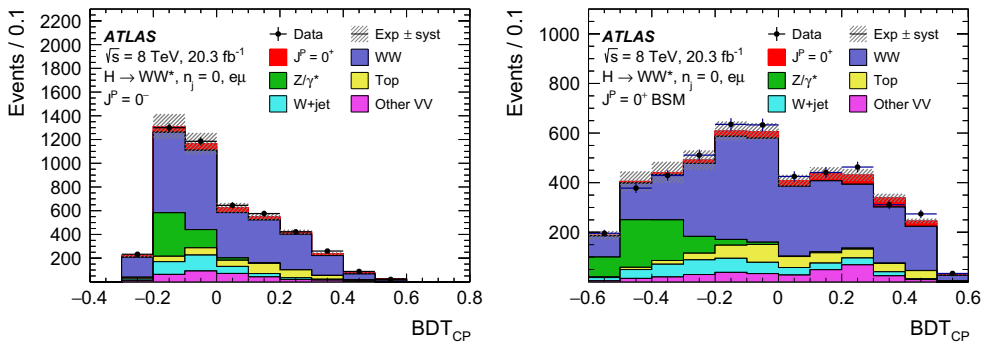

Fig. 14 Distributions of the output of BDT_{CP}, discriminating between the SM signal and the signal for the alternative hypothesis, in the signal region for the SM versus BSM CP-odd (*left*) and SM versus BSM CP-even (*right*) hypotheses. The signal is shown for the SM Higgs-boson hypothesis with $m_H = 125$ GeV. The background yields are corrected with the normalisation factors determined in the control regions

Template histograms representing the nominal signal and background rates are used to construct $\mathcal{L}(\varepsilon, \mu, \boldsymbol{\theta})$, summing over the bins (N_{bins}) of the unrolled BDT output distributions, per jet category in the spin-2 analysis case. $S_{\text{SM},i}$ and $S_{\text{ALT},i}$ are the signal yields for the SM and alternative hypothesis, respectively, while B_i refers to the total background. Systematic uncertainties are represented through the N_{sys} nuisance parameters $\boldsymbol{\theta}$, constrained by the auxiliary measurements $\mathcal{A}(\tilde{\boldsymbol{\theta}}|\boldsymbol{\theta})$, where $\tilde{\boldsymbol{\theta}}$ is the central value of the measurement. The full likelihood can then be written as:

$$\mathcal{L}(\varepsilon, \mu, \boldsymbol{\theta}) = \prod_{i}^{N_{\text{bins}}} P(N_i \,|\, \mu(\varepsilon\, S_{\text{SM},i}(\boldsymbol{\theta}) + (1-\varepsilon)\, S_{\text{ALT},i}(\boldsymbol{\theta})) + B_i(\boldsymbol{\theta})) \times \prod_{i}^{N_{\text{sys}}} \mathcal{A}(\tilde{\theta}_i|\theta_i). \tag{4}$$

The analysis is designed to rely on shape information to distinguish between different signal hypotheses. The overall signal normalisation μ is obtained from the fit and, in the case of the spin analysis, as a combination over both jet categories. Further details of the various likelihood terms can be found in Ref. [9].

The compatibility of the data and two signal hypotheses is then estimated using a test statistic defined as:

$$q = \ln \frac{\mathcal{L}(\varepsilon = 1, \hat{\hat{\mu}}_{\varepsilon=1}, \hat{\hat{\boldsymbol{\theta}}}_{\varepsilon=1})}{\mathcal{L}(\varepsilon = 0, \hat{\hat{\mu}}_{\varepsilon=0}, \hat{\hat{\boldsymbol{\theta}}}_{\varepsilon=0})}. \tag{5}$$

For both the numerator and denominator, the likelihood is maximised independently over all nuisance parameters to obtain the maximum likelihood estimators $\hat{\hat{\mu}}$ and $\hat{\hat{\boldsymbol{\theta}}}$. Pseudo-experiments for the two hypotheses ($\varepsilon = 0, 1$) are used to obtain the corresponding distributions of the test statistic q and subsequently to evaluate the p values, which define the expected and observed sensitivities for various hypotheses. The expected p values are calculated using the fitted signal strength in data, $p^{\text{SM}}_{\text{exp},\ \mu=\hat{\mu}}$ for the SM hypothesis, and $p^{\text{ALT}}_{\text{exp},\ \mu=\hat{\mu}}$ for the alternative hypothesis. In addition, for the SM hypothesis the expected p value fixing the signal normalisation to the SM prediction, $p^{\text{SM}}_{\text{exp},\ \mu=1}$, is given. The observed p values, $p^{\text{SM}}_{\text{obs}}$ and $p^{\text{ALT}}_{\text{obs}}$, are defined as the probability of obtaining a q value smaller (larger) than the observed value under the SM (alternative) signal hypothesis. Pseudo-experiments are needed because the asymptotic approximation [51] does not hold when the parameter of interest, ε in this case, takes only discrete values (0 or 1), and in particular $-2\ln(\mathcal{L})$ does not follow a χ^2 distribution.

The confidence level (CL) for excluding an alternative BSM hypothesis in favour of the SM is evaluated by means of a CL estimator [52]:

$$\text{CL}_{\text{s}} = \frac{p^{\text{ALT}}_{\text{obs}}}{1 - p^{\text{SM}}_{\text{obs}}}, \tag{6}$$

which normalises the rejection power of the alternative hypothesis, p^{ALT}, to the compatibility of the data with the SM case, $1 - p^{\text{SM}}$.

7.2 Procedure for CP-mixing analysis

The likelihood definition for the CP-mixing analysis is the same as for the spin analysis, with $\varepsilon = 1$ corresponding to the SM signal hypothesis and $\varepsilon = 0$ corresponding to the alternative CP hypothesis. Whereas for the fixed-hypothesis test, the sensitivities are estimated by means of pseudo-experiments and follow the procedure explained above, for the CP-mixing analysis, the simpler asymptotic approximation is used, since the fraction of BSM signal events is now considered a continuous parameter. Results using the asymptotic approximation are cross-checked with pseudo-data for a few values of the scan parameter.

The fits to data and to the MC expectation under the SM hypothesis are performed for each value of the scan parameter. Two fits to the SM expectation are evaluated: fixing the signal normalisation to the SM expectation and to the observed SM signal normalisation. From the fit, the value of the log-likelihood (LL) is extracted, as a function of the CP-mixing fraction. The maximum of the LL curve is determined and its difference from all other values is computed, $-2\Delta\text{LL}$. The 1σ and 2σ confidence levels are then found at $-2\Delta\text{LL} = 1$ and $-2\Delta\text{LL} = 3.84$, respectively.

8 Systematic uncertainties

This section describes the systematic uncertainties considered in this analysis, which are divided into two categories: experimental uncertainties and theoretical ones which affect the shape of the BDT output distribution. The systematic uncertainties specific to the normalisation of individual backgrounds are described in Sect. 5.

8.1 Experimental uncertainties

The jet-energy scale and resolution and the b-tagging efficiency are the dominant sources of experimental uncertainty in this category, followed by the lepton resolution, identification and trigger efficiencies and the missing transverse momentum measurement. The latter is calculated as the negative vector sum of the momentum of objects selected according to the ATLAS identification algorithms, such as leptons, photons, and jets, and of the remaining soft objects (referred

Table 6 Sources of experimental systematic uncertainty considered in the analysis. The source and magnitude of the uncertainties and their impact on the reconstructed objects is indicated

Source of uncertainty	Treatment in the analysis and its magnitude
Jet energy scale	1–7 % in total as a function of jet η and p_{T}
Jet energy resolution	5–20 % as a function of jet η and p_{T}
	Relative uncertainty on the resolution is 2–40 %
b-tagging	b-jet identification: 1–8 % decomposed in p_{T} bins
	Light-quark jet misidentification: 9–19 % as a function of η and p_{T}
	c-quark jet misidentification: 6–14 % as a function of p_{T}
Leptons	Reconstruction, identification, isolation, trigger efficiency: below 1 % except for electron identification: 0.2–2.7 % depending on η and p_{T}
	Momentum scale and resolution: <1 %
Missing transverse momentum	Propagated jet-energy and lepton-momentum scale uncertainties
	Resolution (1.5–3.3 GeV) and scale variation (0.3–1.4 GeV)
Pile-up	The number of pile-up events is varied by 10 %
Luminosity	2.8 % [53]

to as soft terms in the following) that typically have low values of p_{T} [9]. The various systematic contributions taken into account in the analysis are listed in Table 6. More information on the experimental systematic uncertainties can be found in Ref. [9].

In the likelihood fit, the experimental uncertainties are varied in a correlated way across all backgrounds and across signal and control regions, so that the uncertainties on the extrapolation factors α described in Sect. 5 are correctly propagated. All sources in Table 6 are analysed to evaluate their impact on both the yield normalisation and on the shape of the BDT discriminant distributions. Shape uncertainties are ignored if they are smaller than 5 % (smaller than the statistical uncertainty) in each bin of the distributions under study. Normalisation uncertainties are ignored as well if they are below 0.1 %.

8.2 Modelling uncertainties

The dominant background is SM WW production, and therefore uncertainties on the shape and yield in the signal region for this background require special attention. The uncertainties on the WW normalisation are discussed in Sect. 5.1; the shape uncertainties are addressed in this section.

An important uncertainty arises from the modelling of the shape of the WW background in the signal region, which is obtained using the same procedure adopted in the evaluation of the theoretical uncertainty on the WW extrapolation parameter. The scale uncertainty on the MC prediction of the BDT discriminants was studied by varying the factorisation and renormalisation scales up and down by a factor of two. The parton shower and generator uncertainties are estimated by comparing the HERWIG and PYTHIA parton shower programs and by comparing POWHEG + HERWIG and aMC@NLO + HERWIG, respectively. Finally, the PDF uncertainty is estimated by combining the CT10 PDF error set with the difference between the central values of NNPDF2.3 and CT10. The procedure is repeated for each of the final BDT output distributions and for each benchmark of the spin and parity analyses.

Modifications to the shape of the final BDT distribution from PDF and scale variations are found to be negligible, and well within the statistical uncertainty of the Monte Carlo predictions. Therefore they are included in the fit model only as overall normalisation effects. The parton shower and generator uncertainties were found to be statistically significant; therefore, a bin-by-bin shape uncertainty is applied.

The interference between the $gg \to WW$ and the $gg \to H$ processes is not taken into account in this study because of its negligible effect. In fact it results in a 4 % decrease in the total yield of events after the selection criteria and is of the same order as in Ref. [9]. These results confirm the expectations in Ref. [54].

The signal final-state observables are affected by the underlying Higgs-boson p_{T} distribution. The Higgs-boson p_{T} distribution for a spin-0 particle is given by the $p_{\mathrm{T}}^{\mathrm{H}}$-reweighted POWHEG + PYTHIA generator prediction as mentioned in Sect. 3. All spin-0 samples are reweighted to the same $p_{\mathrm{T}}^{\mathrm{H}}$ distribution to avoid any impact of the difference in the Higgs-boson p_{T} predictions between MADGRAPH5_aMC@NLO and POWHEG on the CP-analysis results. No additional shape uncertainty is considered. For the spin-2 benchmarks no theoretical uncertainties on the Higgs-boson $p_{\mathrm{T}}^{\mathrm{H}}$ are considered, because they are negligible compared to the effect of the choice of $p_{\mathrm{T}}^{\mathrm{H}}$ requirement in the non-universal couplings models.

Table 7 From top to bottom, systematic uncertainties (in %) with the largest impact on the spin-2 universal couplings, BSM CP-odd and CP-even Higgs-boson fixed-hypothesis tests. This ranking is based on the impact of each systematic uncertainty on the CL_s estimator (see Sect. 7). For the exact meaning of the different uncertainties related to the misidentified lepton rates (the W+jets background estimate uncertainty), see Sect. 5.4 and Ref. [9]

Spin-2		BSM CP-odd		BSM CP-even	
WW generator	2.6	WW generator	0.73	WW UE/PS	21
p_{T}^{Z} reweighting	1.2	WW UE/PS	0.66	Misid. rate (elec. stats)	9.2
Misid. rate (elec. stats)	1.1	QCD scale Wg^*	0.45	Misid. rate (elec. flavour)	8.4
Misid. rate (elec. flavour)	1.0	p_{T}^{Z} reweighting	0.43	Misid. rate (muon flavour)	7.4
WW UE/PS	0.86	QCD scale VV	0.39	Misid. rate (muon stats)	7.3
Misid. rate (muon stats)	0.81	QCD scale Wg	0.38	Misid. rate (elec. other)	7.3
$Z/\gamma^* \to \tau\tau$ generator	0.76	Misid. rate (elec. stats)	0.37	WW PDF qq-production	6.9
Misid. rate (muon flavour)	0.75	Misid. rate (elec. other)	0.34	WW PDF gg-production	6.9
Misid. rate (elec. other)	0.67	Misid. rate (elec. flavour)	0.33	WW generator	3.6

8.3 Ranking of systematics

The impact of each systematic variation on the CL_s estimator gives the measure of the relevance of the systematic uncertainty on the obtained result. The systematic uncertainties that are found to be most important in the various fixed-hypothesis tests are listed for the different cases in Table 7.

The WW modelling uncertainty dominates in all three benchmarks, and another common large uncertainty is due to the W+jets background estimate. The spin-2 and CP-odd analyses are affected by the $Z/\gamma^* \to \tau\tau$ modelling uncertainty. In addition, the CP-odd analysis is impacted by the modelling uncertainties on the non-WW background. The impact of systematics on the CL_s estimator is larger for the CP-even case than for other benchmarks because of the lower sensitivity of the CP-even analysis.

9 Results

The results of the studies of the spin and parity quantum numbers are presented in this section. The SM $J^P = 0^+$ hypothesis is tested against several alternative spin/parity hypotheses, and the mixture of the SM Higgs and a BSM CP-even or CP-odd Higgs bosons is studied by scanning all possible mixing combinations.

This section is organised as follows. The event yields and the BDT output distributions after the fit to data are presented in Sect. 9.1. The results of the fixed-hypotheses tests for spin-2 benchmarks are discussed in Sect. 9.2 and the results for spin-0 and CP-mixed tests are shown in Sect. 9.3.

9.1 Yields and distributions

The post-fit yields for all signals and backgrounds are summarised in Table 8 for the spin and CP analyses. They account for changes in the normalisation factors and for pulls of the nuisance parameters. All the systematic uncertainties discussed in Table 5 and Sect. 8 are included in the fit. The fitted signal yields vary significantly in the BSM scenarios because of the differences in the shapes of the input variable distributions between the benchmark models. A striking example is given by the benchmark models with non-universal couplings: the fitted signal yield varies considerably between the $p_{\mathrm{T}}^{\mathrm{H}} < 125$ GeV and $p_{\mathrm{T}}^{\mathrm{H}} < 300$ GeV selections because of the presence of the tail at high $p_{\mathrm{T}}^{\mathrm{H}}$ values discussed in Sect. 2.1.1. The yield fitted under the SM hypothesis, 270 ± 70 events (see Table 8), is in good agreement with the signal expectation of 238 events, corresponding to the ggF signal strength measured in Ref. [9].

9.2 Spin-2 results

The compatibility of the spin-2 signal model with the observed data is calculated following the prescription explained in Sect. 7.1 for five different benchmarks discussed in Sect. 2.1.2. The expected distributions of the test statistic q, derived from pseudo-experiments, are shown for the universal couplings case in Fig. 15 for 0- and 1-jet combined. The q distributions are symmetric and have no overflow or underflow bins. The expected and observed significances and CL_s are summarised in Table 9. The expected significance $p^{\mathrm{SM}}_{\mathrm{exp},\ \mu=\hat{\mu}}$ using the observed SM normalisation is higher than $p^{\mathrm{SM}}_{\mathrm{exp},\ \mu=1}$, because the observed SM yields in Table 8 are larger than the expected SM yields in Table 3. The SM hypothesis is favoured in all tests in data and the alternative model is disfavoured at 84.5 % CL for the model with universal couplings and excluded at 92.5–99.4 % CL for the benchmark models with non-universal couplings. The exclusion limits for non-universal couplings are stronger for a $p_{\mathrm{T}}^{\mathrm{H}}$

Table 8 Post-fit event yields for the 0- and 1-jet categories for various signal hypotheses. The number of events observed in data, the signal and the total background yields, including their respective post-fit systematic uncertainties, are shown in the top part of the table, assuming in each case the alternative signal hypothesis. The spin-2 $\kappa_g = \kappa_q$ benchmark is used as an example in the bottom part of the table, to show in more detail the results under the SM Higgs-boson hypothesis. For this fit, the individual backgrounds are listed for completeness (see Sect. 5)

Benchmark	Signal		Total background	
	0-jet	1-jet	0-jet	1-jet
$\kappa_g = \kappa_q$	360 ± 100	126 ± 34	4370 ± 240	1430 ± 60
$\kappa_g = 0.5, \kappa_q = 1, p_{\mathrm{T}}^{\mathrm{H}} < 125\,\mathrm{GeV}$	300 ± 100	103 ± 33	4430 ± 240	1390 ± 60
$\kappa_g = 0.5, \kappa_q = 1, p_{\mathrm{T}}^{\mathrm{H}} < 300\,\mathrm{GeV}$	230 ± 80	82 ± 29	4490 ± 230	1460 ± 70
$\kappa_g = 1, \kappa_q = 0, p_{\mathrm{T}}^{\mathrm{H}} < 125\,\mathrm{GeV}$	320 ± 90	111 ± 32	4410 ± 240	1390 ± 60
$\kappa_g = 1, \kappa_q = 0, p_{\mathrm{T}}^{\mathrm{H}} < 300\,\mathrm{GeV}$	200 ± 80	71 ± 28	4520 ± 240	1480 ± 70
BSM CP-odd	240 ± 80	–	4490 ± 260	–
BSM CP-even	180 ± 60	–	4530 ± 240	–

	Data	Signal	Tot. bkg.	WW	Top	DY	W+jets	Other
SM 0-jet	4730	270 ± 70	4460 ± 240	2904	376	464	370	345
SM 1-jet	1569	95 ± 26	1450 ± 70	607	355	233	124	133

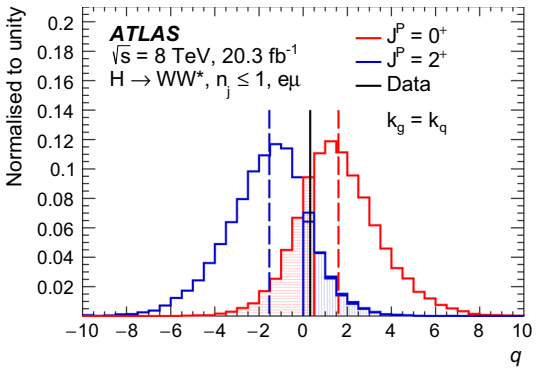

Fig. 15 Test-statistic distribution for the spin-2 benchmark with universal couplings ($\kappa_g = \kappa_q$) including all systematic uncertainties, with 0- and 1-jet categories combined. The median of the expected distributions for the SM (*dashed red line*) and the spin-2 Higgs-boson signal (*dashed blue line*) is also shown, together with the observed result (*solid black line*) from the fit to the data. The *shaded areas* are used to compute the observed p values

cut above 300 GeV because of the enhanced sensitivity at high values of the Higgs-boson p_{T}.

The one-dimensional distribution of the unrolled post-fit BDT output distribution is presented in Fig. 16 for the $\kappa_g = 1$, $\kappa_q = 0$ and $p_{\mathrm{T}}^{\mathrm{H}} < 125$ GeV scenario in the 0-jet case. The distributions are shown for the SM and alternative signal hypotheses separately and compared with the data after the subtraction of all backgrounds. Both the signal and background yields are normalised to the post-fit values. The distributions are ordered in terms of increasing signal yield and, for visualisation purposes, only contain bins that have at least three signal events and a signal-to-background ratio of at least 0.02.

9.3 Spin-0 and CP-mixing results

Similar to the spin-2 fixed-hypothesis tests, the CP-even BSM Higgs and the CP-odd BSM Higgs-boson hypotheses are tested against the SM Higgs-boson hypothesis. The expected distributions of the test statistic q, derived from pseudo-experiments for the SM versus BSM CP-odd and CP-even pure states, are shown in Fig. 17. The distributions are symmetric and have no overflow or underflow bins. The overlap of the test-statistic distributions for the SM hypothesis and the alternative hypothesis indicates the sensitivity of the analysis to distinguish them. The expected sensitivity is higher for the CP-odd hypothesis than for the CP-even hypothesis. The expected and observed significances and $\mathrm{CL_s}$ values are summarised in Table 9. The expected significances $p^{\mathrm{SM}}_{\mathrm{exp},\ \mu=\hat{\mu}}$ and $p^{\mathrm{SM}}_{\mathrm{exp},\ \mu=1}$ are similar, because the observed and the expected SM yields are similar for the spin-0 fixed hypothesis test. The SM hypothesis is favoured in both tests and the alternative hypothesis can be excluded at 96.5 % CL for the CP-odd Higgs boson and disfavoured at 70.8 % CL for the CP-even BSM Higgs boson.

The unrolled BDT output distributions normalised to the post-fit values are shown in Fig. 18. These distributions show the one-dimensional unrolled BDT output for the SM and alternative signal hypotheses separately and compare them with the data after background subtraction. Both the signals and the background yields are normalised to the post-fit values. The distributions are ordered by increasing signal, and they contain bins that have at least three signal events and are above a signal-to-background threshold (S/B) of 0.035. As already mentioned above, these plots are intended for illustrative purposes only. The figure shows that the SM Higgs-

Table 9 Summary of expected and observed sensitivities for various alternative spin/CP benchmarks compared to the SM Higgs-boson hypothesis. The expected and observed p values and the observed $1-\mathrm{CL_s}$ value as defined in Sect. 7 are shown for various benchmarks. The results are computed taking into account systematic uncertainties, using the combined 0-jet and 1-jet categories for the spin analysis and only the 0-jet category for the CP analysis

Channel	$p^{\mathrm{SM}}_{\mathrm{exp},\ \mu=1}$	$p^{\mathrm{SM}}_{\mathrm{exp},\ \mu=\hat{\mu}}$	$p^{\mathrm{ALT}}_{\mathrm{exp},\ \mu=\hat{\mu}}$	$p^{\mathrm{SM}}_{\mathrm{obs}}$	$p^{\mathrm{ALT}}_{\mathrm{obs}}$	$1-\mathrm{CL_s}$
Spin-2, $\kappa_g = \kappa_q$						
$0+1$-jet	0.131	0.039	0.033	0.246	0.117	84.5 %
Spin-2, $\kappa_g = 0.5, \kappa_q = 1, p_{\mathrm{T}}^{\mathrm{H}} < 125$GeV						
$0+1$-jet	0.105	0.047	0.022	0.685	0.007	97.8 %
Spin-2, $\kappa_g = 0.5, \kappa_q = 1, p_{\mathrm{T}}^{\mathrm{H}} < 300$GeV						
$0+1$-jet	0.023	0.014	0.004	0.524	0.003	99.3 %
Spin-2, $\kappa_g = 1, \kappa_q = 0, p_{\mathrm{T}}^{\mathrm{H}} < 125$GeV						
$0+1$-jet	0.109	0.041	0.029	0.421	0.044	92.5 %
Spin-2, $\kappa_g = 1, \kappa_q = 0, p_{\mathrm{T}}^{\mathrm{H}} < 300$GeV						
$0+1$-jet	0.015	0.016	0.004	0.552	0.003	99.4 %
BSM CP-odd						
0-jet	0.078	0.062	0.032	0.652	0.012	96.5 %
BSM CP-even						
0-jet	0.271	0.310	0.287	0.907	0.027	70.8 %

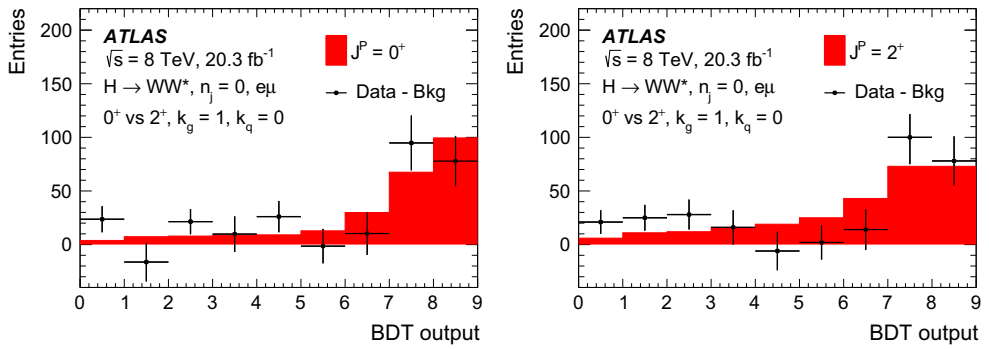

Fig. 16 The unrolled one-dimensional BDT output after background subtraction and using post-fit normalisations, in the case of the spin-2 benchmark with non-universal couplings ($\kappa_g = 1, \kappa_q = 0$), requiring the Higgs-boson p_{T} to be below 125 GeV. The background yields are taken from the fit results, assuming the SM signal hypothesis in the *left-hand plot*, and the alternative spin-2 hypothesis in the *right-hand plot*

boson hypothesis is preferred over the pure BSM CP-even or CP-odd cases. The S/B ratio used for the CP analysis is higher than the one used for the spin-2 analysis because on average the bins with the highest significance have a higher S/B in the CP-mixing than in the spin-2 BDT output.

The compatibility of the CP-mixed signal plus background with the observed data is calculated following the prescription explained in Sect. 7.2 for the two different scans (mixing of an SM Higgs boson with a BSM CP-even or CP-odd boson) as discussed in Sect. 2.2.1. The scan results are presented in Fig. 19.

In the case of the BSM CP-odd mixing scan (top row of Fig. 19), the expected and observed curves are slightly asymmetric, but the sensitivity to the sign of the scan parameter is small. Due to higher observed yields for the SM hypothesis, the expected curve using the observed yields ($\mu = \hat{\mu}$) is above the expected curve for the yields fixed to the SM expectation ($\mu = 1$). The minimum of the -2ΔLL curve is very broad and lies at -0.2. The value at 0 corresponds to the SM hypothesis. The values of $(\tilde{\kappa}_{\mathrm{AWW}}/\kappa_{\mathrm{SM}}) \cdot \tan\alpha$ below -6 and above 5 can be excluded at 95 % CL, while values below -1.6 and above 1.3 at 68 % CL. The fitted signal yields and their relative uncertainties, for the SM and alternative signal hypotheses, are very stable throughout the scan. They are given in Table 8 for the fixed-hypothesis case.

The plot on the bottom of Fig. 19 shows the result of the BSM CP-even scan as a function of $\tilde{\kappa}_{\mathrm{HWW}}/\kappa_{\mathrm{SM}}$. The separa-

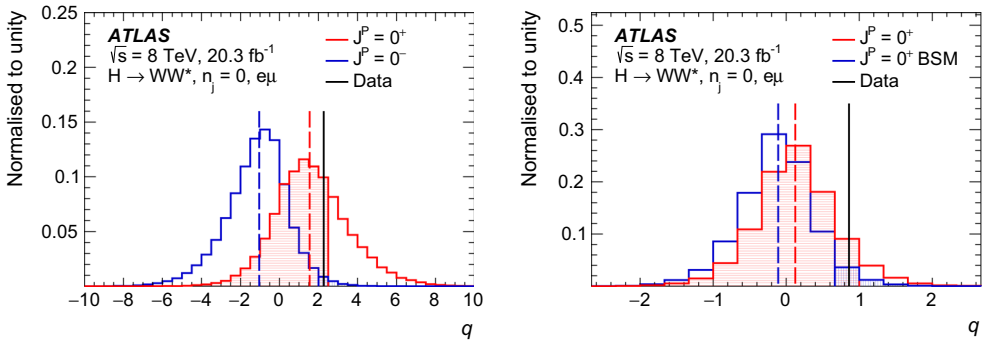

Fig. 17 Test-statistic distribution for the pure BSM CP-odd (*left*) and BSM CP-even (*right*) benchmarks, including all systematic uncertainties. The median of the expected distributions for the SM (*dashed red line*) and the BSM Higgs-boson signal (*dashed blue line*) is also shown, together with the observed result (*solid black line*) from the fit to the data. The *shaded areas* are used to compute the observed p values

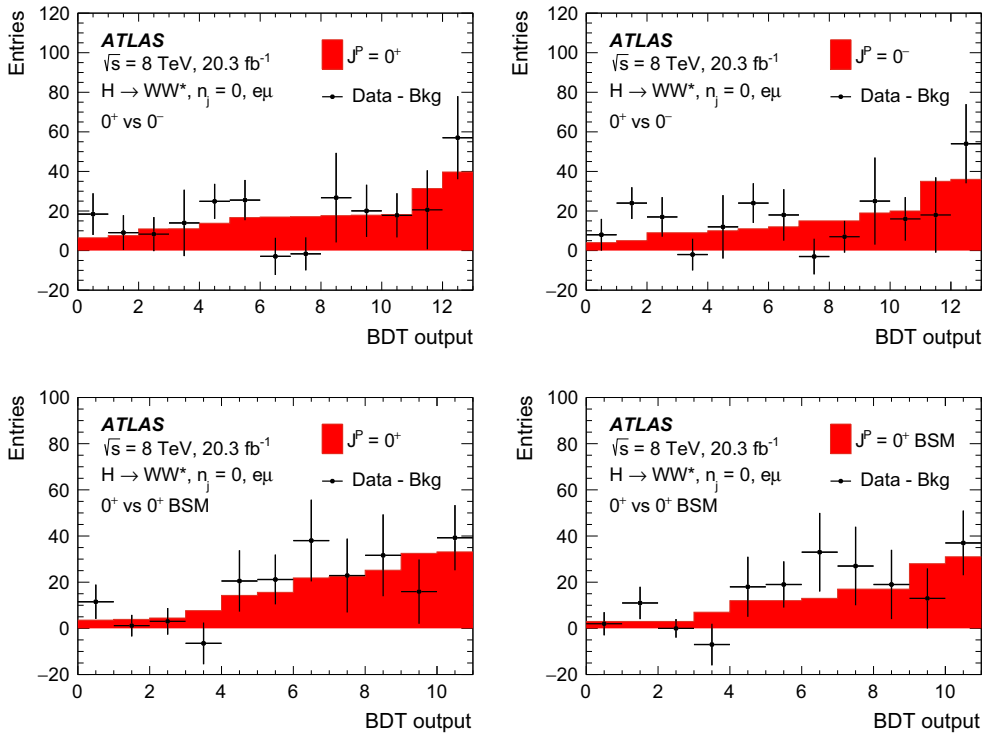

Fig. 18 The unrolled one-dimensional BDT output after background subtraction in the case of the pure BSM CP-odd (*top*) and BSM CP-even (*bottom*) benchmarks. The background yields are taken from the fit results, assuming the SM signal hypothesis in the *left-hand plots*, and the alternative hypothesis in the *right-hand plots*

tion power between the SM Higgs-boson hypothesis and the BSM CP-even mixed hypothesis is enhanced in the region around -1, the observed minimum of the -2ΔLL distribution, because of the interference effect explained in Sect. 4.2. The fitted signal yield, both for the SM and alternative signal hypotheses, is stable for values outside the observed minimum region and similar to the values given in Table 8 for the fixed-hypothesis case. In the region around the minimum, the fitted BSM signal yield is higher, reaching about 370 events. These variations are expected from the significant shape differences of the input variable distributions in this region of the parameter scan, as described in Sect. 4.2. The relative uncertainty is stable throughout the scan, with values around 30 %.

The observed minimum of the -2ΔLL curve is at -1.3 and is compatible with the SM hypothesis within 1.9σ. To further study the compatibility of the SM signal hypothesis with the observed result, several scans are performed, by fitting, instead of the real data, pseudo-data generated around the expected signal-plus-background post-fit BDT distribu-

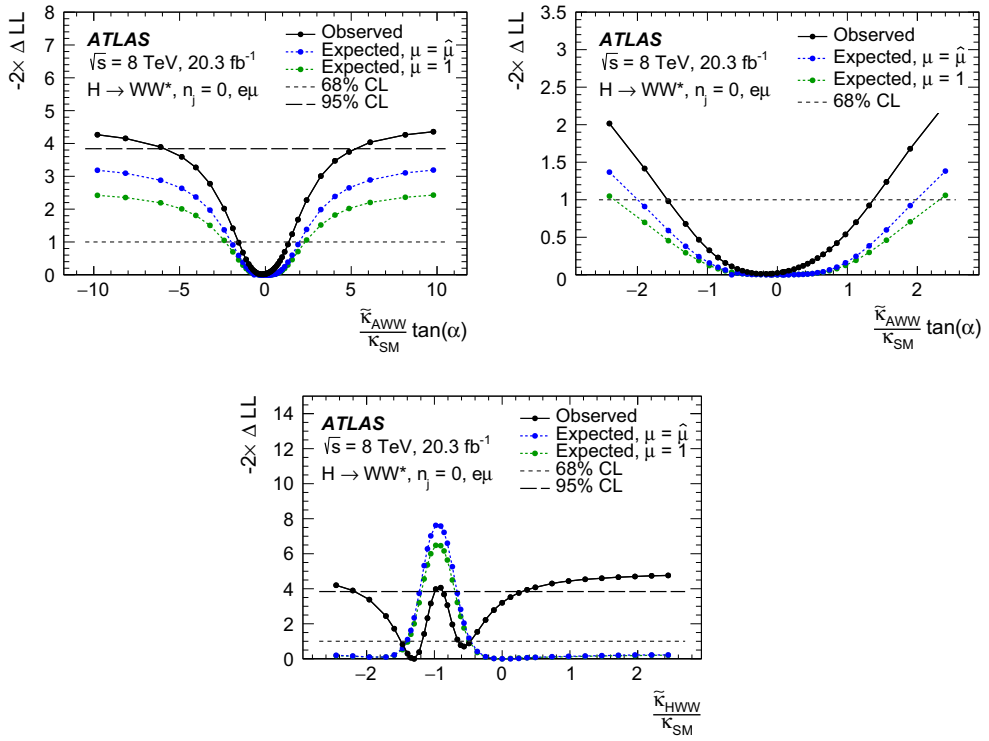

Fig. 19 The BSM CP-odd (*top*) and BSM CP-even (*bottom*) mixing scan results. The *top row* shows the full CP-odd scan (*left*) and the region around the minimum enlarged (*right*). The 68 % and 95 % CL exclusion regions are indicated as lying above the corresponding *horizontal lines*

tion. This means that the nuisance parameters from this test are obtained from the fit of the SM signal to the data. Distributions similar to the one observed in the data are reproduced by pseudo-data. Furthermore, a fixed-hypothesis test is also performed, where the compatibility of the observed data with the SM Higgs boson versus the CP-even mixed signal corresponding to $\tilde{\kappa}_{\mathrm{HWW}}/\kappa_{\mathrm{SM}} = -1.3$ is studied, resulting in a $1 - \mathrm{CL_s}$ of 43 % in favour of the SM and of 93 % in favour of the alternative hypothesis.

Values of the mixing parameter, $\tilde{\kappa}_{\mathrm{HWW}}/\kappa_{\mathrm{SM}}$, above 0.4 and below -2.2 can be excluded at 95 % CL, as well as in the region between -0.85 and -1. Values above -0.5 and below -1.5, as well as between -1.2 and -0.65, can be excluded at 68 % CL.

10 Conclusions

The Standard Model $J^P = 0^+$ hypothesis for the Higgs boson is compared to alternative spin/parity hypotheses using 20.3 fb^{-1} of the proton–proton collision data collected by the ATLAS experiment at the LHC at $\sqrt{s} = 8$ TeV and corresponding to the full data set of 2012. The Higgs-boson decay $WW^* \to e\nu\mu\nu$ is used to test several alternative models, including BSM CP-even and CP-odd Higgs bosons, and a graviton-inspired $J^P = 2^+$ model with minimal couplings to the Standard Model particles. In addition to the tests of pure J^P states, two scenarios are considered where all the CP mixtures of the SM Higgs boson and a BSM CP-even or CP-odd Higgs boson are tested.

For the spin-2 benchmarks, the SM hypothesis is favoured in all tests in data and the alternative model is disfavoured at 84.5 % CL for the model with universal couplings and excluded at 92.5–99.4 % CL for the benchmark models with non-universal couplings.

The SM Higgs-boson hypothesis is tested against a pure BSM CP-even or CP-odd Higgs-boson hypothesis: the results prefer the SM Higgs-boson hypothesis, excluding the alternative hypothesis at the 70.8 and 96.5 % levels, respectively.

The data favour the Standard Model quantum numbers in all cases apart from the scan of a CP-mixed state with a BSM CP-even Higgs boson, where the data prefer a mixed state with $\tilde{\kappa}_{\mathrm{HWW}}/\kappa_{\mathrm{SM}} = -1.3$, which is compatible with the SM hypothesis within 1.9σ. The $\tilde{\kappa}_{\mathrm{HWW}}/\kappa_{\mathrm{SM}}$ values can be excluded at 95 % CL above 0.4 and below -2.2, as well in the region between -0.85 and -1. For the mixing with a BSM CP-odd Higgs boson, the $(\tilde{\kappa}_{\mathrm{AWW}}/\kappa_{\mathrm{SM}}) \cdot \tan\alpha$ values above 5 and below -6 can be excluded at 95 % CL. The preferred value corresponds to $(\tilde{\kappa}_{\mathrm{AWW}}/\kappa_{\mathrm{SM}}) \cdot \tan\alpha = -0.2$, which is compatible with the SM to within 0.5σ.

Acknowledgments We thank CERN for the very successful operation of the LHC, as well as the support staff from our institutions without whom ATLAS could not be operated efficiently. We acknowledge the support of ANPCyT, Argentina; YerPhI, Armenia; ARC, Australia; BMWFW and FWF, Austria; ANAS, Azerbaijan; SSTC, Belarus; CNPq and FAPESP, Brazil; NSERC, NRC and CFI, Canada; CERN; CONICYT, Chile; CAS, MOST and NSFC, China; COLCIENCIAS, Colombia; MSMT CR, MPO CR and VSC CR, Czech Republic; DNRF, DNSRC and Lundbeck Foundation, Denmark; EPLANET, ERC and NSRF, European Union; IN2P3-CNRS, CEA-DSM/IRFU, France; GNSF, Georgia; BMBF, DFG, HGF, MPG and AvH Foundation, Germany; GSRT and NSRF, Greece; RGC, Hong Kong SAR, China; ISF, MINERVA, GIF, I-CORE and Benoziyo Center, Israel; INFN, Italy; MEXT and JSPS, Japan; CNRST, Morocco; FOM and NWO, Netherlands; BRF and RCN, Norway; MNiSW and NCN, Poland; GRICES and FCT, Portugal; MNE/IFA, Romania; MES of Russia and NRC KI, Russian Federation; JINR; MSTD, Serbia; MSSR, Slovakia; ARRS and MIZŠ, Slovenia; DST/NRF, South Africa; MINECO, Spain; SRC and Wallenberg Foundation, Sweden; SER, SNSF and Cantons of Bern and Geneva, Switzerland; NSC, Taiwan; TAEK, Turkey; STFC, the Royal Society and Leverhulme Trust, United Kingdom; DOE and NSF, United States of America. The crucial computing support from all WLCG partners is acknowledged gratefully, in particular from CERN and the ATLAS Tier-1 facilities at TRIUMF (Canada), NDGF (Denmark, Norway, Sweden), CC-IN2P3 (France), KIT/GridKA (Germany), INFN-CNAF (Italy), NL-T1 (Netherlands), PIC (Spain), ASGC (Taiwan), RAL (UK) and BNL (USA) and in the Tier-2 facilities worldwide.

Funded by SCOAP[3].

References

1. ATLAS Collaboration, Observation of a new particle in the search for the standard model Higgs boson with the ATLAS detector at the LHC. Phys. Lett. B **716**, 1–29 (2012). arXiv:1207.7214 [hep-ex]
2. CMS Collaboration, Observation of a new boson at a mass of 125 GeV with the CMS experiment at the LHC. Phys. Lett. B **716**, 30–61 (2012). arXiv:1207.7235 [hep-ex]
3. ATLAS Collaboration, Evidence for the spin-0 nature of the Higgs boson using ATLAS data. Phys. Lett. B **726**, 120–144 (2013). arXiv:1307.1432 [hep-ex]
4. CMS Collaboration, Constraints on the spin-parity and anomalous HVV couplings of the Higgs boson in proton collisions at 7 and 8 TeV (2014). arXiv:1411.3441 [hep-ex]
5. J. Alwall et al., The automated computation of tree-level and next-to-leading order differential cross sections, and their matching to parton shower simulations. JHEP **1407**, 079 (2014). arXiv:1405.0301 [hep-ph]
6. Y. Gao et al., Spin determination of single-produced resonances at hadron colliders. Phys. Rev. D **81**, 075022 (2010). arXiv:1001.3396 [hep-ph]
7. S. Bolognesi et al., On the spin and parity of a single-produced resonance at the LHC. Phys. Rev. D **86**, 095031 (2012). arXiv:1208.4018 [hep-ph]
8. P. Artoisenet et al., A framework for Higgs characterisation. JHEP **1311**, 043 (2013). arXiv:1306.6464 [hep-ph]
9. ATLAS Collaboration, Observation and measurement of Higgs boson decays to WW^* with the ATLAS detector (2014). arXiv:1412.2641 [hep-ex]
10. P. Speckmayer et al., The toolkit for multivariate data analysis, TMVA 4. J. Phys. Conf. Ser. **219**, 032057 (2010)
11. L. Randall, R. Sundrum, A Large mass hierarchy from a small extra dimension. Phys. Rev. Lett. **83**, 3370–3373 (1999). arXiv:hep-ph/9905221 [hep-ph]
12. ATLAS Collaboration, Measurements of fiducial and differential cross sections for Higgs boson production in the diphoton decay channel at $\sqrt{s} = 8$ TeV with ATLAS. JHEP **1409**, 112 (2014). arXiv:1407.4222 [hep-ex]
13. ATLAS Collaboration, Fiducial and differential cross sections of Higgs boson production measured in the four-lepton decay channel in pp collisions at $\sqrt{s}$= 8 TeV with the ATLAS detector. Phys. Lett. B **738**, 234 (2014). arXiv:1408.3226 [hep-ex]
14. E. Accomando et al., Workshop on CP studies and non-standard Higgs physics (2006). arXiv:hep-ph/0608079 [hep-ph]
15. M.S. Carena et al., CP violating MSSM Higgs bosons in the light of LEP-2. Phys. Lett. B **495**, 155–163 (2000). arXiv:hep-ph/0009212 [hep-ph]
16. J.F. Gunion et al., The Higgs Hunter's guide. Front. Phys. **80**, 1–448 (2000)
17. ATLAS Collaboration, The ATLAS experiment at the CERN large hadron collider. JINST **3**, S08003 (2008)
18. P. Nason, A new method for combining NLO QCD with shower Monte Carlo algorithms. JHEP **0411**, 040 (2004). arXiv:hep-ph/0409146 [hep-ph]
19. M.L. Mangano et al., ALPGEN, a generator for hard multiparton processes in hadronic collisions. JHEP **0307**, 001 (2003). arXiv:hep-ph/0206293 [hep-ph]
20. T. Gleisberg et al., Event generation with SHERPA 1.1. JHEP **0902**, 007 (2009). arXiv:0811.4622 [hep-ph]
21. B.P. Kersevan, E. Richter-Was, The Monte Carlo event generator AcerMC versions 2.0 to 3.8 with interfaces to PYTHIA 6.4, HERWIG 6.5 and ARIADNE 4.1. Comput. Phys. Commun. **184**, 919–985 (2013). arXiv:hep-ph/0405247 [hep-ph]
22. N. Kauer, Interference effects for H $\to$ WW/ZZ $\to$ $\ell\bar{\nu}_\ell\bar{\ell}\nu_\ell$ searches in gluon fusion at the LHC. JHEP **1312**, 082 (2013). arXiv:1310.7011 [hep-ph]
23. T. Sjostrand, S. Mrenna, P.Z. Skands, PYTHIA 6.4 physics and manual. JHEP **0605**, 026 (2006). arXiv:hep-ph/0603175 [hep-ph]
24. T. Sjostrand, S. Mrenna, P.Z. Skands, A brief introduction to PYTHIA 8.1. Comput. Phys. Commun. **178**, 852–867 (2008). arXiv:0710.3820 [hep-ph]
25. G. Corcella et al., HERWIG 6: an event generator for hadron emission reactions with interfering gluons (including supersymmetric processes). JHEP **0101**, 010 (2001). arXiv:hep-ph/0011363 [hep-ph]
26. J. Butterworth, J.R. Forshaw, M. Seymour, Multiparton interactions in photoproduction at HERA. Z. Phys. C **72**, 637–646 (1996). arXiv:hep-ph/9601371 [hep-ph]
27. H.-L. Lai et al., New parton distributions for collider physics. Phys. Rev. D **82**, 074024 (2010). arXiv:1007.2241 [hep-ph]
28. P.M. Nadolsky et al., Implications of CTEQ global analysis for collider observables. Phys. Rev. D **78**, 013004 (2008). arXiv:0802.0007 [hep-ph]
29. A. Sherstnev, R. Thorne, Parton distributions for LO generators. Eur. Phys. J. C **55**, 553–575 (2008). arXiv:0711.2473 [hep-ph]
30. ATLAS Collaboration, The ATLAS simulation infrastructure. Eur. Phys. J. C **70**, 823–874 (2010). arXiv:1005.4568 [physics.ins-det]
31. S. Agostinelli et al., GEANT4: a simulation toolkit. Nucl. Instrum. Methods A **506**, 250–303 (2003)
32. ATLAS Collaboration, The simulation principle and performance of the ATLAS fast calorimeter simulation FastCaloSim. ATL-PHYS-PUB-2010-013 (2010). http://cds.cern.ch/record/1300517

33. E. Bagnaschi et al., Higgs production via gluon fusion in the POWHEG approach in the SM and in the MSSM. JHEP **1202**, 088 (2012) (Powheg-Box 1.0 r1655). arXiv:1111.2854 [hep-ph]
34. P. Nason, C. Oleari, NLO Higgs boson production via vector-boson fusion matched with shower in POWHEG. JHEP **1002**, 037 (2010) (Powheg-Box 1.0 r1655). arXiv:0911.5299 [hep-ph]
35. D. de Florian et al., Transverse-momentum resummation: Higgs boson production at the Tevatron and the LHC. JHEP **1111**, 064 (2011). arXiv:1109.2109 [hep-ph]
36. M. Grazzini, H. Sargsyan, Heavy-quark mass effects in Higgs boson production at the LHC. JHEP **1309**, 129 (2013). arXiv:1306.4581 [hep-ph]
37. J.M. Campbell, R.K. Ellis, C. Williams, Vector boson pair production at the LHC. JHEP **1107**, 018 (2011). arXiv:1105.0020 [hep-ph]
38. M. Czakon, A. Mitov, Top++: a program for the calculation of the top-pair cross-section at hadron colliders. Comput. Phys. Commun. **185**, 2930 (2014). arXiv:1112.5675 [hep-ph]
39. N. Kidonakis, NNLL resummation for s-channel single top quark production. Phys. Rev. D **81**, 054028 (2010). arXiv:1001.5034 [hep-ph]
40. N. Kidonakis, Next-to-next-to-leading-order collinear and soft gluon corrections for t-channel single top quark production. Phys. Rev. D **83**, 091503 (2011). arXiv:1103.2792 [hep-ph]
41. N. Kidonakis, Two-loop soft anomalous dimensions for single top quark associated production with a W− or H−. Phys. Rev. D **82**, 054018 (2010). arXiv:1005.4451 [hep-ph]
42. T. Melia et al., W+W−, WZ and ZZ production in the POWHEG BOX. JHEP **1111**, 078 (2011) (Powheg-Box 1.0 r1556 for WW, ZZ (r1508 for WZ)). arXiv:1107.5051 [hep-ph]
43. S. Frixione, P. Nason, G. Ridolfi, A positive-weight next-to-leading-order Monte Carlo for heavy flavour hadroproduction. JHEP **0709**, 126 (2007) (Powheg-Box 1.0 r2129). arXiv:0707.3088 [hep-ph]
44. E. Re, Single-top Wt-channel production matched with parton showers using the POWHEG method. Eur. Phys. J. C **71**, 1547 (2011) (Powheg-Box 1.0 r2092). arXiv:1009.2450 [hep-ph]
45. S. Alioli et al., NLO single-top production matched with shower in POWHEG: s- and t-channel contributions. JHEP **0909**, 111 (2009) (Powheg-Box 1.0 r2092). arXiv:0907.4076 [hep-ph]
46. S. Catani et al., Vector boson production at hadron colliders: a fully exclusive QCD calculation at NNLO. Phys. Rev. Lett. **103**, 082001 (2009). arXiv:0903.2120 [hep-ph]
47. ATLAS Collaboration, Calibration of the performance of b-tagging for c and light-flavour jets in the 2012 ATLAS data. ATLAS-CONF-2014-046 (2014). http://cds.cern.ch/record/1741020
48. R.K. Ellis et al., Higgs decay to $\tau^+\tau^-$: a possible signature of intermediate mass Higgs bosons at the SSC. Nucl. Phys. B **297**, 221 (1988)
49. A. Martin et al., Parton distributions for the LHC. Eur. Phys. J. C **63**, 189–285 (2009). arXiv:0901.0002 [hep-ph]
50. R.D. Ball et al., Parton distributions with LHC data. Nucl. Phys. B **867**, 244–289 (2013). arXiv:1207.1303 [hep-ph]
51. G. Cowan et al., Asymptotic formulae for likelihood-based tests of new physics. Eur. Phys. J. C **71**, 1554 (2011). arXiv:1007.1727 [physics.data-an]
52. A.L. Read, Presentation of search results: The CL(s) technique. J. Phys. G **28**, 2693–2704 (2002)
53. ATLAS Collaboration, Improved luminosity determination in pp collisions at $\sqrt{s}$ = 7 TeV using the ATLAS detector at the LHC. Eur. Phys. J. C **73.8**, 2518 (2013). arXiv:1302.4393 [hep-ex]
54. N. Kauer, G. Passarino, Inadequacy of zero-width approximation for a light Higgs boson signal. JHEP **1208**, 116 (2012). arXiv:1206.4803 [hep-ph]

ATLAS Collaboration

G. Aad[85], B. Abbott[113], J. Abdallah[152], O. Abdinov[11], R. Aben[107], M. Abolins[90], O. S. AbouZeid[159], H. Abramowicz[154], H. Abreu[153], R. Abreu[30], Y. Abulaiti[147a,147b], B. S. Acharya[165a,165a,b], L. Adamczyk[38a], D. L. Adams[25], J. Adelman[108], S. Adomeit[100], T. Adye[131], A. A. Affolder[74], T. Agatonovic-Jovin[13], J. A. Aguilar-Saavedra[126a,126f], M. Agustoni[17], S. P. Ahlen[22], F. Ahmadov[65,b], G. Aielli[134a,134b], H. Akerstedt[147a,147b], T. P. A. Åkesson[81], G. Akimoto[156], A. V. Akimov[96], G. L. Alberghi[20a,20b], J. Albert[170], S. Albrand[55], M. J. Alconada Verzini[71], M. Aleksa[30], I. N. Aleksandrov[65], C. Alexa[26a], G. Alexander[154], T. Alexopoulos[10], M. Alhroob[113], G. Alimonti[91a], L. Alio[85], J. Alison[31], S. P. Alkire[35], B. M. M. Allbrooke[18], P. P. Allport[74], A. Aloisio[104a,104b], A. Alonso[36], F. Alonso[71], C. Alpigiani[76], A. Altheimer[35], B. Alvarez Gonzalez[90], D. Álvarez Piqueras[168], M. G. Alviggi[104a,104b], K. Amako[66], Y. Amaral Coutinho[24a], C. Amelung[23], D. Amidei[89], S. P. Amor Dos Santos[126a,126c], A. Amorim[126a,126b], S. Amoroso[48], N. Amram[154], G. Amundsen[23], C. Anastopoulos[140], L. S. Ancu[49], N. Andari[30], T. Andeen[35], C. F. Anders[58b], G. Anders[30], K. J. Anderson[31], A. Andreazza[91a,91b], V. Andrei[58a], S. Angelidakis[9], I. Angelozzi[107], P. Anger[44], A. Angerami[35], F. Anghinolfi[30], A. V. Anisenkov[109,c], N. Anjos[12], A. Annovi[124a,124b], M. Antonelli[47], A. Antonov[98], J. Antos[145b], F. Anulli[133a], M. Aoki[66], L. Aperio Bella[18], G. Arabidze[90], Y. Arai[66], J. P. Araque[126a], A. T. H. Arce[45], F. A Arduh[71], J.-F. Arguin[95], S. Argyropoulos[42], M. Arik[19a], A. J. Armbruster[30], O. Arnaez[30], V. Arnal[82], H. Arnold[48], M. Arratia[28], O. Arslan[21], A. Artamonov[97], G. Artoni[23], S. Asai[156], N. Asbah[42], A. Ashkenazi[154], B. Åsman[147a,147b], L. Asquith[150], K. Assamagan[25], R. Astalos[145a], M. Atkinson[166], N. B. Atlay[142], B. Auerbach[6], K. Augsten[128], M. Aurousseau[146b], G. Avolio[30], B. Axen[15], M. K. Ayoub[117], G. Azuelos[95,d], M. A. Baak[30], A. E. Baas[58a], C. Bacci[135a,135b], H. Bachacou[137], K. Bachas[155], M. Backes[30], M. Backhaus[30], E. Badescu[26a], P. Bagiacchi[133a,133b], P. Bagnaia[133a,133b], Y. Bai[33a], T. Bain[35], J. T. Baines[131], O. K. Baker[177], P. Balek[129], T. Balestri[149], F. Balli[84], E. Banas[39], Sw. Banerjee[174], A. A. E. Bannoura[176], H. S. Bansil[18], L. Barak[30], S. P. Baranov[96], E. L. Barberio[88], D. Barberis[50a,50b], M. Barbero[85], T. Barillari[101], M. Barisonzi[165a,165b], T. Barklow[144], N. Barlow[28], S. L. Barnes[84], B. M. Barnett[131], R. M. Barnett[15], Z. Barnovska[5], A. Baroncelli[135a], G. Barone[49], A. J. Barr[120], F. Barreiro[82], J. Barreiro Guimarães da Costa[57], R. Bartoldus[144], A. E. Barton[72], P. Bartos[145a], A. Bassalat[117], A. Basye[166], R. L. Bates[53], S. J. Batista[159], J. R. Batley[28], M. Battaglia[138], M. Bauce[133a,133b],

F. Bauer[137], H. S. Bawa[144,e], J. B. Beacham[111], M. D. Beattie[72], T. Beau[80], P. H. Beauchemin[162], R. Beccherle[124a,124b], P. Bechtle[21], H. P. Beck[17,f], K. Becker[120], M. Becker[83], S. Becker[100], M. Beckingham[171], C. Becot[117], A. J. Beddall[19c], A. Beddall[19c], V. A. Bednyakov[65], C. P. Bee[149], L. J. Beemster[107], T. A. Beermann[176], M. Begel[25], J. K. Behr[120], C. Belanger-Champagne[87], P. J. Bell[49], W. H. Bell[49], G. Bella[154], L. Bellagamba[20a], A. Bellerive[29], M. Bellomo[86], K. Belotskiy[98], O. Beltramello[30], O. Benary[154], D. Benchekroun[136a], M. Bender[100], K. Bendtz[147a,147b], N. Benekos[10], Y. Benhammou[154], E. Benhar Noccioli[49], J. A. Benitez Garcia[160b], D. P. Benjamin[45], J. R. Bensinger[23], S. Bentvelsen[107], L. Beresford[120], M. Beretta[47], D. Berge[107], E. Bergeaas Kuutmann[167], N. Berger[5], F. Berghaus[170], J. Beringer[15], C. Bernard[22], N. R. Bernard[86], C. Bernius[110], F. U. Bernlochner[21], T. Berry[77], P. Berta[129], C. Bertella[83], G. Bertoli[147a,147b], F. Bertolucci[124a,124b], C. Bertsche[113], D. Bertsche[113], M. I. Besana[91a], G. J. Besjes[106], O. Bessidskaia Bylund[147a,147b], M. Bessner[42], N. Besson[137], C. Betancourt[48], S. Bethke[101], A. J. Beven[76], W. Bhimji[46], R. M. Bianchi[125], L. Bianchini[23], M. Bianco[30], O. Biebel[100], S. P. Bieniek[78], M. Biglietti[135a], J. Bilbao De Mendizabal[49], H. Bilokon[47], M. Bindi[54], S. Binet[117], A. Bingul[19c], C. Bini[133a,133b], C. W. Black[151], J. E. Black[144], K. M. Black[22], D. Blackburn[139], R. E. Blair[6], J.-B. Blanchard[137], J.E. Blanco[77], T. Blazek[145a], I. Bloch[42], C. Blocker[23], W. Blum[83,*], U. Blumenschein[54], G. J. Bobbink[107], V. S. Bobrovnikov[109,c], S. S. Bocchetta[81], A. Bocci[45], C. Bock[100], M. Boehler[48], J. A. Bogaerts[30], A. G. Bogdanchikov[109], C. Bohm[147a], V. Boisvert[77], T. Bold[38a], V. Boldea[26a], A. S. Boldyrev[99], M. Bomben[80], M. Bona[76], M. Boonekamp[137], A. Borisov[130], G. Borissov[72], S. Borroni[42], J. Bortfeldt[100], V. Bortolotto[60a,60b,60c], K. Bos[107], D. Boscherini[20a], M. Bosman[12], J. Boudreau[125], J. Bouffard[2], E. V. Bouhova-Thacker[72], D. Boumediene[34], C. Bourdarios[117], N. Bousson[114], A. Boveia[30], J. Boyd[30], I. R. Boyko[65], I. Bozic[13], J. Bracinik[18], A. Brandt[8], G. Brandt[15], O. Brandt[58a], U. Bratzler[157], B. Brau[86], J. E. Brau[116], H. M. Braun[176,*], S. F. Brazzale[165a,165c], K. Brendlinger[122], A. J. Brennan[88], L. Brenner[107], R. Brenner[167], S. Bressler[173], K. Bristow[146c], T. M. Bristow[46], D. Britton[53], D. Britzger[42], F. M. Brochu[28], I. Brock[21], R. Brock[90], J. Bronner[101], G. Brooijmans[35], T. Brooks[77], W. K. Brooks[32b], J. Brosamer[15], E. Brost[116], J. Brown[55], P. A. Bruckman de Renstrom[39], D. Bruncko[145b], R. Bruneliere[48], A. Bruni[20a], G. Bruni[20a], M. Bruschi[20a], L. Bryngemark[81], T. Buanes[14], Q. Buat[143], P. Buchholz[142], A. G. Buckley[53], S. I. Buda[26a], I. A. Budagov[65], F. Buehrer[48], L. Bugge[119], M. K. Bugge[119], O. Bulekov[98], H. Burckhart[30], S. Burdin[74], B. Burghgrave[108], S. Burke[131], I. Burmeister[43], E. Busato[34], D. Büscher[48], V. Büscher[83], P. Bussey[53], C. P. Buszello[167], J. M. Butler[22], A. I. Butt[3], C. M. Buttar[53], J. M. Butterworth[78], P. Butti[107], W. Buttinger[25], A. Buzatu[53], R. Buzykaev[109,c], S. Cabrera Urbán[168], D. Caforio[128], O. Cakir[4a], P. Calafiura[15], A. Calandri[137], G. Calderini[80], P. Calfayan[100], L. P. Caloba[24a], D. Calvet[34], S. Calvet[34], R. Camacho Toro[49], S. Camarda[42], D. Cameron[119], L. M. Caminada[15], R. Caminal Armadans[12], S. Campana[30], M. Campanelli[78], A. Campoverde[149], V. Canale[104a,104b], A. Canepa[160a], M. Cano Bret[76], J. Cantero[82], R. Cantrill[126a], T. Cao[40], M. D. M. Capeans Garrido[30], I. Caprini[26a], M. Caprini[26a], M. Capua[37a,37b], R. Caputo[83], R. Cardarelli[134a], T. Carli[30], G. Carlino[104a], L. Carminati[91a,91b], S. Caron[106], E. Carquin[32a], G. D. Carrillo-Montoya[8], J. R. Carter[28], J. Carvalho[126a,126c], D. Casadei[78], M. P. Casado[12], M. Casolino[12], E. Castaneda-Miranda[146b], A. Castelli[107], V. Castillo Gimenez[168], N. F. Castro[126a,g], P. Catastini[57], A. Catinaccio[30], J. R. Catmore[119], A. Cattai[30], J. Caudron[83], V. Cavaliere[166], D. Cavalli[91a], M. Cavalli-Sforza[12], V. Cavasinni[124a,124b], F. Ceradini[135a,135b], B. Cerio[45], K. Cerny[129], A. S. Cerqueira[24b], A. Cerri[150], L. Cerrito[76], F. Cerutti[15], M. Cerv[30], A. Cervelli[17], S. A. Cetin[19b], A. Chafaq[136a], D. Chakraborty[108], I. Chalupkova[129], P. Chang[166], B. Chapleau[87], J. D. Chapman[28], D. G. Charlton[18], C. C. Chau[159], C. A. Chavez Barajas[150], S. Cheatham[153], A. Chegwidden[90], S. Chekanov[6], S. V. Chekulaev[160a], G. A. Chelkov[65,h], M. A. Chelstowska[89], C. Chen[64], H. Chen[25], K. Chen[149], L. Chen[33d,i], S. Chen[33c], X. Chen[33f], Y. Chen[67], H. C. Cheng[89], Y. Cheng[31], A. Cheplakov[65], E. Cheremushkina[130], R. Cherkaoui El Moursli[136e], V. Chernyatin[25,*], E. Cheu[7], L. Chevalier[137], V. Chiarella[47], J. T. Childers[6], G. Chiodini[73a], A. S. Chisholm[18], R. T. Chislett[78], A. Chitan[26a], M. V. Chizhov[65], K. Choi[61], S. Chouridou[9], B. K. B. Chow[100], V. Christodoulou[78], D. Chromek-Burckhart[30], M. L. Chu[152], J. Chudoba[127], A. J. Chuinard[87], J. J. Chwastowski[39], L. Chytka[115], G. Ciapetti[133a,133b], A. K. Ciftci[4a], D. Cinca[53], V. Cindro[75], I. A. Cioara[21], A. Ciocio[15], Z. H. Citron[173], M. Ciubancan[26a], A. Clark[49], B. L. Clark[57], P. J. Clark[46], R. N. Clarke[15], W. Cleland[125], C. Clement[147a,147b], Y. Coadou[85], M. Cobal[165a,165c], A. Coccaro[139], J. Cochran[64], L. Coffey[23], J. G. Cogan[144], B. Cole[35], S. Cole[108], A. P. Colijn[107], J. Collot[55], T. Colombo[58c], G. Compostella[101], P. Conde Muiño[126a,126b], E. Coniavitis[48], S. H. Connell[146b], I. A. Connelly[77], S. M. Consonni[91a,91b], V. Consorti[48], S. Constantinescu[26a], C. Conta[121a,121b], G. Conti[30], F. Conventi[104a,j], M. Cooke[15], B. D. Cooper[78], A. M. Cooper-Sarkar[120], K. Copic[15], T. Cornelissen[176], M. Corradi[20a], F. Corriveau[87,k], A. Corso-Radu[164], A. Cortes-Gonzalez[12], G. Cortiana[101], G. Costa[91a], M. J. Costa[168], D. Costanzo[140], D. Côté[8], G. Cottin[28], G. Cowan[77], B. E. Cox[84], K. Cranmer[110], G. Cree[29], S. Crépé-Renaudin[55], F. Crescioli[80], W. A. Cribbs[147a,147b], M. Crispin Ortuzar[120], M. Cristinziani[21], V. Croft[106], G. Crosetti[37a,37b], T. Cuhadar Donszelmann[140], J. Cummings[177], M. Curatolo[47], C. Cuthbert[151], H. Czirr[142], P. Czodrowski[3], S. D'Auria[53], M. D'Onofrio[74], M. J. Da Cunha Sargedas De Sousa[126a,126b], C. Da Via[84], W. Dabrowski[38a], A. Dafinca[120], T. Dai[89], O. Dale[14], F. Dallaire[95], C. Dallapiccola[86], M. Dam[36], J. R. Dandoy[31],

A. C. Daniells[18], M. Danninger[169], M. Dano Hoffmann[137], V. Dao[48], G. Darbo[50a], S. Darmora[8], J. Dassoulas[3], A. Dattagupta[61], W. Davey[21], C. David[170], T. Davidek[129], E. Davies[120,l], M. Davies[154], P. Davison[78], Y. Davygora[58a], E. Dawe[88], I. Dawson[140], R. K. Daya-Ishmukhametova[86], K. De[8], R. de Asmundis[104a], S. De Castro[20a,20b], S. De Cecco[80], N. De Groot[106], P. de Jong[107], H. De la Torre[82], F. De Lorenzi[64], L. De Nooij[107], D. De Pedis[133a], A. De Salvo[133a], U. De Sanctis[150], A. De Santo[150], J. B. De Vivie De Regie[117], W. J. Dearnaley[72], R. Debbe[25], C. Debenedetti[138], D. V. Dedovich[65], I. Deigaard[107], J. Del Peso[82], T. Del Prete[124a,124b], D. Delgove[117], F. Deliot[137], C. M. Delitzsch[49], M. Deliyergiyev[75], A. Dell'Acqua[30], L. Dell'Asta[22], M. Dell'Orso[124a,124b], M. Della Pietra[104a,j], D. della Volpe[49], M. Delmastro[5], P. A. Delsart[55], C. Deluca[107], D. A. DeMarco[159], S. Demers[177], M. Demichev[65], A. Demilly[80], S. P. Denisov[130], D. Derendarz[39], J. E. Derkaoui[136d], F. Derue[80], P. Dervan[74], K. Desch[21], C. Deterre[42], P. O. Deviveiros[30], A. Dewhurst[131], S. Dhaliwal[107], A. Di Ciaccio[134a,134b], L. Di Ciaccio[5], A. Di Domenico[133a,133b], C. Di Donato[104a,104b], A. Di Girolamo[30], B. Di Girolamo[30], A. Di Mattia[153], B. Di Micco[135a,135b], R. Di Nardo[47], A. Di Simone[48], R. Di Sipio[159], D. Di Valentino[29], C. Diaconu[85], M. Diamond[159], F. A. Dias[46], M. A. Diaz[32a], E. B. Diehl[89], J. Dietrich[16], S. Diglio[85], A. Dimitrievska[13], J. Dingfelder[21], F. Dittus[30], F. Djama[85], T. Djobava[51b], J. I. Djuvsland[58a], M. A. B. do Vale[24c], D. Dobos[30], M. Dobre[26a], C. Doglioni[49], T. Dohmae[156], J. Dolejsi[129], Z. Dolezal[129], B. A. Dolgoshein[98,*], M. Donadelli[24d], S. Donati[124a,124b], P. Dondero[121a,121b], J. Donini[34], J. Dopke[131], A. Doria[104a], M. T. Dova[71], A. T. Doyle[53], E. Drechsler[54], M. Dris[10], E. Dubreuil[34], E. Duchovni[173], G. Duckeck[100], O. A. Ducu[26a,85], D. Duda[176], A. Dudarev[30], L. Duflot[117], L. Duguid[77], M. Dührssen[30], M. Dunford[58a], H. Duran Yildiz[4a], M. Düren[52], A. Durglishvili[51b], D. Duschinger[44], M. Dwuznik[38a], M. Dyndal[38a], C. Eckardt[42], K. M. Ecker[101], W. Edson[2], N. C. Edwards[46], W. Ehrenfeld[21], T. Eifert[30], G. Eigen[14], K. Einsweiler[15], T. Ekelof[167], M. El Kacimi[136c], M. Ellert[167], S. Elles[5], F. Ellinghaus[83], A. A. Elliot[170], N. Ellis[30], J. Elmsheuser[100], M. Elsing[30], D. Emeliyanov[131], Y. Enari[156], O. C. Endner[83], M. Endo[118], R. Engelmann[149], J. Erdmann[43], A. Ereditato[17], G. Ernis[176], J. Ernst[2], M. Ernst[25], S. Errede[166], E. Ertel[83], M. Escalier[117], H. Esch[43], C. Escobar[125], B. Esposito[47], A. I. Etienvre[137], E. Etzion[154], H. Evans[61], A. Ezhilov[123], L. Fabbri[20a,20b], G. Facini[31], R. M. Fakhrutdinov[130], S. Falciano[133a], R. J. Falla[78], J. Faltova[129], Y. Fang[33a], M. Fanti[91a,91b], A. Farbin[8], A. Farilla[135a], T. Farooque[12], S. Farrell[15], S. M. Farrington[171], P. Farthouat[30], F. Fassi[136e], P. Fassnacht[30], D. Fassouliotis[9], A. Favareto[50a,50b], L. Fayard[117], P. Federic[145a], O. L. Fedin[123,m], W. Fedorko[169], S. Feigl[30], L. Feligioni[85], C. Feng[33d], E. J. Feng[6], H. Feng[89], A. B. Fenyuk[130], P. Fernandez Martinez[168], S. Fernandez Perez[30], S. Ferrag[53], J. Ferrando[53], A. Ferrari[167], P. Ferrari[107], R. Ferrari[121a], D. E. Ferreira de Lima[53], A. Ferrer[168], D. Ferrere[49], C. Ferretti[89], A. Ferretto Parodi[50a,50b], M. Fiascaris[31], F. Fiedler[83], A. Filipčič[75], M. Filipuzzi[42], F. Filthaut[106], M. Fincke-Keeler[170], K. D. Finelli[151], M. C. N. Fiolhais[126a,126c], L. Fiorini[168], A. Firan[40], A. Fischer[2], C. Fischer[12], J. Fischer[176], W. C. Fisher[90], E. A. Fitzgerald[23], M. Flechl[48], I. Fleck[142], P. Fleischmann[89], S. Fleischmann[176], G. T. Fletcher[140], G. Fletcher[76], T. Flick[176], A. Floderus[81], L. R. Flores Castillo[60a], M. J. Flowerdew[101], A. Formica[137], A. Forti[84], D. Fournier[117], H. Fox[72], S. Fracchia[12], P. Francavilla[80], M. Franchini[20a,20b], D. Francis[30], L. Franconi[119], M. Franklin[57], M. Fraternali[121a,121b], D. Freeborn[78], S. T. French[28], F. Friedrich[44], D. Froidevaux[30], J. A. Frost[120], C. Fukunaga[157], E. Fullana Torregrosa[83], B. G. Fulsom[144], J. Fuster[168], C. Gabaldon[55], O. Gabizon[176], A. Gabrielli[20a,20b], A. Gabrielli[133a,133b], S. Gadatsch[107], S. Gadomski[49], G. Gagliardi[50a,50b], P. Gagnon[61], C. Galea[106], B. Galhardo[126a,126c], E. J. Gallas[120], B. J. Gallop[131], P. Gallus[128], G. Galster[36], K. K. Gan[111], J. Gao[33b,85], Y. Gao[46], Y. S. Gao[144,e], F. M. Garay Walls[46], F. Garberson[177], C. García[168], J. E. García Navarro[168], M. Garcia-Sciveres[15], R. W. Gardner[31], N. Garelli[144], V. Garonne[119], C. Gatti[47], A. Gaudiello[50a,50b], G. Gaudio[121a], B. Gaur[142], L. Gauthier[95], P. Gauzzi[133a,133b], I. L. Gavrilenko[96], C. Gay[169], G. Gaycken[21], E. N. Gazis[10], P. Ge[33d], Z. Gecse[169], C. N. P. Gee[131], D. A. A. Geerts[107], Ch. Geich-Gimbel[21], M. P. Geisler[58a], C. Gemme[50a], M. H. Genest[55], S. Gentile[133a,133b], M. George[54], S. George[77], D. Gerbaudo[164], A. Gershon[154], H. Ghazlane[136b], N. Ghodbane[34], B. Giacobbe[20a], S. Giagu[133a,133b], V. Giangiobbe[12], P. Giannetti[124a,124b], B. Gibbard[25], S. M. Gibson[77], M. Gilchriese[15], T. P. S. Gillam[28], D. Gillberg[30], G. Gilles[34], D. M. Gingrich[3,d], N. Giokaris[9], M. P. Giordani[165a,165c], F. M. Giorgi[20a], F. M. Giorgi[16], P. F. Giraud[137], P. Giromini[47], D. Giugni[91a], C. Giuliani[48], M. Giulini[58b], B. K. Gjelsten[119], S. Gkaitatzis[155], I. Gkialas[155], E. L. Gkougkousis[117], L. K. Gladilin[99], C. Glasman[82], J. Glatzer[30], P. C. F. Glaysher[46], A. Glazov[42], G. L. Glonti[62], M. Goblirsch-Kolb[101], J. R. Goddard[76], J. Godlewski[39], S. Goldfarb[89], T. Golling[49], D. Golubkov[130], A. Gomes[126a,126b,126d], R. Gonçalo[126a], J. Goncalves Pinto Firmino Da Costa[137], L. Gonella[21], S. González de la Hoz[168], G. Gonzalez Parra[12], S. Gonzalez-Sevilla[49], L. Goossens[30], P. A. Gorbounov[97], H. A. Gordon[25], I. Gorelov[105], B. Gorini[30], E. Gorini[73a,73b], A. Gorišek[75], E. Gornicki[39], A. T. Goshaw[45], C. Gössling[43], M. I. Gostkin[65], D. Goujdami[136c], A. G. Goussiou[139], N. Govender[146b], H. M. X. Grabas[138], L. Graber[54], I. Grabowska-Bold[38a], P. Grafström[20a,20b], K-J. Grahn[42], J. Gramling[49], E. Gramstad[119], S. Grancagnolo[16], V. Grassi[149], V. Gratchev[123], H. M. Gray[30], E. Graziani[135a], Z. D. Greenwood[79,n], K. Gregersen[78], I. M. Gregor[42], P. Grenier[144], J. Griffiths[8], A. A. Grillo[138], K. Grimm[72], S. Grinstein[12,o], Ph. Gris[34], Y. V. Grishkevich[99], J.-F. Grivaz[117], J. P. Grohs[44], A. Grohsjean[42], E. Gross[173],

J. Grosse-Knetter[54], G. C. Grossi[134a,134b], Z. J. Grout[150], L. Guan[33b], J. Guenther[128], F. Guescini[49], D. Guest[177], O. Gueta[154], E. Guido[50a,50b], T. Guillemin[117], S. Guindon[2], U. Gul[53], C. Gumpert[44], J. Guo[33e], S. Gupta[120], P. Gutierrez[113], N. G. Gutierrez Ortiz[53], C. Gutschow[44], C. Guyot[137], C. Gwenlan[120], C. B. Gwilliam[74], A. Haas[110], C. Haber[15], H. K. Hadavand[8], N. Haddad[136e], P. Haefner[21], S. Hageböck[21], Z. Hajduk[39], H. Hakobyan[178], M. Haleem[42], J. Haley[114], D. Hall[120], G. Halladjian[90], G. D. Hallewell[85], K. Hamacher[176], P. Hamal[115], K. Hamano[170], M. Hamer[54], A. Hamilton[146a], S. Hamilton[162], G. N. Hamity[146c], P. G. Hamnett[42], L. Han[33b], K. Hanagaki[118], K. Hanawa[156], M. Hance[15], P. Hanke[58a], R. Hanna[137], J. B. Hansen[36], J. D. Hansen[36], M. C. Hansen[21], P. H. Hansen[36], K. Hara[161], A. S. Hard[174], T. Harenberg[176], F. Hariri[117], S. Harkusha[92], R. D. Harrington[46], P. F. Harrison[171], F. Hartjes[107], M. Hasegawa[67], S. Hasegawa[103], Y. Hasegawa[141], A. Hasib[113], S. Hassani[137], S. Haug[17], R. Hauser[90], L. Hauswald[44], M. Havranek[127], C. M. Hawkes[18], R. J. Hawkings[30], A. D. Hawkins[81], T. Hayashi[161], D. Hayden[90], C. P. Hays[120], J. M. Hays[76], H. S. Hayward[74], S. J. Haywood[131], S. J. Head[18], T. Heck[83], V. Hedberg[81], L. Heelan[8], S. Heim[122], T. Heim[176], B. Heinemann[15], L. Heinrich[110], J. Hejbal[127], L. Helary[22], S. Hellman[147a,147b], D. Hellmich[21], C. Helsens[30], J. Henderson[120], R. C. W. Henderson[72], Y. Heng[174], C. Hengler[42], A. Henrichs[177], A. M. Henriques Correia[30], S. Henrot-Versille[117], G. H. Herbert[16], Y. Hernández Jiménez[168], R. Herrberg-Schubert[16], G. Herten[48], R. Hertenberger[100], L. Hervas[30], G. G. Hesketh[78], N. P. Hessey[107], J. W. Hetherly[40], R. Hickling[76], E. Higón-Rodriguez[168], E. Hill[170], J. C. Hill[28], K. H. Hiller[42], S. J. Hillier[18], I. Hinchliffe[15], E. Hines[122], R. R. Hinman[15], M. Hirose[158], D. Hirschbuehl[176], J. Hobbs[149], N. Hod[107], M. C. Hodgkinson[140], P. Hodgson[140], A. Hoecker[30], M. R. Hoeferkamp[105], F. Hoenig[100], M. Hohlfeld[83], D. Hohn[21], T. R. Holmes[15], T. M. Hong[122], L. Hooft van Huysduynen[110], W. H. Hopkins[116], Y. Horii[103], A. J. Horton[143], J-Y. Hostachy[55], S. Hou[152], A. Hoummada[136a], J. Howard[120], J. Howarth[42], M. Hrabovsky[115], I. Hristova[16], J. Hrivnac[117], T. Hryn'ova[5], A. Hrynevich[93], C. Hsu[146c], P. J. Hsu[152,p], S.-C. Hsu[139], D. Hu[35], Q. Hu[33b], X. Hu[89], Y. Huang[42], Z. Hubacek[30], F. Hubaut[85], F. Huegging[21], T. B. Huffman[120], E. W. Hughes[35], G. Hughes[72], M. Huhtinen[30], T. A. Hülsing[83], N. Huseynov[65,b], J. Huston[90], J. Huth[57], G. Iacobucci[49], G. Iakovidis[25], I. Ibragimov[142], L. Iconomidou-Fayard[117], E. Ideal[177], Z. Idrissi[136e], P. Iengo[30], O. Igonkina[107], T. Iizawa[172], Y. Ikegami[66], K. Ikematsu[142], M. Ikeno[66], Y. Ilchenko[31,q], D. Iliadis[155], N. Ilic[159], Y. Inamaru[67], T. Ince[101], P. Ioannou[9], M. Iodice[135a], K. Iordanidou[9], V. Ippolito[57], A. Irles Quiles[168], C. Isaksson[167], M. Ishino[68], M. Ishitsuka[158], R. Ishmukhametov[111], C. Issever[120], S. Istin[19a], J. M. Iturbe Ponce[84], R. Iuppa[134a,134b], J. Ivarsson[81], W. Iwanski[39], H. Iwasaki[66], J. M. Izen[41], V. Izzo[104a], S. Jabbar[3], B. Jackson[122], M. Jackson[74], P. Jackson[1], M. R. Jaekel[30], V. Jain[2], K. Jakobs[48], S. Jakobsen[30], T. Jakoubek[127], J. Jakubek[128], D. O. Jamin[152], D. K. Jana[79], E. Jansen[78], R. W. Jansky[62], J. Janssen[21], M. Janus[171], G. Jarlskog[81], N. Javadov[65,b], T. Javůrek[48], L. Jeanty[15], J. Jejelava[51a,r], G.-Y. Jeng[151], D. Jennens[88], P. Jenni[48,s], J. Jentzsch[43], C. Jeske[171], S. Jézéquel[5], H. Ji[174], J. Jia[149], Y. Jiang[33b], S. Jiggins[78], J. Jimenez Pena[168], S. Jin[33a], A. Jinaru[26a], O. Jinnouchi[158], M. D. Joergensen[36], P. Johansson[140], K. A. Johns[7], K. Jon-And[147a,147b], G. Jones[171], R. W. L. Jones[72], T. J. Jones[74], J. Jongmanns[58a], P. M. Jorge[126a,126b], K. D. Joshi[84], J. Jovicevic[160a], X. Ju[174], C. A. Jung[43], P. Jussel[62], A. Juste Rozas[12,o], M. Kaci[168], A. Kaczmarska[39], M. Kado[117], H. Kagan[111], M. Kagan[144], S. J. Kahn[85], E. Kajomovitz[45], C. W. Kalderon[120], S. Kama[40], A. Kamenshchikov[130], N. Kanaya[156], M. Kaneda[30], S. Kaneti[28], V. A. Kantserov[98], J. Kanzaki[66], B. Kaplan[110], A. Kapliy[31], D. Kar[53], K. Karakostas[10], A. Karamaoun[3], N. Karastathis[10,107], M. J. Kareem[54], M. Karnevskiy[83], S. N. Karpov[65], Z. M. Karpova[65], K. Karthik[110], V. Kartvelishvili[72], A. N. Karyukhin[130], L. Kashif[174], R. D. Kass[111], A. Kastanas[14], Y. Kataoka[156], A. Katre[49], J. Katzy[42], K. Kawagoe[70], T. Kawamoto[156], G. Kawamura[54], S. Kazama[156], V. F. Kazanin[109,c], M. Y. Kazarinov[65], R. Keeler[170], R. Kehoe[40], M. Keil[54], J. S. Keller[42], J. J. Kempster[77], H. Keoshkerian[84], O. Kepka[127], B. P. Kerševan[75], S. Kersten[176], R. A. Keyes[87], F. Khalil-zada[11], H. Khandanyan[147a,147b], A. Khanov[114], A.G. Kharlamov[109,c], T. J. Khoo[28], G. Khoriauli[21], V. Khovanskiy[97], E. Khramov[65], J. Khubua[51b,t], H. Y. Kim[8], H. Kim[147a,147b], S. H. Kim[161], Y. Kim[31], N. Kimura[155], O. M. Kind[16], B. T. King[74], M. King[168], R. S. B. King[120], S. B. King[169], J. Kirk[131], A. E. Kiryunin[101], T. Kishimoto[67], D. Kisielewska[38a], F. Kiss[48], K. Kiuchi[161], O. Kivernyk[137], E. Kladiva[145b], M. H. Klein[35], M. Klein[74], U. Klein[74], K. Kleinknecht[83], P. Klimek[147a,147b], A. Klimentov[25], R. Klingenberg[43], J. A. Klinger[84], T. Klioutchnikova[30], P. F. Klok[106], E.-E. Kluge[58a], P. Kluit[107], S. Kluth[101], E. Kneringer[62], E. B. F. G. Knoops[85], A. Knue[53], D. Kobayashi[158], T. Kobayashi[156], M. Kobel[44], M. Kocian[144], P. Kodys[129], T. Koffas[29], E. Koffeman[107], L. A. Kogan[120], S. Kohlmann[176], Z. Kohout[128], T. Kohriki[66], T. Koi[144], H. Kolanoski[16], I. Koletsou[5], A. A. Komar[96,*], Y. Komori[156], T. Kondo[66], N. Kondrashova[42], K. Köneke[48], A. C. König[106], S. König[83], T. Kono[66,u], R. Konoplich[110,v], N. Konstantinidis[78], R. Kopeliansky[153], S. Koperny[38a], L. Köpke[83], A. K. Kopp[48], K. Korcyl[39], K. Kordas[155], A. Korn[78], A. A. Korol[109,c], I. Korolkov[12], E. V. Korolkova[140], O. Kortner[101], S. Kortner[101], T. Kosek[129], V. V. Kostyukhin[21], V. M. Kotov[65], A. Kotwal[45], A. Kourkoumeli-Charalampidi[155], C. Kourkoumelis[9], V. Kouskoura[25], A. Koutsman[160a], R. Kowalewski[170], T. Z. Kowalski[38a], W. Kozanecki[137], A. S. Kozhin[130], V. A. Kramarenko[99], G. Kramberger[75], D. Krasnopevtsev[98], M. W. Krasny[80], A. Krasznahorkay[30], J. K. Kraus[21], A. Kravchenko[25], S. Kreiss[110], M. Kretz[58c], J. Kretzschmar[74],

K. Kreutzfeldt[52], P. Krieger[159], K. Krizka[31], K. Kroeninger[43], H. Kroha[101], J. Kroll[122], J. Kroseberg[21], J. Krstic[13], U. Kruchonak[65], H. Krüger[21], N. Krumnack[64], Z. V. Krumshteyn[65], A. Kruse[174], M. C. Kruse[45], M. Kruskal[22], T. Kubota[88], H. Kucuk[78], S. Kuday[4b], S. Kuehn[48], A. Kugel[58c], F. Kuger[175], A. Kuhl[138], T. Kuhl[42], V. Kukhtin[65], Y. Kulchitsky[92], S. Kuleshov[32b], M. Kuna[133a,133b], T. Kunigo[68], A. Kupco[127], H. Kurashige[67], Y. A. Kurochkin[92], R. Kurumida[67], V. Kus[127], E. S. Kuwertz[148], M. Kuze[158], J. Kvita[115], T. Kwan[170], D. Kyriazopoulos[140], A. La Rosa[49], J. L. La Rosa Navarro[24d], L. La Rotonda[37a,37b], C. Lacasta[168], F. Lacava[133a,133b], J. Lacey[29], H. Lacker[16], D. Lacour[80], V. R. Lacuesta[168], E. Ladygin[65], R. Lafaye[5], B. Laforge[80], T. Lagouri[177], S. Lai[48], L. Lambourne[78], S. Lammers[61], C. L. Lampen[7], W. Lampl[7], E. Lançon[137], U. Landgraf[48], M. P. J. Landon[76], V. S. Lang[58a], J. C. Lange[12], A. J. Lankford[164], F. Lanni[25], K. Lantzsch[30], S. Laplace[80], C. Lapoire[30], J. F. Laporte[137], T. Lari[91a], F. Lasagni Manghi[20a,20b], M. Lassnig[30], P. Laurelli[47], W. Lavrijsen[15], A. T. Law[138], P. Laycock[74], O. Le Dortz[80], E. Le Guirriec[85], E. Le Menedeu[12], M. LeBlanc[170], T. LeCompte[6], F. Ledroit-Guillon[55], C. A. Lee[146b], S. C. Lee[152], L. Lee[1], G. Lefebvre[80], M. Lefebvre[170], F. Legger[100], C. Leggett[15], A. Lehan[74], G. Lehmann Miotto[30], X. Lei[7], W. A. Leight[29], A. Leisos[155], A. G. Leister[177], M. A. L. Leite[24d], R. Leitner[129], D. Lellouch[173], B. Lemmer[54], K. J. C. Leney[78], T. Lenz[21], G. Lenzen[176], B. Lenzi[30], R. Leone[7], S. Leone[124a,124b], C. Leonidopoulos[46], S. Leontsinis[10], C. Leroy[95], C. G. Lester[28], M. Levchenko[123], J. Levêque[5], D. Levin[89], L. J. Levinson[173], M. Levy[18], A. Lewis[120], A. M. Leyko[21], M. Leyton[41], B. Li[33b,w], H. Li[149], H. L. Li[31], L. Li[45], L. Li[33e], S. Li[45], Y. Li[33c,x], Z. Liang[138], H. Liao[34], B. Liberti[134a], A. Liblong[159], P. Lichard[30], K. Lie[166], J. Liebal[21], W. Liebig[14], C. Limbach[21], A. Limosani[151], S. C. Lin[152,y], T. H. Lin[83], F. Linde[107], B. E. Lindquist[149], J. T. Linnemann[90], E. Lipeles[122], A. Lipniacka[14], M. Lisovyi[42], T. M. Liss[166], D. Lissauer[25], A. Lister[169], A. M. Litke[138], B. Liu[152], D. Liu[152], J. Liu[85], J. B. Liu[33b], K. Liu[85], L. Liu[166], M. Liu[45], M. Liu[33b], Y. Liu[33b], M. Livan[121a,121b], A. Lleres[55], J. Llorente Merino[82], S. L. Lloyd[76], F. Lo Sterzo[152], E. Lobodzinska[42], P. Loch[7], W. S. Lockman[138], F. K. Loebinger[84], A. E. Loevschall-Jensen[36], A. Loginov[177], T. Lohse[16], K. Lohwasser[42], M. Lokajicek[127], B. A. Long[22], J. D. Long[89], R. E. Long[72], K. A. Looper[111], L. Lopes[126a], D. Lopez Mateos[57], B. Lopez Paredes[140], I. Lopez Paz[12], J. Lorenz[100], N. Lorenzo Martinez[61], M. Losada[163], P. Loscutoff[15], P. J. Lösel[100], X. Lou[33a], A. Lounis[117], J. Love[6], P. A. Love[72], N. Lu[89], H. J. Lubatti[139], C. Luci[133a,133b], A. Lucotte[55], F. Luehring[61], W. Lukas[62], L. Luminari[133a], O. Lundberg[147a,147b], B. Lund-Jensen[148] and M. Lungwitz[83], D. Lynn[25], R. Lysak[127], E. Lytken[81], H. Ma[25], L. L. Ma[33d], G. Maccarrone[47], A. Macchiolo[101], C. M. Macdonald[140], J. Machado Miguens[122,126b], D. Macina[30], D. Madaffari[85], R. Madar[34], H. J. Maddocks[72], W. F. Mader[44], A. Madsen[167], S. Maeland[14], T. Maeno[25], A. Maevskiy[99], E. Magradze[54], K. Mahboubi[48], J. Mahlstedt[107], C. Maiani[137], C. Maidantchik[24a], A. A. Maier[101], T. Maier[100], A. Maio[126a,126b,126d], S. Majewski[116], Y. Makida[66], N. Makovec[117], B. Malaescu[80], Pa. Malecki[39], V. P. Maleev[123], F. Malek[55], U. Mallik[63], D. Malon[6], C. Malone[144], S. Maltezos[10], V. M. Malyshev[109], S. Malyukov[30], J. Mamuzic[42], G. Mancini[47], B. Mandelli[30], L. Mandelli[91a], I. Mandić[75], R. Mandrysch[63], J. Maneira[126a,126b], A. Manfredini[101], L. Manhaes de Andrade Filho[24b], J. Manjarres Ramos[160b], A. Mann[100], P. M. Manning[138], A. Manousakis-Katsikakis[9], B. Mansoulie[137], R. Mantifel[87], M. Mantoani[54], L. Mapelli[30], L. March[146c], G. Marchiori[80], M. Marcisovsky[127], C. P. Marino[170], M. Marjanovic[13], F. Marroquim[24a], S. P. Marsden[84], Z. Marshall[15], L. F. Marti[17], S. Marti-Garcia[168], B. Martin[90], T. A. Martin[171], V. J. Martin[46], B. Martin dit Latour[14], M. Martinez[12,o], S. Martin-Haugh[131], V. S. Martoiu[26a], A. C. Martyniuk[78], M. Marx[139], F. Marzano[133a], A. Marzin[30], L. Masetti[83], T. Mashimo[156], R. Mashinistov[96], J. Masik[84], A. L. Maslennikov[109,c], I. Massa[20a,20b], L. Massa[20a,20b], N. Massol[5], P. Mastrandrea[149], A. Mastroberardino[37a,37b], T. Masubuchi[156], P. Mättig[176], J. Mattmann[83], J. Maurer[26a], S. J. Maxfield[74], D. A. Maximov[109,c], R. Mazini[152], S. M. Mazza[91a,91b], L. Mazzaferro[134a,134b], G. Mc Goldrick[159], S. P. Mc Kee[89], A. McCarn[89], R. L. McCarthy[149], T. G. McCarthy[29], N. A. McCubbin[131], K. W. McFarlane[56,*], J. A. Mcfayden[78], G. Mchedlidze[54], S. J. McMahon[131], R. A. McPherson[170,k], M. Medinnis[42], S. Meehan[146a], S. Mehlhase[100], A. Mehta[74], K. Meier[58a], C. Meineck[100], B. Meirose[41], B. R. Mellado Garcia[146c], F. Meloni[17], A. Mengarelli[20a,20b], S. Menke[101], E. Meoni[162], K. M. Mercurio[57], S. Mergelmeyer[21], P. Mermod[49], L. Merola[104a,104b], C. Meroni[91a], F. S. Merritt[31], A. Messina[133a,133a], J. Metcalfe[25], A. S. Mete[164], C. Meyer[83], C. Meyer[122], J-P. Meyer[137], J. Meyer[107], R. P. Middleton[131], S. Miglioranzi[165a,165c], L. Mijović[21], G. Mikenberg[173], M. Mikestikova[127], M. Mikuž[75], M. Milesi[88], A. Milic[30], D. W. Miller[31], C. Mills[46], A. Milov[173], D. A. Milstead[147a,147b], A. A. Minaenko[130], Y. Minami[156], I. A. Minashvili[65], A. I. Mincer[110], B. Mindur[38a], M. Mineev[65], Y. Ming[174], L. M. Mir[12], T. Mitani[172], J. Mitrevski[100], V. A. Mitsou[168], A. Miucci[49], P. S. Miyagawa[140], J. U. Mjörnmark[81], T. Moa[147a,147b], K. Mochizuki[85], S. Mohapatra[35], W. Mohr[48], S. Molander[147a,147b], R. Moles-Valls[168], K. Mönig[42], C. Monini[55], J. Monk[36], E. Monnier[85], J. Montejo Berlingen[12], F. Monticelli[71], S. Monzani[133a,133b], R. W. Moore[3], N. Morange[117], D. Moreno[163], M. Moreno Llácer[54], P. Morettini[50a], M. Morgenstern[44], M. Morii[57], V. Morisbak[119], S. Moritz[83], A. K. Morley[148], G. Mornacchi[30], J. D. Morris[76], S. S. Mortensen[36], A. Morton[53], L. Morvaj[103], H. G. Moser[101], M. Mosidze[51b], J. Moss[111], K. Motohashi[158], R. Mount[144], E. Mountricha[25], S. V. Mouraviev[96,*], E. J. W. Moyse[86], S. Muanza[85], R. D. Mudd[18], F. Mueller[101], J. Mueller[125], K. Mueller[21],

R. S. P. Mueller[100], T. Mueller[28], D. Muenstermann[49], P. Mullen[53], Y. Munwes[154], J. A. Murillo Quijada[18], W. J. Murray[171,131], H. Musheghyan[54], E. Musto[153], A. G. Myagkov[130,z], M. Myska[128], O. Nackenhorst[54], J. Nadal[54], K. Nagai[120], R. Nagai[158], Y. Nagai[85], K. Nagano[66], A. Nagarkar[111], Y. Nagasaka[59], K. Nagata[161], M. Nagel[101], E. Nagy[85], A. M. Nairz[30], Y. Nakahama[30], K. Nakamura[66], T. Nakamura[156], I. Nakano[112], H. Namasivayam[41], G. Nanava[21], R. F. Naranjo Garcia[42], R. Narayan[58b], T. Naumann[42], G. Navarro[163], R. Nayyar[7], H. A. Neal[89], P. Yu. Nechaeva[96], T. J. Neep[84], P. D. Nef[144], A. Negri[121a,121b], M. Negrini[20a], S. Nektarijevic[106], C. Nellist[117], A. Nelson[164], S. Nemecek[127], P. Nemethy[110], A. A. Nepomuceno[24a], M. Nessi[30,aa], M. S. Neubauer[166], M. Neumann[176], R. M. Neves[110], P. Nevski[25], P. R. Newman[18], D. H. Nguyen[6], R. B. Nickerson[120], R. Nicolaidou[137], B. Nicquevert[30], J. Nielsen[138], N. Nikiforou[35], A. Nikiforov[16], V. Nikolaenko[130,z], I. Nikolic-Audit[80], K. Nikolopoulos[18], J. K. Nilsen[119], P. Nilsson[25], Y. Ninomiya[156], A. Nisati[133a], R. Nisius[101], T. Nobe[158], M. Nomachi[118], I. Nomidis[29], T. Nooney[76], S. Norberg[113], M. Nordberg[30], O. Novgorodova[44], S. Nowak[101], M. Nozaki[66], L. Nozka[115], K. Ntekas[10], G. Nunes Hanninger[88], T. Nunnemann[100], E. Nurse[78], F. Nuti[88], B. J. O'Brien[46], F. O'grady[7], D. C. O'Neil[143], V. O'Shea[53], F. G. Oakham[29,d], H. Oberlack[101], T. Obermann[21], J. Ocariz[80], A. Ochi[67], I. Ochoa[78], S. Oda[70], S. Odaka[66], H. Ogren[61], A. Oh[84], S. H. Oh[45], C. C. Ohm[15], H. Ohman[167], H. Oide[30], W. Okamura[118], H. Okawa[161], Y. Okumura[31], T. Okuyama[156], A. Olariu[26a], S. A. Olivares Pino[46], D. Oliveira Damazio[25], E. Oliver Garcia[168], A. Olszewski[39], J. Olszowska[39], A. Onofre[126a,126e], P. U. E. Onyisi[31,q], C. J. Oram[160a], M. J. Oreglia[31], Y. Oren[154], D. Orestano[135a,135b], N. Orlando[155], C. Oropeza Barrera[53], R. S. Orr[159], B. Osculati[50a,50b], R. Ospanov[84], G. Otero y Garzon[27], H. Otono[70], M. Ouchrif[136d], E. A. Ouellette[170], F. Ould-Saada[119], A. Ouraou[137], K. P. Oussoren[107], Q. Ouyang[33a], A. Ovcharova[15], M. Owen[53], R. E. Owen[18], V. E. Ozcan[19a], N. Ozturk[8], K. Pachal[120], A. Pacheco Pages[12], C. Padilla Aranda[12], M. Pagáčová[48], S. Pagan Griso[15], E. Paganis[140], C. Pahl[101], F. Paige[25], P. Pais[86], K. Pajchel[119], G. Palacino[160b], S. Palestini[30], M. Palka[38b], D. Pallin[34], A. Palma[126a,126b], Y. B. Pan[174], E. Panagiotopoulou[10], C. E. Pandini[80], J. G. Panduro Vazquez[77], P. Pani[147a,147b], S. Panitkin[25], L. Paolozzi[134a,134b], Th. D. Papadopoulou[10], K. Papageorgiou[155], A. Paramonov[6], D. Paredes Hernandez[155], M. A. Parker[28], K. A. Parker[140], F. Parodi[50a,50b], J. A. Parsons[35], U. Parzefall[48], E. Pasqualucci[133a], S. Passaggio[50a], F. Pastore[135a,135b,*], Fr. Pastore[77], G. Pásztor[29], S. Pataraia[176], N. D. Patel[151], J. R. Pater[84], T. Pauly[30], J. Pearce[170], B. Pearson[113], L. E. Pedersen[36], M. Pedersen[119], S. Pedraza Lopez[168], R. Pedro[126a,126b], S. V. Peleganchuk[109], D. Pelikan[167], H. Peng[33b], B. Penning[31], J. Penwell[61], D. V. Perepelitsa[25], E. Perez Codina[160a], M. T. Pérez García-Estañ[168], L. Perini[91a,91b], H. Pernegger[30], S. Perrella[104a,104b], R. Peschke[42], V. D. Peshekhonov[65], K. Peters[30], R. F. Y. Peters[84], B. A. Petersen[30], T. C. Petersen[36], E. Petit[42], A. Petridis[147a,147b], C. Petridou[155], E. Petrolo[133a], F. Petrucci[135a,135b], N. E. Pettersson[158], R. Pezoa[32b], P. W. Phillips[131], G. Piacquadio[144], E. Pianori[171], A. Picazio[49], E. Piccaro[76], M. Piccinini[20a,20b], M. A. Pickering[120], R. Piegaia[27], D. T. Pignotti[111], J. E. Pilcher[31], A. D. Pilkington[78], J. Pina[126a,126b,126d], M. Pinamonti[165a,165c,ab], J. L. Pinfold[3], A. Pingel[36], B. Pinto[126a], S. Pires[80], M. Pitt[173], C. Pizio[91a,91b], L. Plazak[145a], M.-A. Pleier[25], V. Pleskot[129], E. Plotnikova[65], P. Plucinski[147a,147b], D. Pluth[64], R. Poettgen[83], L. Poggioli[117], D. Pohl[21], G. Polesello[121a], A. Policicchio[37a,37b], R. Polifka[159], A. Polini[20a], C. S. Pollard[53], V. Polychronakos[25], K. Pommès[30], L. Pontecorvo[133a], B. G. Pope[90], G. A. Popeneciu[26b], D. S. Popovic[13], A. Poppleton[30], S. Pospisil[128], K. Potamianos[15], I. N. Potrap[65], C. J. Potter[150], C. T. Potter[116], G. Poulard[30], J. Poveda[30], V. Pozdnyakov[65], P. Pralavorio[85], A. Pranko[15], S. Prasad[30], S. Prell[64], D. Price[84], J. Price[74], L. E. Price[6], M. Primavera[73a], S. Prince[87], M. Proissl[46], K. Prokofiev[60c], F. Prokoshin[32b], E. Protopapadaki[137], S. Protopopescu[25], J. Proudfoot[6], M. Przybycien[38a], E. Ptacek[116], D. Puddu[135a,135b], E. Pueschel[86], D. Puldon[149], M. Purohit[25,ac], P. Puzo[117], J. Qian[89], G. Qin[53], Y. Qin[84], A. Quadt[54], D. R. Quarrie[15], W. B. Quayle[165a,165b], M. Queitsch-Maitland[84], D. Quilty[53], S. Raddum[119], V. Radeka[25], V. Radescu[42], S. K. Radhakrishnan[149], P. Radloff[116], P. Rados[88], F. Ragusa[91a,91b], G. Rahal[179], S. Rajagopalan[25], M. Rammensee[30], C. Rangel-Smith[167], F. Rauscher[100], S. Rave[83], T. Ravenscroft[53], M. Raymond[30], A. L. Read[119], N. P. Readioff[74], D. M. Rebuzzi[121a,121b], A. Redelbach[175], G. Redlinger[25], R. Reece[138], K. Reeves[41], L. Rehnisch[16], H. Reisin[27], M. Relich[164], C. Rembser[30], H. Ren[33a], A. Renaud[117], M. Rescigno[133a], S. Resconi[91a], O. L. Rezanova[109,c], P. Reznicek[129], R. Rezvani[95], R. Richter[101], S. Richter[78], E. Richter-Was[38b], O. Ricken[21], M. Ridel[80], P. Rieck[16], C. J. Riegel[176], J. Rieger[54], M. Rijssenbeek[149], A. Rimoldi[121a,121b], L. Rinaldi[20a], B. Ristić[49], E. Ritsch[62], I. Riu[12], F. Rizatdinova[114], E. Rizvi[76], S. H. Robertson[87,k], A. Robichaud-Veronneau[87], D. Robinson[28], J. E. M. Robinson[84], A. Robson[53], C. Roda[124a,124b], S. Roe[30], O. Røhne[119], S. Rolli[162], A. Romaniouk[98], M. Romano[20a,20b], S. M. Romano Saez[34], E. Romero Adam[168], N. Rompotis[139], M. Ronzani[48], L. Roos[80], E. Ros[168], S. Rosati[133a], K. Rosbach[48], P. Rose[138], P. L. Rosendahl[14], O. Rosenthal[142], V. Rossetti[147a,147b], E. Rossi[104a,104b], L. P. Rossi[50a], R. Rosten[139], M. Rotaru[26a], I. Roth[173], J. Rothberg[139], D. Rousseau[117], C. R. Royon[137], A. Rozanov[85], Y. Rozen[153], X. Ruan[146c], F. Rubbo[144], I. Rubinskiy[42], V. I. Rud[99], C. Rudolph[44], M. S. Rudolph[159], F. Rühr[48], A. Ruiz-Martinez[30], Z. Rurikova[48], N. A. Rusakovich[65], A. Ruschke[100], H. L. Russell[139], J. P. Rutherfoord[7], N. Ruthmann[48], Y. F. Ryabov[123], M. Rybar[129], G. Rybkin[117], N. C. Ryder[120], A. F. Saavedra[151], G. Sabato[107], S. Sacerdoti[27], A. Saddique[3], H. F-W. Sadrozinski[138], R. Sadykov[65], F. Safai Tehrani[133a], M. Saimpert[137],

H. Sakamoto[156], Y. Sakurai[172], G. Salamanna[135a,135b], A. Salamon[134a], M. Saleem[113], D. Salek[107], P. H. Sales De Bruin[139], D. Salihagic[101], A. Salnikov[144], J. Salt[168], D. Salvatore[37a,37b], F. Salvatore[150], A. Salvucci[106], A. Salzburger[30], D. Sampsonidis[155], A. Sanchez[104a,104b], J. Sánchez[168], V. Sanchez Martinez[168], H. Sandaker[14], R. L. Sandbach[76], H. G. Sander[83], M. P. Sanders[100], M. Sandhoff[176], C. Sandoval[163], R. Sandstroem[101], D. P. C. Sankey[131], M. Sannino[50a,50b], A. Sansoni[47], C. Santoni[34], R. Santonico[134a,134b], H. Santos[126a], I. Santoyo Castillo[150], K. Sapp[125], A. Sapronov[65], J. G. Saraiva[126a,126d], B. Sarrazin[21], O. Sasaki[66], Y. Sasaki[156], K. Sato[161], G. Sauvage[5,*], E. Sauvan[5], G. Savage[77], P. Savard[159,d], C. Sawyer[120], L. Sawyer[79,n], J. Saxon[31], C. Sbarra[20a], A. Sbrizzi[20a,20b], T. Scanlon[78], D. A. Scannicchio[164], M. Scarcella[151], V. Scarfone[37a,37b], J. Schaarschmidt[173], P. Schacht[101], D. Schaefer[30], R. Schaefer[42], J. Schaeffer[83], S. Schaepe[21], S. Schaetzel[58b], U. Schäfer[83], A. C. Schaffer[117], D. Schaile[100], R. D. Schamberger[149], V. Scharf[58a], V. A. Schegelsky[123], D. Scheirich[129], M. Schernau[164], C. Schiavi[50a,50b], C. Schillo[48], M. Schioppa[37a,37b], S. Schlenker[30], E. Schmidt[48], K. Schmieden[30], C. Schmitt[83], S. Schmitt[58b], S. Schmitt[42], B. Schneider[160a], Y. J. Schnellbach[74], U. Schnoor[44], L. Schoeffel[137], A. Schoening[58b], B. D. Schoenrock[90], E. Schopf[21], A. L. S. Schorlemmer[54], M. Schott[83], D. Schouten[160a], J. Schovancova[8], S. Schramm[159], M. Schreyer[175], C. Schroeder[83], N. Schuh[83], M. J. Schultens[21], H.-C. Schultz-Coulon[58a], H. Schulz[16], M. Schumacher[48], B. A. Schumm[138], Ph. Schune[137], C. Schwanenberger[84], A. Schwartzman[144], T. A. Schwarz[89], Ph. Schwegler[101], Ph. Schwemling[137], R. Schwienhorst[90], J. Schwindling[137], T. Schwindt[21], M. Schwoerer[5], F. G. Sciacca[17], E. Scifo[117], G. Sciolla[23], F. Scuri[124a,124b], F. Scutti[21], J. Searcy[89], G. Sedov[42], E. Sedykh[123], P. Seema[21], S. C. Seidel[105], A. Seiden[138], F. Seifert[128], J. M. Seixas[24a], G. Sekhniaidze[104a], S. J. Sekula[40], K. E. Selbach[46], D. M. Seliverstov[123,*], N. Semprini-Cesari[20a,20b], C. Serfon[30], L. Serin[117], L. Serkin[165a,165b], T. Serre[85], R. Seuster[160a], H. Severini[113], T. Sfiligoj[75], F. Sforza[101], A. Sfyrla[30], E. Shabalina[54], M. Shamim[116], L. Y. Shan[33a], R. Shang[166], J. T. Shank[22], M. Shapiro[15], P. B. Shatalov[97], K. Shaw[165a,165b], A. Shcherbakova[147a,147b], C. Y. Shehu[150], P. Sherwood[78], L. Shi[152,ad], S. Shimizu[67], C. O. Shimmin[164], M. Shimojima[102], M. Shiyakova[65], A. Shmeleva[96], D. Shoaleh Saadi[95], M. J. Shochet[31], S. Shojaii[91a,91b], S. Shrestha[111], E. Shulga[98], M. A. Shupe[7], S. Shushkevich[42], P. Sicho[127], O. Sidiropoulou[175], D. Sidorov[114], A. Sidoti[20a,20b], F. Siegert[44], Dj. Sijacki[13], J. Silva[126a,126d], Y. Silver[154], S. B. Silverstein[147a], V. Simak[128], O. Simard[5], Lj. Simic[13], S. Simion[117], E. Simioni[83], B. Simmons[78], D. Simon[34], R. Simoniello[91a,91b], P. Sinervo[159], N. B. Sinev[116], G. Siragusa[175], A. N. Sisakyan[65,*], S. Yu. Sivoklokov[99], J. Sjölin[147a,147b], T. B. Sjursen[14], M. B. Skinner[72], H. P. Skottowe[57], P. Skubic[113], M. Slater[18], T. Slavicek[128], M. Slawinska[107], K. Sliwa[162], V. Smakhtin[173], B. H. Smart[46], L. Smestad[14], S. Yu. Smirnov[98], Y. Smirnov[98], L. N. Smirnova[99,ae], O. Smirnova[81], M. N. K. Smith[35], M. Smizanska[72], K. Smolek[128], A. A. Snesarev[96], G. Snidero[76], S. Snyder[25], R. Sobie[170,k], F. Socher[44], A. Soffer[154], D. A. Soh[152,ad], C. A. Solans[30], M. Solar[128], J. Solc[128], E. Yu. Soldatov[98], U. Soldevila[168], A. A. Solodkov[130], A. Soloshenko[65], O. V. Solovyanov[130], V. Solovyev[123], P. Sommer[48], H. Y. Song[33b], N. Soni[1], A. Sood[15], A. Sopczak[128], B. Sopko[128], V. Sopko[128], V. Sorin[12], D. Sosa[58b], M. Sosebee[8], C. L. Sotiropoulou[155], R. Soualah[165a,165c], P. Soueid[95], A. M. Soukharev[109,c], D. South[42], S. Spagnolo[73a,73b], M. Spalla[124a,124b], F. Spanò[77], W. R. Spearman[57], F. Spettel[101], R. Spighi[20a], G. Spigo[30], L. A. Spiller[88], M. Spousta[129], T. Spreitzer[159], R. D. St. Denis[53,*], S. Staerz[44], J. Stahlman[122], R. Stamen[58a], S. Stamm[16], E. Stanecka[39], C. Stanescu[135a], M. Stanescu-Bellu[42], M. M. Stanitzki[42], S. Stapnes[119], E. A. Starchenko[130], J. Stark[55], P. Staroba[127], P. Starovoitov[42], R. Staszewski[39], P. Stavina[145a,*], P. Steinberg[25], B. Stelzer[143], H. J. Stelzer[30], O. Stelzer-Chilton[160a], H. Stenzel[52], S. Stern[101], G. A. Stewart[53], J. A. Stillings[21], M. C. Stockton[87], M. Stoebe[87], G. Stoicea[26a], P. Stolte[54], S. Stonjek[101], A. R. Stradling[8], A. Straessner[44], M. E. Stramaglia[17], J. Strandberg[148], S. Strandberg[147a,147b], A. Strandlie[119], E. Strauss[144], M. Strauss[113], P. Strizenec[145b], R. Ströhmer[175], D. M. Strom[116], R. Stroynowski[40], A. Strubig[106], S. A. Stucci[17], B. Stugu[14], N. A. Styles[42], D. Su[144], J. Su[125], R. Subramaniam[79], A. Succurro[12], Y. Sugaya[118], C. Suhr[108], M. Suk[128], V. V. Sulin[96], S. Sultansoy[4c], T. Sumida[68], S. Sun[57], X. Sun[33a], J. E. Sundermann[48], K. Suruliz[150], G. Susinno[37a,37b], M. R. Sutton[150], S. Suzuki[66], Y. Suzuki[66], M. Svatos[127], S. Swedish[169], M. Swiatlowski[144], I. Sykora[145a], T. Sykora[129], D. Ta[90], C. Taccini[135a,135b], K. Tackmann[42], J. Taenzer[159], A. Taffard[164], R. Tafirout[160a], N. Taiblum[154], H. Takai[25], R. Takashima[69], H. Takeda[67], T. Takeshita[141], Y. Takubo[66], M. Talby[85], A. A. Talyshev[109,c], J. Y. C. Tam[175], K. G. Tan[88], J. Tanaka[156], R. Tanaka[117], S. Tanaka[132], S. Tanaka[66], B. B. Tannenwald[111], N. Tannoury[21], S. Tapprogge[83], S. Tarem[153], F. Tarrade[29], G. F. Tartarelli[91a], P. Tas[129], M. Tasevsky[127], T. Tashiro[68], E. Tassi[37a,37b], A. Tavares Delgado[126a,126b], Y. Tayalati[136d], F. E. Taylor[94], G. N. Taylor[88], W. Taylor[160b], F. A. Teischinger[30], M. Teixeira Dias Castanheira[76], P. Teixeira-Dias[77], K. K. Temming[48], H. Ten Kate[30], P. K. Teng[152], J. J. Teoh[118], F. Tepel[176], S. Terada[66], K. Terashi[156], J. Terron[82], S. Terzo[101], M. Testa[47], R. J. Teuscher[159,k], J. Therhaag[21], T. Theveneaux-Pelzer[34], J. P. Thomas[18], J. Thomas-Wilsker[77], E. N. Thompson[35], P. D. Thompson[18], R. J. Thompson[84], A. S. Thompson[53], L. A. Thomsen[36], E. Thomson[122], M. Thomson[28], R. P. Thun[89,*], M. J. Tibbetts[15], R. E. Ticse Torres[85], V. O. Tikhomirov[96,af], Yu. A. Tikhonov[109,c], S. Timoshenko[98], E. Tiouchichine[85], P. Tipton[177], S. Tisserant[85], T. Todorov[5,*], S. Todorova-Nova[129], J. Tojo[70], S. Tokár[145a], K. Tokushuku[66], K. Tollefson[90], E. Tolley[57],

L. Tomlinson[84], M. Tomoto[103], L. Tompkins[144,ag], K. Toms[105], E. Torrence[116], H. Torres[143], E. Torró Pastor[168], J. Toth[85,ah], F. Touchard[85], D. R. Tovey[140], T. Trefzger[175], L. Tremblet[30], A. Tricoli[30], I. M. Trigger[160a], S. Trincaz-Duvoid[80], M. F. Tripiana[12], W. Trischuk[159], B. Trocmé[55], C. Troncon[91a], M. Trottier-McDonald[15], M. Trovatelli[135a,135b], P. True[90], M. Trzebinski[39], A. Trzupek[39], C. Tsarouchas[30], J. C-L. Tseng[120], P. V. Tsiareshka[92], D. Tsionou[155], G. Tsipolitis[10], N. Tsirintanis[9], S. Tsiskaridze[12], V. Tsiskaridze[48], E. G. Tskhadadze[51a], I. I. Tsukerman[97], V. Tsulaia[15], S. Tsuno[66], D. Tsybychev[149], A. Tudorache[26a], V. Tudorache[26a], A. N. Tuna[122], S. A. Tupputi[20a,20b], S. Turchikhin[99,ae], D. Turecek[128], R. Turra[91a,91b], A. J. Turvey[40], P. M. Tuts[35], A. Tykhonov[49], M. Tylmad[147a,147b], M. Tyndel[131], I. Ueda[156], R. Ueno[29], M. Ughetto[147a,147b], M. Ugland[14], M. Uhlenbrock[21], F. Ukegawa[161], G. Unal[30], A. Undrus[25], G. Unel[164], F. C. Ungaro[48], Y. Unno[66], C. Unverdorben[100], J. Urban[145b], P. Urquijo[88], P. Urrejola[83], G. Usai[8], A. Usanova[62], L. Vacavant[85], V. Vacek[128], B. Vachon[87], C. Valderanis[83], N. Valencic[107], S. Valentinetti[20a,20b], A. Valero[168], L. Valery[12], S. Valkar[129], E. Valladolid Gallego[168], S. Vallecorsa[49], J. A. Valls Ferrer[168], W. Van Den Wollenberg[107], P. C. Van Der Deijl[107], R. van der Geer[107], H. van der Graaf[107], R. Van Der Leeuw[107], N. van Eldik[153], P. van Gemmeren[6], J. Van Nieuwkoop[143], I. van Vulpen[107], M. C. van Woerden[30], M. Vanadia[133a,133b], W. Vandelli[30], R. Vanguri[122], A. Vaniachine[6], F. Vannucci[80], G. Vardanyan[178], R. Vari[133a], E. W. Varnes[7], T. Varol[40], D. Varouchas[80], A. Vartapetian[8], K. E. Varvell[151], F. Vazeille[34], T. Vazquez Schroeder[87], J. Veatch[7], F. Veloso[126a,126c], T. Velz[21], S. Veneziano[133a], A. Ventura[73a,73b], D. Ventura[86], M. Venturi[170], N. Venturi[159], A. Venturini[23], V. Vercesi[121a], M. Verducci[133a,133b], W. Verkerke[107], J. C. Vermeulen[107], A. Vest[44], M. C. Vetterli[143,d], O. Viazlo[81], I. Vichou[166], T. Vickey[140], O. E. Vickey Boeriu[140], G. H. A. Viehhauser[120], S. Viel[15], R. Vigne[30], M. Villa[20a,20b], M. Villaplana Perez[91a,91b], E. Vilucchi[47], M. G. Vincter[29], V. B. Vinogradov[65], I. Vivarelli[150], F. Vives Vaque[3], S. Vlachos[10], D. Vladoiu[100], M. Vlasak[128], M. Vogel[32a], P. Vokac[128], G. Volpi[124a,124b], M. Volpi[88], H. von der Schmitt[101], H. von Radziewski[48], E. von Toerne[21], V. Vorobel[129], K. Vorobev[98], M. Vos[168], R. Voss[30], J. H. Vossebeld[74], N. Vranjes[13], M. Vranjes Milosavljevic[13], V. Vrba[127], M. Vreeswijk[107], R. Vuillermet[30], I. Vukotic[31], Z. Vykydal[128], P. Wagner[21], W. Wagner[176], H. Wahlberg[71], S. Wahrmund[44], J. Wakabayashi[103], J. Walder[72], R. Walker[100], W. Walkowiak[142], C. Wang[33c], F. Wang[174], H. Wang[15], H. Wang[40], J. Wang[42], J. Wang[33a], K. Wang[87], R. Wang[6], S. M. Wang[152], T. Wang[21], X. Wang[177], C. Wanotayaroj[116], A. Warburton[87], C. P. Ward[28], D. R. Wardrope[78], M. Warsinsky[48], A. Washbrook[46], C. Wasicki[42], P. M. Watkins[18], A. T. Watson[18], I. J. Watson[151], M. F. Watson[18], G. Watts[139], S. Watts[84], B. M. Waugh[78], S. Webb[84], M. S. Weber[17], S. W. Weber[175], J. S. Webster[31], A. R. Weidberg[120], B. Weinert[61], J. Weingarten[54], C. Weiser[48], H. Weits[107], P. S. Wells[30], T. Wenaus[25], T. Wengler[30], S. Wenig[30], N. Wermes[21], M. Werner[48], P. Werner[30], M. Wessels[58a], J. Wetter[162], K. Whalen[29], A. M. Wharton[72], A. White[8], M. J. White[1], R. White[32b], S. White[124a,124b], D. Whiteson[164], F. J. Wickens[131], W. Wiedenmann[174], M. Wielers[131], P. Wienemann[21], C. Wiglesworth[36], L. A. M. Wiik-Fuchs[21], A. Wildauer[101], H. G. Wilkens[30], H. H. Williams[122], S. Williams[107], C. Willis[90], S. Willocq[86], A. Wilson[89], J. A. Wilson[18], I. Wingerter-Seez[5], F. Winklmeier[116], B. T. Winter[21], M. Wittgen[144], J. Wittkowski[100], S. J. Wollstadt[83], M. W. Wolter[39], H. Wolters[126a,126c], B. K. Wosiek[39], J. Wotschack[30], M. J. Woudstra[84], K. W. Wozniak[39], M. Wu[55], M. Wu[31], S. L. Wu[174], X. Wu[49], Y. Wu[89], T. R. Wyatt[84], B. M. Wynne[46], S. Xella[36], D. Xu[33a], L. Xu[33b,ai], B. Yabsley[151], S. Yacoob[146b,aj], R. Yakabe[67], M. Yamada[66], Y. Yamaguchi[118], A. Yamamoto[66], S. Yamamoto[156], T. Yamanaka[156], K. Yamauchi[103], Y. Yamazaki[67], Z. Yan[22], H. Yang[33e], H. Yang[174], Y. Yang[152], L. Yao[33a], W-M. Yao[15], Y. Yasu[66], E. Yatsenko[42], K. H. Yau Wong[21], J. Ye[40], S. Ye[25], I. Yeletskikh[65], A. L. Yen[57], E. Yildirim[42], K. Yorita[172], R. Yoshida[6], K. Yoshihara[122], C. Young[144], C. J. S. Young[30], S. Youssef[22], D. R. Yu[15], J. Yu[8], J. M. Yu[89], J. Yu[114], L. Yuan[67], A. Yurkewicz[108], I. Yusuff[28,ak], B. Zabinski[39], R. Zaidan[63], A. M. Zaitsev[130,z], J. Zalieckas[14], A. Zaman[149], S. Zambito[23], L. Zanello[133a,133b], D. Zanzi[88], C. Zeitnitz[176], M. Zeman[128], A. Zemla[38a], K. Zengel[23], O. Zenin[130], T. Ženiš[145a], D. Zerwas[117], D. Zhang[89], F. Zhang[174], J. Zhang[6], L. Zhang[48], R. Zhang[33b], X. Zhang[33d], Z. Zhang[117], X. Zhao[40], Y. Zhao[33d,117], Z. Zhao[33b], A. Zhemchugov[65], J. Zhong[120], B. Zhou[89], C. Zhou[45], L. Zhou[35], L. Zhou[40], N. Zhou[164], C. G. Zhu[33d], H. Zhu[33a], J. Zhu[89], Y. Zhu[33b], X. Zhuang[33a], K. Zhukov[96], A. Zibell[175], D. Zieminska[61], N. I. Zimine[65], C. Zimmermann[83], R. Zimmermann[21], S. Zimmermann[48], Z. Zinonos[54], M. Zinser[83], M. Ziolkowski[142], L. Živković[13], G. Zobernig[174], A. Zoccoli[20a,20b], M. zur Nedden[16], G. Zurzolo[104a,104b], L. Zwalinski[30]

[1] Department of Physics, University of Adelaide, Adelaide, Australia
[2] Physics Department, SUNY Albany, Albany, NY, USA
[3] Department of Physics, University of Alberta, Edmonton, AB, Canada
[4] [(a)]Department of Physics, Ankara University, Ankara, Turkey; [(b)]Istanbul Aydin University, Istanbul, Turkey; [(c)]Division of Physics, TOBB University of Economics and Technology, Ankara, Turkey
[5] LAPP, CNRS/IN2P3 and Université Savoie Mont Blanc, Annecy-le-Vieux, France
[6] High Energy Physics Division, Argonne National Laboratory, Argonne, IL, USA
[7] Department of Physics, University of Arizona, Tucson, AZ, USA

[8] Department of Physics, The University of Texas at Arlington, Arlington, TX, USA
[9] Physics Department, University of Athens, Athens, Greece
[10] Physics Department, National Technical University of Athens, Zografou, Greece
[11] Institute of Physics, Azerbaijan Academy of Sciences, Baku, Azerbaijan
[12] Institut de Física d'Altes Energies and Departament de Física de la Universitat Autònoma de Barcelona, Barcelona, Spain
[13] Institute of Physics, University of Belgrade, Belgrade, Serbia
[14] Department for Physics and Technology, University of Bergen, Bergen, Norway
[15] Physics Division, Lawrence Berkeley National Laboratory and University of California, Berkeley, CA, USA
[16] Department of Physics, Humboldt University, Berlin, Germany
[17] Albert Einstein Center for Fundamental Physics and Laboratory for High Energy Physics, University of Bern, Bern, Switzerland
[18] School of Physics and Astronomy, University of Birmingham, Birmingham, UK
[19] [(a)]Department of Physics, Bogazici University, Istanbul, Turkey; [(b)]Department of Physics, Dogus University, Istanbul, Turkey; [(c)]Department of Physics Engineering, Gaziantep University, Gaziantep, Turkey
[20] [(a)]INFN Sezione di Bologna, Bologna, Italy; [(b)]Dipartimento di Fisica e Astronomia, Università di Bologna, Bologna, Italy
[21] Physikalisches Institut, University of Bonn, Bonn, Germany
[22] Department of Physics, Boston University, Boston, MA, USA
[23] Department of Physics, Brandeis University, Waltham, MA, USA
[24] [(a)]Universidade Federal do Rio De Janeiro COPPE/EE/IF, Rio de Janeiro, Brazil; [(b)]Electrical Circuits Department, Federal University of Juiz de Fora (UFJF), Juiz de Fora, Brazil; [(c)]Federal University of Sao Joao del Rei (UFSJ), Sao Joao del Rei, Brazil; [(d)]Instituto de Fisica, Universidade de Sao Paulo, São Paulo, Brazil
[25] Physics Department, Brookhaven National Laboratory, Upton, NY, USA
[26] [(a)]National Institute of Physics and Nuclear Engineering, Bucharest, Romania; [(b)]Physics Department, National Institute for Research and Development of Isotopic and Molecular Technologies, Cluj Napoca, Romania; [(c)]University Politehnica Bucharest, Bucharest, Romania; [(d)]West University in Timisoara, Timisoara, Romania
[27] Departamento de Física, Universidad de Buenos Aires, Buenos Aires, Argentina
[28] Cavendish Laboratory, University of Cambridge, Cambridge, UK
[29] Department of Physics, Carleton University, Ottawa, ON, Canada
[30] CERN, Geneva, Switzerland
[31] Enrico Fermi Institute, University of Chicago, Chicago, IL, USA
[32] [(a)]Departamento de Física, Pontificia Universidad Católica de Chile, Santiago, Chile; [(b)]Departamento de Física, Universidad Técnica Federico Santa María, Valparaiso, Chile
[33] [(a)]Institute of High Energy Physics, Chinese Academy of Sciences, Beijing, China; [(b)]Department of Modern Physics, University of Science and Technology of China, Anhui, China; [(c)]Department of Physics, Nanjing University, Jiangsu, China; [(d)]School of Physics, Shandong University, Shandong, China; [(e)]Department of Physics and Astronomy, Shanghai Key Laboratory for Particle Physics and Cosmology, Shanghai Jiao Tong University, Shanghai, China; [(f)]Physics Department, Tsinghua University, Beijing 100084, China
[34] Laboratoire de Physique Corpusculaire, Clermont Université and Université Blaise Pascal and CNRS/IN2P3, Clermont-Ferrand, France
[35] Nevis Laboratory, Columbia University, Irvington, NY, USA
[36] Niels Bohr Institute, University of Copenhagen, Copenhagen, Denmark
[37] [(a)]INFN Gruppo Collegato di Cosenza, Laboratori Nazionali di Frascati, Frascati, Italy; [(b)]Dipartimento di Fisica, Università della Calabria, Rende, Italy
[38] [(a)]Faculty of Physics and Applied Computer Science, AGH University of Science and Technology, Kraków, Poland; [(b)]Marian Smoluchowski Institute of Physics, Jagiellonian University, Kraków, Poland
[39] Institute of Nuclear Physics, Polish Academy of Sciences, Kraków, Poland
[40] Physics Department, Southern Methodist University, Dallas, TX, USA
[41] Physics Department, University of Texas at Dallas, Richardson, TX, USA
[42] DESY, Hamburg and Zeuthen, Germany
[43] Institut für Experimentelle Physik IV, Technische Universität Dortmund, Dortmund, Germany
[44] Institut für Kern- und Teilchenphysik, Technische Universität Dresden, Dresden, Germany

[45] Department of Physics, Duke University, Durham, NC, USA
[46] SUPA, School of Physics and Astronomy, University of Edinburgh, Edinburgh, UK
[47] INFN Laboratori Nazionali di Frascati, Frascati, Italy
[48] Fakultät für Mathematik und Physik, Albert-Ludwigs-Universität, Freiburg, Germany
[49] Section de Physique, Université de Genève, Geneva, Switzerland
[50] [(a)]INFN Sezione di Genova, Genoa, Italy; [(b)]Dipartimento di Fisica, Università di Genova, Genoa, Italy
[51] [(a)]E. Andronikashvili Institute of Physics, Iv. Javakhishvili Tbilisi State University, Tbilisi, Georgia; [(b)]High Energy Physics Institute, Tbilisi State University, Tbilisi, Georgia
[52] II Physikalisches Institut, Justus-Liebig-Universität Giessen, Giessen, Germany
[53] SUPA, School of Physics and Astronomy, University of Glasgow, Glasgow, UK
[54] II Physikalisches Institut, Georg-August-Universität, Göttingen, Germany
[55] Laboratoire de Physique Subatomique et de Cosmologie, Université Grenoble-Alpes, CNRS/IN2P3, Grenoble, France
[56] Department of Physics, Hampton University, Hampton, VA, USA
[57] Laboratory for Particle Physics and Cosmology, Harvard University, Cambridge, MA, USA
[58] [(a)]Kirchhoff-Institut für Physik, Ruprecht-Karls-Universität Heidelberg, Heidelberg, Germany; [(b)]Physikalisches Institut, Ruprecht-Karls-Universität Heidelberg, Heidelberg, Germany; [(c)]ZITI Institut für technische Informatik, Ruprecht-Karls-Universität Heidelberg, Mannheim, Germany
[59] Faculty of Applied Information Science, Hiroshima Institute of Technology, Hiroshima, Japan
[60] [(a)]Department of Physics, The Chinese University of Hong Kong, Shatin, NT, Hong Kong; [(b)]Department of Physics, The University of Hong Kong, Pok Fu Lam, Hong Kong; [(c)]Department of Physics, The Hong Kong University of Science and Technology, Clear Water Bay, Kowloon, Hong Kong, China
[61] Department of Physics, Indiana University, Bloomington, IN, USA
[62] Institut für Astro- und Teilchenphysik, Leopold-Franzens-Universität, Innsbruck, Austria
[63] University of Iowa, Iowa City, IA, USA
[64] Department of Physics and Astronomy, Iowa State University, Ames, IA, USA
[65] Joint Institute for Nuclear Research, JINR Dubna, Dubna, Russia
[66] KEK, High Energy Accelerator Research Organization, Tsukuba, Japan
[67] Graduate School of Science, Kobe University, Kobe, Japan
[68] Faculty of Science, Kyoto University, Kyoto, Japan
[69] Kyoto University of Education, Kyoto, Japan
[70] Department of Physics, Kyushu University, Fukuoka, Japan
[71] Instituto de Física La Plata, Universidad Nacional de La Plata and CONICET, La Plata, Argentina
[72] Physics Department, Lancaster University, Lancaster, UK
[73] [(a)]INFN Sezione di Lecce, Lecce, Italy; [(b)]Dipartimento di Matematica e Fisica, Università del Salento, Lecce, Italy
[74] Oliver Lodge Laboratory, University of Liverpool, Liverpool, UK
[75] Department of Physics, Jožef Stefan Institute and University of Ljubljana, Ljubljana, Slovenia
[76] School of Physics and Astronomy, Queen Mary University of London, London, UK
[77] Department of Physics, Royal Holloway University of London, Surrey, UK
[78] Department of Physics and Astronomy, University College London, London, UK
[79] Louisiana Tech University, Ruston, LA, USA
[80] Laboratoire de Physique Nucléaire et de Hautes Energies, UPMC and Université Paris-Diderot and CNRS/IN2P3, Paris, France
[81] Fysiska institutionen, Lunds universitet, Lund, Sweden
[82] Departamento de Fisica Teorica C-15, Universidad Autonoma de Madrid, Madrid, Spain
[83] Institut für Physik, Universität Mainz, Mainz, Germany
[84] School of Physics and Astronomy, University of Manchester, Manchester, UK
[85] CPPM, Aix-Marseille Université and CNRS/IN2P3, Marseille, France
[86] Department of Physics, University of Massachusetts, Amherst, MA, USA
[87] Department of Physics, McGill University, Montreal, QC, Canada
[88] School of Physics, University of Melbourne, Melbourne, VIC, Australia
[89] Department of Physics, The University of Michigan, Ann Arbor, MI, USA
[90] Department of Physics and Astronomy, Michigan State University, East Lansing, MI, USA
[91] [(a)]INFN Sezione di Milano, Milan, Italy; [(b)]Dipartimento di Fisica, Università di Milano, Milan, Italy

[92] B.I. Stepanov Institute of Physics, National Academy of Sciences of Belarus, Minsk, Republic of Belarus
[93] National Scientific and Educational Centre for Particle and High Energy Physics, Minsk, Republic of Belarus
[94] Department of Physics, Massachusetts Institute of Technology, Cambridge, MA, USA
[95] Group of Particle Physics, University of Montreal, Montreal, QC, Canada
[96] P.N. Lebedev Institute of Physics, Academy of Sciences, Moscow, Russia
[97] Institute for Theoretical and Experimental Physics (ITEP), Moscow, Russia
[98] National Research Nuclear University MEPhI, Moscow, Russia
[99] D.V. Skobeltsyn Institute of Nuclear Physics, M.V. Lomonosov Moscow State University, Moscow, Russia
[100] Fakultät für Physik, Ludwig-Maximilians-Universität München, Munich, Germany
[101] Max-Planck-Institut für Physik (Werner-Heisenberg-Institut), Munich, Germany
[102] Nagasaki Institute of Applied Science, Nagasaki, Japan
[103] Graduate School of Science and Kobayashi-Maskawa Institute, Nagoya University, Nagoya, Japan
[104] [(a)]INFN Sezione di Napoli, Naples, Italy; [(b)]Dipartimento di Fisica, Università di Napoli, Naples, Italy
[105] Department of Physics and Astronomy, University of New Mexico, Albuquerque, NM, USA
[106] Institute for Mathematics, Astrophysics and Particle Physics, Radboud University Nijmegen/Nikhef, Nijmegen, The Netherlands
[107] Nikhef National Institute for Subatomic Physics and University of Amsterdam, Amsterdam, The Netherlands
[108] Department of Physics, Northern Illinois University, De Kalb, IL, USA
[109] Budker Institute of Nuclear Physics, SB RAS, Novosibirsk, Russia
[110] Department of Physics, New York University, New York, NY, USA
[111] Ohio State University, Columbus, OH, USA
[112] Faculty of Science, Okayama University, Okayama, Japan
[113] Homer L. Dodge Department of Physics and Astronomy, University of Oklahoma, Norman, OK, USA
[114] Department of Physics, Oklahoma State University, Stillwater, OK, USA
[115] Palacký University, RCPTM, Olomouc, Czech Republic
[116] Center for High Energy Physics, University of Oregon, Eugene, OR, USA
[117] LAL, Université Paris-Sud and CNRS/IN2P3, Orsay, France
[118] Graduate School of Science, Osaka University, Osaka, Japan
[119] Department of Physics, University of Oslo, Oslo, Norway
[120] Department of Physics, Oxford University, Oxford, UK
[121] [(a)]INFN Sezione di Pavia, Pavia, Italy; [(b)]Dipartimento di Fisica, Università di Pavia, Pavia, Italy
[122] Department of Physics, University of Pennsylvania, Philadelphia, PA, USA
[123] Petersburg Nuclear Physics Institute, Gatchina, Russia
[124] [(a)]INFN Sezione di Pisa, Pisa, Italy; [(b)]Dipartimento di Fisica E. Fermi, Università di Pisa, Pisa, Italy
[125] Department of Physics and Astronomy, University of Pittsburgh, Pittsburgh, PA, USA
[126] [(a)]Laboratorio de Instrumentacao e Fisica Experimental de Particulas, LIP, Lisbon, Portugal; [(b)]Faculdade de Ciências, Universidade de Lisboa, Lisbon, Portugal; [(c)]Department of Physics, University of Coimbra, Coimbra, Portugal; [(d)]Centro de Física Nuclear da Universidade de Lisboa, Lisbon, Portugal; [(e)]Departamento de Fisica, Universidade do Minho, Braga, Portugal; [(f)]Departamento de Fisica Teorica y del Cosmos and CAFPE, Universidad de Granada, Granada, Spain; [(g)]Dep Fisica and CEFITEC of Faculdade de Ciencias e Tecnologia, Universidade Nova de Lisboa, Caparica, Portugal
[127] Institute of Physics, Academy of Sciences of the Czech Republic, Prague, Czech Republic
[128] Czech Technical University in Prague, Prague, Czech Republic
[129] Faculty of Mathematics and Physics, Charles University in Prague, Prague, Czech Republic
[130] State Research Center Institute for High Energy Physics, Protvino, Russia
[131] Particle Physics Department, Rutherford Appleton Laboratory, Didcot, UK
[132] Ritsumeikan University, Kusatsu, Shiga, Japan
[133] [(a)]INFN Sezione di Roma, Rome, Italy; [(b)]Dipartimento di Fisica, Sapienza Università di Roma, Rome, Italy
[134] [(a)]INFN Sezione di Roma Tor Vergata, Rome, Italy; [(b)]Dipartimento di Fisica, Università di Roma Tor Vergata, Rome, Italy
[135] [(a)]INFN Sezione di Roma Tre, Rome, Italy; [(b)]Dipartimento di Matematica e Fisica, Università Roma Tre, Rome, Italy
[136] [(a)]Faculté des Sciences Ain Chock, Réseau Universitaire de Physique des Hautes Energies-Université Hassan II, Casablanca, Morocco; [(b)]Centre National de l'Energie des Sciences Techniques Nucleaires, Rabat, Morocco; [(c)]Faculté

des Sciences Semlalia, Université Cadi Ayyad, LPHEA-Marrakech, Marrakech, Morocco; [d]Faculté des Sciences, Université Mohamed Premier and LPTPM, Oujda, Morocco; [e]Faculté des Sciences, Université Mohammed V-Agdal, Rabat, Morocco
[137] DSM/IRFU (Institut de Recherches sur les Lois Fondamentales de l'Univers), CEA Saclay (Commissariat à l'Energie Atomique et aux Energies Alternatives), Gif-sur-Yvette, France
[138] Santa Cruz Institute for Particle Physics, University of California Santa Cruz, Santa Cruz, CA, USA
[139] Department of Physics, University of Washington, Seattle, WA, USA
[140] Department of Physics and Astronomy, University of Sheffield, Sheffield, UK
[141] Department of Physics, Shinshu University, Nagano, Japan
[142] Fachbereich Physik, Universität Siegen, Siegen, Germany
[143] Department of Physics, Simon Fraser University, Burnaby, BC, Canada
[144] SLAC National Accelerator Laboratory, Stanford, CA, USA
[145] [a]Faculty of Mathematics, Physics and Informatics, Comenius University, Bratislava, Slovak Republic; [b]Department of Subnuclear Physics, Institute of Experimental Physics of the Slovak Academy of Sciences, Kosice, Slovak Republic
[146] [a]Department of Physics, University of Cape Town, Cape Town, South Africa; [b]Department of Physics, University of Johannesburg, Johannesburg, South Africa; [c]School of Physics, University of the Witwatersrand, Johannesburg, South Africa
[147] [a]Department of Physics, Stockholm University, Stockholm, Sweden; [b]The Oskar Klein Centre, Stockholm, Sweden
[148] Physics Department, Royal Institute of Technology, Stockholm, Sweden
[149] Departments of Physics and Astronomy and Chemistry, Stony Brook University, Stony Brook, NY, USA
[150] Department of Physics and Astronomy, University of Sussex, Brighton, UK
[151] School of Physics, University of Sydney, Sydney, Australia
[152] Institute of Physics, Academia Sinica, Taipei, Taiwan
[153] Department of Physics, Technion: Israel Institute of Technology, Haifa, Israel
[154] Raymond and Beverly Sackler School of Physics and Astronomy, Tel Aviv University, Tel Aviv, Israel
[155] Department of Physics, Aristotle University of Thessaloniki, Thessaloníki, Greece
[156] International Center for Elementary Particle Physics and Department of Physics, The University of Tokyo, Tokyo, Japan
[157] Graduate School of Science and Technology, Tokyo Metropolitan University, Tokyo, Japan
[158] Department of Physics, Tokyo Institute of Technology, Tokyo, Japan
[159] Department of Physics, University of Toronto, Toronto, ON, Canada
[160] [a]TRIUMF, Vancouver, BC, Canada; [b]Department of Physics and Astronomy, York University, Toronto, ON, Canada
[161] Faculty of Pure and Applied Sciences, University of Tsukuba, Tsukuba, Japan
[162] Department of Physics and Astronomy, Tufts University, Medford, MA, USA
[163] Centro de Investigaciones, Universidad Antonio Narino, Bogotá, Colombia
[164] Department of Physics and Astronomy, University of California Irvine, Irvine, CA, USA
[165] [a]INFN Gruppo Collegato di Udine, Sezione di Trieste, Udine, Italy; [b]ICTP, Trieste, Italy; [c]Dipartimento di Chimica, Fisica e Ambiente, Università di Udine, Udine, Italy
[166] Department of Physics, University of Illinois, Urbana, IL, USA
[167] Department of Physics and Astronomy, University of Uppsala, Uppsala, Sweden
[168] Instituto de Física Corpuscular (IFIC) and Departamento de Física Atómica, Molecular y Nuclear and Departamento de Ingeniería Electrónica and Instituto de Microelectrónica de Barcelona (IMB-CNM), University of Valencia and CSIC, Valencia, Spain
[169] Department of Physics, University of British Columbia, Vancouver, BC, Canada
[170] Department of Physics and Astronomy, University of Victoria, Victoria, BC, Canada
[171] Department of Physics, University of Warwick, Coventry, UK
[172] Waseda University, Tokyo, Japan
[173] Department of Particle Physics, The Weizmann Institute of Science, Rehovot, Israel
[174] Department of Physics, University of Wisconsin, Madison, WI, USA
[175] Fakultät für Physik und Astronomie, Julius-Maximilians-Universität, Würzburg, Germany
[176] Fachbereich C Physik, Bergische Universität Wuppertal, Wuppertal, Germany
[177] Department of Physics, Yale University, New Haven, CT, USA
[178] Yerevan Physics Institute, Yerevan, Armenia

[179] Centre de Calcul de l'Institut National de Physique Nucléaire et de Physique des Particules (IN2P3), Villeurbanne, France

[a] Also at Department of Physics, King's College London, London, UK
[b] Also at Institute of Physics, Azerbaijan Academy of Sciences, Baku, Azerbaijan
[c] Also at Novosibirsk State University, Novosibirsk, Russia
[d] Also at TRIUMF, Vancouver, BC, Canada
[e] Also at Department of Physics, California State University, Fresno, CA, USA
[f] Also at Department of Physics, University of Fribourg, Fribourg, Switzerland
[g] Also at Departamento de Fisica e Astronomia, Faculdade de Ciencias, Universidade do Porto, Porto, Portugal
[h] Also at Tomsk State University, Tomsk, Russia
[i] Also at CPPM, Aix-Marseille Université and CNRS/IN2P3, Marseille, France
[j] Also at Università di Napoli Parthenope, Naples, Italy
[k] Also at Institute of Particle Physics (IPP), Victoria, Canada
[l] Also at Also at Particle Physics Department, Rutherford Appleton Laboratory, Didcot, UK
[m] Also at Department of Physics, St. Petersburg State Polytechnical University, St. Petersburg, Russia
[n] Also at Louisiana Tech University, Ruston, LA, USA
[o] Also at Institucio Catalana de Recerca i Estudis Avancats, ICREA, Barcelona, Spain
[p] Also at Department of Physics, National Tsing Hua University, Hsinchu, Taiwan
[q] Also at Department of Physics, The University of Texas at Austin, Austin, TX, USA
[r] Also at Institute of Theoretical Physics, Ilia State University, Tbilisi, Georgia
[s] Also at CERN, Geneva, Switzerland
[t] Also at Georgian Technical University (GTU), Tbilisi, Georgia
[u] Also at Ochadai Academic Production, Ochanomizu University, Tokyo, Japan
[v] Also at Manhattan College, New York, NY, USA
[w] Also at Institute of Physics, Academia Sinica, Taipei, Taiwan
[x] Also at LAL, Université Paris-Sud and CNRS/IN2P3, Orsay, France
[y] Also at Academia Sinica Grid Computing, Institute of Physics, Academia Sinica, Taipei, Taiwan
[z] Also at Moscow Institute of Physics and Technology State University, Dolgoprudny, Russia
[aa] Also at Section de Physique, Université de Genève, Geneva, Switzerland
[ab] Also at International School for Advanced Studies (SISSA), Trieste, Italy
[ac] Also at Department of Physics and Astronomy, University of South Carolina, Columbia, SC, USA
[ad] Also at School of Physics and Engineering, Sun Yat-sen University, Guangzhou, China
[ae] Also at Faculty of Physics, M.V. Lomonosov Moscow State University, Moscow, Russia
[af] Also at National Research Nuclear University MEPhI, Moscow, Russia
[ag] Also at Department of Physics, Stanford University, Stanford, CA, USA
[ah] Also at Institute for Particle and Nuclear Physics, Wigner Research Centre for Physics, Budapest, Hungary
[ai] Also at Department of Physics, The University of Michigan, Ann Arbor, MI, USA
[aj] Also at Discipline of Physics, University of KwaZulu-Natal, Durban, South Africa
[ak] Also at University of Malaya, Department of Physics, Kuala Lumpur, Malaysia
* Deceased